

Regulators of synaptic vesicle docking and priming

BY

SZI-CHIEH YU

B.S., National Chung Hsing University, Taiwan, 2004

M.S., University of Pennsylvania, 2006

THESIS

Submitted as partial fulfillment of the requirements
for the degree of Doctor of Philosophy in Biological Sciences
in the Graduate College of the
University of Illinois at Chicago, 2013

Chicago, Illinois

Defense Committee:

David Featherstone, Chair
Janet Richmond, Advisor
Liang-Wei Gong
Simon Alford
David Biron, University of Chicago

ACKNOWLEDGMENTS

I am grateful to my advisor Dr. Janet Richmond for her support and guidance. Her expertise in molecular mechanisms of synaptic transmission in *C. elegans* improved my research skills and prepared me for future challenges. Particularly, her inspiration and enthusiasm in science leads me to be creative and productive. I thank her for demanding a high quality of work in all my endeavors. I also enjoyed the memories that we shared for the past two summers in Germany and the time outside the lab when we had our special Christmas parties and celebrate Oktoberfest as well as Halloween. Additionally, I would like to thank my committee members, Dr. David Featherstone, Dr. Liang-Wei Gong, Dr. Simon Alford and Dr. David Biron for providing insightful suggestions and encouragement. I could never have reached the heights or explored the depths without the help of my advisor and committees.

Very special thanks to the members of Richmond and Featherstone labs, to our collaborator Dr. Kenneth Miller, and to the people from ENI in Germany. Specifically, to Elena Gracheva and Carolin Wichmann who are my teachers in electron microscopy, to Susan Klosterman and Ashley Martin for part of the molecular and behavior experiments, and to Kaiyun Chen for the fly electrophysiological data in my thesis.

I cannot finish without saying how thankful I am with the care and love from my parents and my brother. Without their support and encouragement, I am not able to study in U.S and finish my Ph.D. Additionally, I would like to extend my gratitude to my dearest friends, Po-jen Yen, Peng-hsiang Chen and Zi Yang for their prayer and unyielding friendship. Above all, thanks be to God for granting me wisdom and strength to undertake my research project and enabling me to its completion.

TABLE OF CONTENT

| | |
|--|-------------|
| LIST OF FIGURES | vi |
| LIST OF ABBREVIATIONS | viii |
| ABSTRACT | x |
| I. INTRODUCTION | 1 |
| 1.1 Synaptic transmission and central role of the SNARE complex..... | 1 |
| 1.2 Controversial role of the SNARE complex assembly in vesicle docking..... | 5 |
| 1.3 Is Snapin required to stabilize the Synaptotagmin/SNARE complex? | 6 |
| 1.4 Does the HOPS complex component VPS-39 regulate synaptic transmission? ... | 8 |
| 1.5 Does acute activation of adenylate cyclase promote synaptic transmission in a Tomosyn-dependent manner? | 9 |
| II: Differential roles for Snapin and Synaptotagmin in the synaptic vesicle cycle | 11 |
| 2.1 Abstract | 11 |
| 2.2 Introduction | 12 |
| 2.3 Materials and Methods | 14 |
| Genetics | 14 |
| Quantitative RT-PCR..... | 16 |
| Behavioral assay | 16 |
| Electrophysiology | 17 |
| Confocal imaging and analysis | 17 |
| Electron microscopy..... | 18 |
| Statistical analysis..... | 19 |
| 2.4 Results | 19 |
| <i>snpn-1</i> mutants exhibit locomotory defects..... | 19 |
| <i>snpn-1</i> mutants exhibit synaptic defects | 22 |
| SNPN-1 acts presynaptically to regulate release..... | 23 |
| SNPN-1 does not affect synaptic density in <i>C. elegans</i> | 25 |
| SNPN-1 functions in synaptic vesicle docking | 27 |
| 2.5 Discussion..... | 32 |
| 2.6 Acknowledgements | 36 |
| III. VPS-39 promotes fusion competent vesicles in <i>C. elegans</i> | 37 |
| 3.1 Introduction | 37 |
| 3.2 Materials and Methods | 39 |
| Genetics | 39 |
| Molecular Biology..... | 39 |
| Confocal Microscopy | 40 |
| Pharmacology | 41 |
| Electrophysiology | 41 |
| Electron Microscopy..... | 42 |
| Statistical analysis..... | 43 |
| 3.3 Results | 43 |
| <i>vps-39</i> encodes a component of the HOPS complex | 43 |
| Neuronal expression of VPS-39 is required for early development | 45 |

| | |
|--|------------|
| VPS-39 is required for GFP processing in the coelomocytes | 47 |
| VPS-39 transport is kinesin-dependent..... | 49 |
| VPS-39 functions in neurons to promote cholinergic synaptic transmission | 51 |
| Neuronal cytoarchitecture is normal in <i>vps-39</i> mutants | 53 |
| VPS-39 regulates synaptic transmission..... | 55 |
| VPS-39 functions to dock synaptic vesicles | 57 |
| VPS-39/HOPS does not bypass UNC-13 function | 60 |
| Open Syntaxin partially bypasses <i>vps-39</i> mutants | 62 |
| Neuronal VPS-39 compensates for open Syntaxin evoked defects in low calcium | 67 |
| 3.4 Discussion | 70 |
| 3.5 Acknowledgements | 74 |
| VI. Photoactivation of adenylate cyclase promotes synaptic vesicle docking and release in a Tomosyn-dependent pathway | 75 |
| 4.1 Introduction | 75 |
| 4.2 Materials and Methods | 78 |
| Electrophysiology | 78 |
| Confocal Microscopy | 79 |
| Electron Microscopy | 79 |
| 4.3 Results | 80 |
| Photoactivatable adenylate cyclase (PAC) regulates synaptic transmission at the fly NMJ | 80 |
| bPAC activation of fly larvae increases synaptic vesicle docking | 86 |
| Increased synaptic vesicle docking is observed following Tomosyn RNAi | 89 |
| bPAC activation results in synaptic redistribution of Tomosyn..... | 91 |
| Tomosyn functions as an important effector in the cAMP-signaling pathway | 93 |
| 4.4 Discussion | 96 |
| bPAC as an optogenetic tool to acutely and reversibly increase intracellular cAMP | 97 |
| The enhanced release associated with Tomosyn and cAMP correlates with an increase in vesicle docking at <i>Drosophila</i> synapses | 98 |
| cAMP signaling regulates Tomosyn membrane localization and leads to enhanced synaptic strength <i>in vivo</i> | 100 |
| V. Future directions | 102 |
| Reference | 104 |
| VITA | 114 |

LIST OF FIGURES

Chapter I

- Figure 1.1. The synaptic vesicle cycle and the key SNARE proteins that mediate vesicle fusion4

Chapter II

- Figure 2.1. Neuronally expressed *C. elegans* Snapin and Synaptotagmin regulate locomotion.....21
- Figure 2.2. Synaptic defects of *snpn-1* and *snt-1* mutants.....24
- Figure 2.3. *snpn-1* and *snt-1* mutants have normal synaptic density.....26
- Figure 2.4. The additive ultrastructural phenotypes of *snpn-1* and *snt-1* mutants suggest independent roles in the vesicle cycle.....29
- Figure 2.5. PD proximal docked vesicle numbers in *snt-1* and *snt-1;snpn-1* mutants correlate with their release defects31

Chapter III

- Figure 3.1. VPS-39 is a member of the HOPS complex44
- Figure 3.2. VPS-39 expression and rescue of *vps-39* mutant embryonic lethality.....46
- Figure 3.3. VPS-39 is required for coelomocyte processing.....48
- Figure 3.4. Axonal expression of *VPS-39::mCherry* is *UNC-104*/Kinesin-dependent.50
- Figure 3.5. VPS-39 regulates ACh release in intact worms52
- Figure 3.6. VPS-39 is not required for synaptic development.....54
- Figure 3.7. VPS-39 promotes evoked release at the NMJ.....56
- Figure 3.8. VPS-39 is required for vesicle docking/priming59
- Figure 3.9. Expression of VPS-39 in neurons does not rescue *unc-13(L)* mutants61
- Figure 3.10. Open Syntaxin rescues the dylox resistance of *vps-39* mutants63
- Figure 3.11. Open Syntaxin partially rescues the *vps-39* mutant evoked defect.....65
- Figure 3.12. Open Syntaxin partially rescues *vps-39* mutant docking defects66
- Figure 3.13. VPS-39/open Syntaxin co-expression enhances release at low calcium .68

Figure 3.14. VPS-39 and open Syntaxin exhibit differential docked vesicle distributions69

Figure 3.15. Model of VPS-39 function73

Chapter IV

Figure 4.1. The optogenetic tool bPAC acutely and reversibly increases spacial cAMP level.....82

Figure 4.2 bPAC activation enhances synaptic release at NMJs85

Figure 4.3. bPAC activation increases plasma membrane synaptic vesicle docking .88

Figure 4.4. Tomosyn RNAi increases plasma membrane synaptic vesicle docking...90

Figure 4.5. bPAC activation translocates Tomosyn from the plasma membrane to the synaptic lumen.....92

Figure 4.6. bPAC activation in the Tomosyn RNAi background shows no additivity of synaptic vesicle docking95

LIST OF ABBREVIATIONS

| | |
|---------|--|
| ACh | Acetylcholine |
| BLOC | Biogenesis of lysosome-related organelle complex |
| BLUF | Blue light receptor using FAD |
| cAMP | Cyclic adenosine monophosphate |
| CGC | Caenorhabditis Genetics Center |
| CHCR | Clathrin heavy chain repeat |
| DNC | Dorsal nerve cord |
| EJC | Evoked junctional current |
| EM | Electron microscopy |
| FS | Freeze substitution |
| GFP | Green fluorescent protein |
| qRT-PCR | Quantitative real-time PCR |
| HOPS | Homotypic fusion and vacuole protein sorting |
| HPF | High-pressure freeze fixation |
| miniEJC | Miniature excitatory junctional currents |
| MLD | Membrane localization domain |
| NMJ | Neuromuscular junction |
| NSF | N-ethylmaleimide sensitive factor |
| PAC | Photoactivatable adenylate cyclase |
| PD | Presynaptic density |
| PKA | Protein kinase A |
| RBD | Rab binding domain |

| | |
|---------|---|
| RNAi | RNA interference |
| SCG | Superior cervical ganglion |
| SDS | Sodium dodecyl sulfate |
| SNAP-25 | Synaptosome-associated protein of 25 kDa |
| SNARE | Soluble <i>N</i> -ethylmaleimide-sensitive factor attachment receptor |
| SV | Synaptic vesicle |
| VAMP | Vesicle-associated protein |
| VNC | Ventral nerve cord |
| VPS | Vacuole protein sorting |
| WT | Wild-type |
| Y2H | Yeast-two hybrid |

ABSTRACT

Synaptic vesicle priming is dependent on the assembly of SNARE (soluble-N-ethylmaleimide-sensitive factor attachment receptor) complexes formed between Synaptobrevin, SNAP-25 and Syntaxin. The subsequent calcium-dependent release of primed vesicles requires the recruitment of the calcium-sensor, Synaptotagmin, a protein also implicated in endocytosis. As a consequence, proteins that regulate SNARE complex formation or stabilization can profoundly alter the synaptic strength. This thesis focuses on four SNARE interacting proteins, Snapin, Synaptotagmin, VPS-39 as well as Tomosyn, and explores their neuronal function by primarily using high pressure freezing/ freeze substitution (HPF/FS) electron microscope (EM) combined with other techniques. Specifically, the results presented in this thesis establish that Snapin stabilizes the SNARE complex to promote fusion in a Synaptotagmin-independent manner in *C. elegans*, that *C. elegans* VPS-39 alters Syntaxin conformation to enable fusogenic SNARE complex assembly, and that *Drosophila* Tomosyn functions as an important effector in the cAMP signaling pathway.

I. INTRODUCTION

1.1 Synaptic transmission and central role of the SNARE complex

Communication within the nervous system requires chemical release from synaptic vesicles, which undergo cycles of exocytosis and endocytic retrieval. Newly recycled vesicles are rapidly refilled with neurotransmitter, and are then targeted to presynaptic densities where they become primed to fuse in response to a Ca^{2+} signal. This is a highly regulated process requiring many synaptic proteins. Several lines of evidence have established that neuronally enriched members of the conserved SNARE (soluble N-ethylmaleimide sensitive factor attachment protein receptors) protein family play an essential role in neurotransmitter release (Weber et al., 1998). Specifically, the plasma membrane associated SNARE proteins-SNAP-25 (25 kDa synaptosome-associated protein) and Syntaxin as well as the vesicle-associated SNARE-Synaptobrevin (VAMP - vesicle-associated membrane protein) were identified as key components of the vesicle fusion machinery. These three proteins assemble in trans beginning at their N-terminals and subsequently zipper toward their membrane proximal C-terminals to form a four α -helical bundle known as the SNARE core complex (Broadie et al., 1995; Sollner et al., 1993; Sutton et al., 1998) (Figure 1.1). This complex is very stable, is resistant to sodium dodecyl sulfate (SDS) and requires the ATPase, NSF (N-ethylmaleimide sensitive factor) for disassembly (Hayashi et al., 1994). Disruption of any of the three SNARE complex proteins profoundly impairs synaptic transmission. For example, it has been shown that the clostridial toxins (botulinum and tetanus) abolish evoked neurotransmitter release by cleaving neuronal SNARE proteins (Blasi et al., 1993a; Blasi et al., 1993b; Schiavo et al., 1992). Similarly, genetic deletion of any

of the three SNARE proteins produces lethal phenotypes in both vertebrates and invertebrate systems, due to the loss of synaptic transmission (O'Connor et al., 1997; Saifee et al., 1998; Schoch et al., 2001; Washbourne et al., 2001). Consistent with these observations, SNARE containing reconstituted vesicles exhibit fusion, demonstrating that SNARE proteins alone are able to promote membrane fusion (Weber et al., 1998). However, the time required for these reconstituted vesicles to fuse is slow (hours) compared to physiological fusion rates at synapses (millisecond).

Subsequent studies have shown that additional SNARE binding proteins are required for efficient vesicle fusion, including members of the Sec1/Munc18 (SM), UNC-13/Munc13, and Synaptotagmin protein families. All three of these protein classes are now known to regulate the assembly and function of the SNARE complex, in part through their interactions with Syntaxin. Syntaxin exhibits a closed conformation with its N-terminal regulatory domain (H_{abc}) blocking the Syntaxin SNARE domain. At least one role of Munc-18 is to stabilize this closed Syntaxin conformation during intracellular transport to the synapse, after which Munc-18 also appears to play an important role in the fusion process itself through interactions with the assembled SNARE complex (Dulubova et al., 1999; Khvotchev et al., 2007; Ma et al., 2013). UNC-13, which is highly enriched at the presynaptic plasma membrane protein and interacts with the N-terminal of Syntaxin (Madison et al., 2005; Stevens et al., 2005) has been proposed to stabilize its open configuration (Stevens et al., 2005) promoting vesicle priming and neurotransmission (Betz et al., 1998; Maruyama and Brenner, 1991; Richmond et al., 1999). Consistent with this model, in *C. elegans* a constitutively open form of Syntaxin can bypass the requirement for UNC-13 in vesicle priming (Richmond et al., 2001).

Synaptotagmin then interacts with the assembled SNARE complex, and upon Ca^{2+} -binding triggers the fusion of primed vesicles with the presynaptic membrane through SNARE and phospholipid interactions (Geppert et al., 1991; Jorgensen et al., 1995; Perin et al., 1990; Sudhof and Rizo, 1996; Yoshihara and Littleton, 2002).

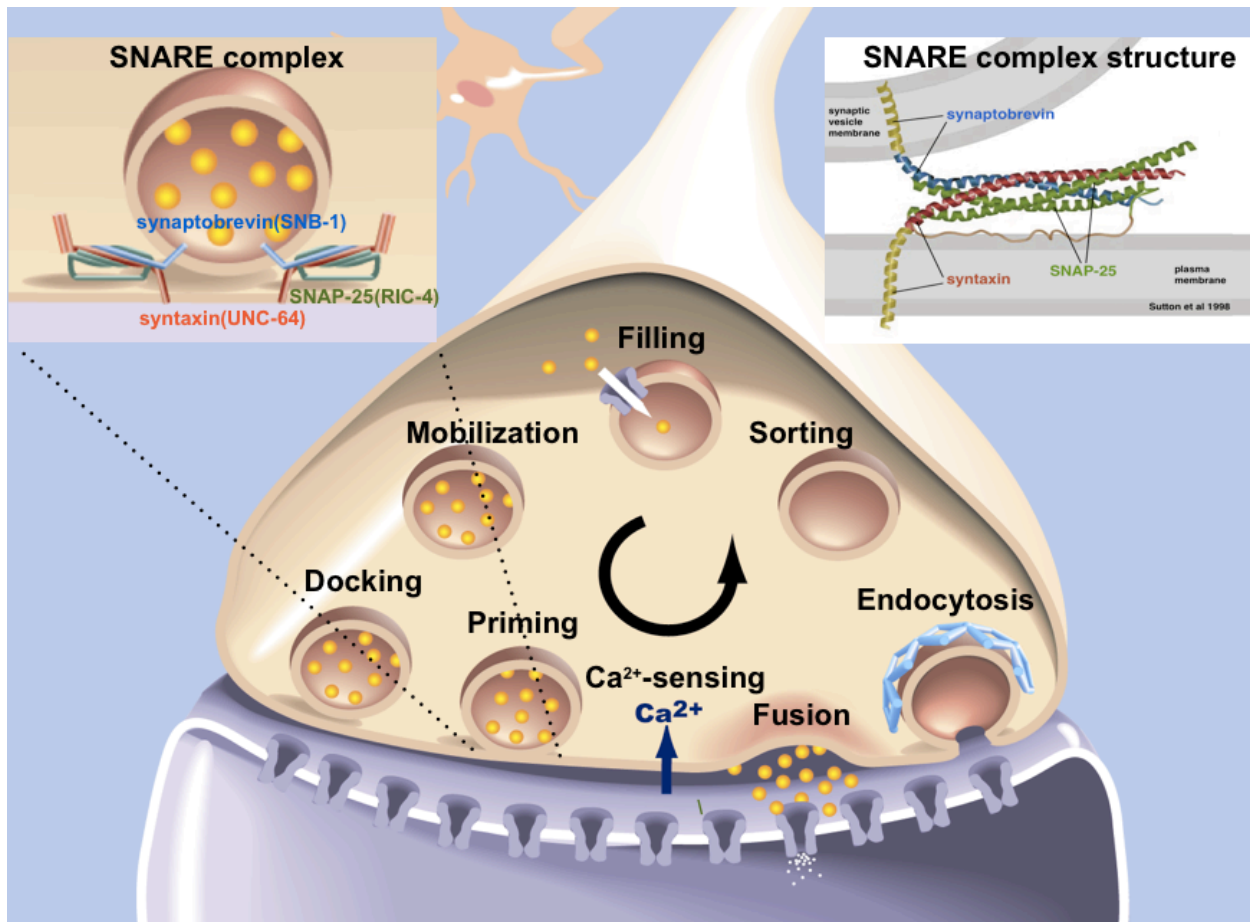


Figure 1.1. The synaptic vesicle cycle and the key SNARE proteins that mediate vesicle fusion. During priming, the α -helical domains of the three SNARE proteins: Syntaxin, SNAP-25 and Synaptobrevin, zipper together to form a highly stable SNARE complex that is essential for synaptic transmission.

1.2 Controversial role of the SNARE complex assembly in vesicle docking

Since Syntaxin and Synaptobrevin C-terminals have trans-membrane domains in the plasma and vesicle membranes, respectively, SNARE complex assembly was originally predicted to result in vesicle docking. However, early ultrastructural studies suggested that neither loss of SNARE protein nor UNC-13/Munc13 function reduced the number of membrane contacting vesicles (Aravamudan et al., 1999; Augustin et al., 1999; Broadie et al., 1995; Deak et al., 2004; Hunt et al., 1994; Richmond et al., 1999) leading to the hypothesis that vesicle docking must precede SNARE complex assembly. However, all of these original studies relied on the use of classical chemical fixation methods to prepare specimens for ultrastructural analysis. One disadvantage of this method is that fixation takes tens of minutes to fully immobilize tissues. In addition, the fixatives are hyperosmotic, which can cause cell shrinkage, possible redistribution of synaptic vesicles as well as exocytosis of primed vesicles (Rostaing et al., 2004). To circumvent these technical limitations, high pressure freezing/freeze substitution (HPF/FS) electron microscopy (EM) has recently been applied to the study of synaptic ultrastructure (Rostaing et al., 2004). HPF permits the almost instantaneous freezing immobilization of specimens (down to -180 C in ~10ms), the rapid cooling step excellently preserving cellular architecture by solidifying water within tissues as vitreous ice, an amorphous state that avoids ice crystal formation. Following HPF, freeze substitution is applied and organic solvents, such as anhydrous acetone, are used to replace amorphous ice at low temperature. By slowly substituting water along with introduction of chemical fixatives, cell morphology is well-preserved minimizing cell shrinkage and ultrastructural rearrangements. *C. elegans unc-13* and Syntaxin (*unc-*

64) were two of the first mutants re-analyzed following HPF/FS specimen preparation. In striking contrast to previous studies, the number of membrane contacting vesicles in both mutants were found to be profoundly reduced following HPF, suggesting that under these fixation conditions, morphological docking closely correlates with SNARE complex formation and the functional priming of synaptic vesicles (Hammarlund et al., 2007; Siksou et al., 2009; Weimer et al., 2006).

My expertise in HPF/FS electron microscopy thus provides an opportunity to study specimens in their near-native morphometric state. This thesis will use this and other techniques to focus on the following three questions addressing the roles of other SNARE interacting proteins, namely Snapin, Synaptotagmin, VPS-39 and Tomosyn, in the regulation of the synaptic vesicle cycle.

1.3 Is Snapin required to stabilize the Synaptotagmin/SNARE complex?

Snapin is a 15 kDa soluble protein which was first identified as a SNAP-25 binding partner in a yeast two-hybrid screen (Y2H); hence the name Snapin (SNAP-25 interacting protein) (Ilardi et al., 1999). Analysis from gel filtration and comparative protein structure modeling showed that Snapin has a predominantly α -helical secondary structure and forms dimers that bind to the two SNAP-25 alpha helices (Gowthaman et al., 2006; Vites et al., 2004). Subsequently, biochemical data indicated that Snapin dimers can simultaneously interact with both SNAP-25 and the calcium sensor, Synaptotagmin-1 (Chheda et al., 2001; Ilardi et al., 1999; Tian et al., 2005). This led to the hypothesis that Snapin is required to stabilize the interaction between Synaptotagmin and the SNARE complex. Given the importance of Synaptotagmin-1 in triggering the synchronous release of vesicles upon calcium-entry at the presynaptic

terminal, disruption of the Synaptotagmin/SNARE interaction in the absence of Snapin would be expected to have a similar effect. Consistent with this prediction, electrophysiological data from Snapin mouse mutants exhibited a loss of evoked release synchronicity, as well as a smaller primed vesicle pool. Interestingly, analysis of a dimerization defective Snapin construct with impaired ability to couple Synaptotagmin with the SNARE complex at rest restored release synchronicity but failed to rescue the priming defect in Snapin mutants. These results suggested that Snapin dimerization is somehow required to promote the full complement of fusion competent vesicles, but not the release kinetics. However one concern about these data is that since mouse Snapin mutants die at birth, all of the above functional experiments had to be performed on embryonically derived cultured neurons from Snapin mutant mice. Furthermore, these cultured neurons exhibit synaptogenesis defects and reduced vesicle numbers based on conventional electron microscopic analysis, all of which could impact the interpretation of the observed exocytic defects (Pan et al., 2009). These previous studies also failed to examine genetic interactions between Snapin and Synaptotagmin mutants which would be expected to further resolve the interdependence of Snapin and Synaptotagmin in their functions.

To address these potential concerns, we undertook a functional characterization of *C. elegans* Snapin mutants (*snpn-1*), which are viable and exhibit no obvious synaptogenesis defects, as well as Synaptotagmin (*snt-1*) mutants, using a combination of behavioral assays, electrophysiology and electron microscopy. We also examined whether there were any genetic interactions between these two binding partners. Our results, presented in Chapter 2, suggest that Snapin plays a role in vesicle docking and

fusion competence but does not regulate the kinetics of evoked synaptic transmission. Additionally, ultrastructural analyses of *snt-1* and *snt-1;snpn-1* double mutants suggest that the function of SNPN-1 in vesicle docking is independent of SNT-1. Therefore, we propose a model that *C. elegans* SNPN-1 is required for the stabilization of primed vesicles through SNARE complex interactions and acts upstream of SNT-1 which functions after docking both as a calcium-sensor to promote vesicle fusion and during endocytosis.

1.4 Does the HOPS complex component VPS-39 regulate synaptic transmission?

Components of the mammalian HOPS complex (hVps-11, 16 and 18) have been shown to co-immunoprecipitate Syntaxin1A and Munc18 from rat brain homogenate, (Kim et al., 2006). The incorporation of Munc18 and Syntaxin into large heterooligomeric complexes with the HOPS complex occurs at the expense of Munc18/Syntaxin dimers (Kim et al., 2006). The HOPS complex is also enriched in presynaptic synaptosomal fractions. Furthermore, overexpression of the HOPS components hVps 11, 16 and 18 potentiate Ca^{2+} -dependent hormone release from PC12 cells. While the precise role of the HOPS complex in neurons remains to be determined, the fact that this complex binds to Syntaxin and Munc18 and promotes release has given rise to the hypothesis that it may regulate vesicle fusion (Kim et al., 2006). To address this question *in vivo* we obtained a putative null mutant of the *C. elegans* HOPS complex gene *vps-39*. In Chapter 3, we performed a detailed characterization of *C. elegans vps-39* mutants and uncovered multiple roles for VPS-38

in embryonic survival, coelomocyte function as well as synaptic vesicle docking and release.

1.5 Does acute activation of adenylate cyclase promote synaptic transmission in a Tomosyn-dependent manner?

Biochemical data suggest that cAMP (cyclic adenosine monophosphate)-dependent Protein Kinase A (PKA) phosphorylation of Tomosyn reduces its Syntaxin-binding affinity, thereby enhancing the formation of SNARE complexes *in vitro* (Baba et al., 2005). The PKA phosphorylation site of Tomosyn is upstream of a “tail” domain that links the large N-terminal WD40 repeats of Tomosyn to the C-terminal SNARE domain. Intramolecular interactions between the tail and the SNARE domain prevent Tomosyn from forming Tomosyn complexes. However, the tail can also undergo a molecular switch, interacting instead with the N-terminal, freeing the Tomosyn SNARE domain. It has been postulated that PKA phosphorylation of Tomosyn may regulate this intramolecular switch, leading to repression of the Tomosyn SNARE motif function (Yamamoto et al., 2009). In this model PKA-phosphorylation of Tomosyn could lead to enhanced priming.

To test this hypothesis, we needed to acutely trigger cAMP signaling at presynaptic synapses to examine the functional consequences and establish whether these changes phenocopied those of Tomosyn knockdown. This was achieved by expressing an optogenetic tool, photoactivatable adenylate cyclase from soil bacterium *Beggiatoa* (bPAC) in *Drosophila*. bPAC rapidly generates intracellular cAMP upon blue light activation (Stierl et al., 2011). Compared to the adenylate-cyclase activator, forskolin, and mutants in the cAMP pathway, the manipulation of blue light-activated

bPAC is able to enhance intracellular cAMP non-invasively, in a tissue-specific manner and avoids developmental defects associated with chronic cAMP signaling (Bellen et al., 1987; Guan et al., 2011). Using bPAC, we were able to record the evoked synaptic responses of dissected larvae to acutely increase neuronal specific cAMP. This represents the first *Drosophila* study in which the electrophysiological consequences of activated bPAC have been analyzed.

Additionally, introduction of bPAC allowed us to examine intact larvae at the EM level immediately after blue light activation. Because this study is the first to conduct a detailed morphometric analysis of synapses at *Drosophila* neuromuscular junctions (NMJs) following HPF/FS, we first characterized wild-type synaptic ultrastructure and then observed changes due to bPAC activation, Tomosyn knockdown and the two conditions combined.

Our electrophysiological results, presented in Chapter 4, indicate that activation of neuronally expressed bPAC phenocopies the prolonged release observed following Tomosyn-knockdown. This phenotype correlates with a significant increase in plasma membrane docked synaptic vesicles. Furthermore, bPAC activation also results in the translocation of Tomosyn away from the plasma membrane into the synaptic lumen, consistent with the notion that cAMP-dependent signaling impacts the ability of Tomosyn to bind plasma-membrane SNAREs. Lastly, the number of docked vesicles of Tomosyn knockdown in the bPAC activated background shows no further increase compared to bPAC activation only, suggesting that adenylate cyclase promotes synaptic transmission through the addition of primed/docked synaptic vesicles in a Tomosyn-dependent manner.

II: Differential roles for Snapin and Synaptotagmin in the synaptic vesicle cycle

Szi-Chieh Yu¹, Susan M. Klosterman¹, Ashley A. Martin¹, Elena O. Gracheva², and Janet E. Richmond^{1*}

¹Biological Sciences, University of Illinois at Chicago, Chicago, Illinois, USA

²Biological and Biomedical Sciences, Yale University, New Haven, Connecticut, USA

* Corresponding author: jer@uic.edu

2.1 **Abstract**

Evoked synaptic transmission requires interactions between the calcium sensor Synaptotagmin I and the three essential SNARE proteins, Syntaxin, SNAP-25, and Synaptobrevin. Evidence suggests that Snapin may be a functionally important intermediate in this process through simultaneous interactions of Snapin dimers with both SNAP-25 and Synaptotagmin. This model is supported by data from cultured neurons from embryonically lethal Snapin null mutant mice, which exhibit desynchronized release and a reduced primed vesicle pool. Based on observations that dimerization-defective Snapin mutants specifically disrupt priming, Snapin is hypothesized to stabilize primed vesicles by coupling Synaptotagmin and SNAP-25. To test this model *in vivo* we examined synaptic transmission in adult *C. elegans* Snapin (*snpn-1*) mutants, which are viable. Unlike Snapin mutant mice synapses, synaptic transmission was unaffected at *C. elegans snpn-1* mutant neuromuscular junctions (NMJs), but similar to the mouse mutant, the number of morphologically docked, fusion competent vesicles was significantly reduced. However, comparison of *snt-1* and *snt-1;snpn-1* double mutants suggests that the docking role of SNPN-1 is independent of

Synaptotagmin. We therefore, propose that the primary role of *C. elegans* Snapin is to promote vesicle priming, through the stabilization of SNARE complexes via established interactions with SNAP-25, which is upstream and independent of Synaptotagmin roles in calcium-sensing and endocytosis.

2.2 Introduction

Neurotransmission is critically dependent on the formation of SNARE (soluble *N*-ethylmaleimide sensitive factor adaptor protein receptor) complexes that form between plasma membrane associated Syntaxin and SNAP-25 (synaptosomal-associated protein 25 kDa) and vesicle-associated Synaptobrevin (VAMP-2) (Fasshauer et al., 1998; Sollner et al., 1993; Sutton et al., 1998; Trimble et al., 1988). The zippering together of the SNARE motifs of all three SNARE proteins brings the vesicle membrane into close apposition with the plasma membrane, producing a fusion competent state known as priming (Jahn et al., 2003; Matos et al., 2003). The essential role that SNARE proteins play in priming is supported by clostridial toxin as well as SNARE protein knockout studies, either of which completely eliminate evoked neurotransmitter release indicating that the SNAREs are components of the minimal membrane fusion machinery (Augustine et al., 1996; Schiavo et al., 2000; Schoch et al., 2001).

In addition to the SNAREs, the synaptic vesicle protein Synaptotagmin I plays an important role as a Ca^{2+} sensor (Brose et al., 1992), triggering the fusion of primed vesicles in response to Ca^{2+} entry in the terminal through voltage-gated Ca^{2+} channels (Geppert et al., 1994). Two Ca^{2+} binding domains (C2A and C2B) within the cytoplasmic region of Synaptotagmin are critical for this function. Ca^{2+} binding to both C2 domains increases the binding affinity of Synaptotagmin for the SNARE complex

and membrane lipids, events that promote the exocytic event (Davletov and Sudhof, 1993). The speed of the Synaptotagmin/SNARE complex interaction is thus an important determinant of the kinetics of exocytosis (Fernandez-Chacon et al., 2001; Striegel et al., 2012).

Recent studies suggest that the highly conserved protein, Snapin, may also contribute to the timing and efficacy of synaptic transmission (Pan et al., 2009). Snapin first isolated as a SNAP-25 interacting protein in a yeast two-hybrid assay of human brain cDNA, was subsequently shown to also bind Synaptotagmin I (Ilardi et al., 1999). By binding simultaneously with the SNARE complex and Synaptotagmin I, Snapin dimers have been postulated to promote the Synaptotagmin I/ SNARE complex interaction. Interestingly, the phosphorylation of Snapin by protein kinase A (PKA) enhances its association with Synaptotagmin I and the SNARE complex thus, Snapin is also a potential effector of PKA-dependent synaptic facilitation (Chheda et al., 2001; Thakur et al., 2004; Tian et al., 2005).

Despite evidence that Snapin and Synaptotagmin I act in the same biochemical pathway, analysis of vertebrate Snapin and Synaptotagmin I mutant neuronal cultures reveal different phenotypes. Specifically, Snapin mutants neurons have reduced synaptic event frequency (Pan et al., 2009) whereas Synaptotagmin I mutants exhibit increased endogenous rates in most cases (Broadie et al., 1994; Littleton et al., 1994; Pang et al., 2006), although not in autaptic cultures (Geppert et al., 1994). This latter discrepancy has been attributed to differences in synaptic behavior under different culture conditions (Xu et al., 2009). In other studies Synaptotagmin I has also been implicated in endocytosis through interactions with the heterooligomeric AP-2 protein

complex which is responsible for recruiting clathrin which is required for clathrin-mediated endocytosis (Jorgensen et al., 1995; Poskanzer et al., 2003; Yao et al., 2012; Zhang et al., 1994). It is less clear whether Snapin has an endocytic role, although cultured Snapin mutant neurons have fewer vesicles, possibly reflecting a vesicle recycling defect (Pan et al., 2009). One shortcoming of the Snapin and Synaptotagmin research field is that the lethality of both mutants has necessitated performing functional experiments on cultured neurons derived from embryonic tissues, which may not always fully recapitulate protein function in the intact nervous system. Since neither the role of Snapin nor its functional interplay with Synaptotagmin has been examined *in vivo* we undertook an evaluation of *C. elegans snpn-1* and *snt-1* mutants. Since these mutants are viable and reach adulthood we were able to perform behavioral, electrophysiological, and ultrastructural analyses within an intact nervous system, revealing new insights into the function of these two synaptic proteins.

2.3 Materials and Methods

Genetics

Nematodes were maintained on agar plates with OP50 bacteria as a food source. Strains used were the N2 reference strain, *snpn-1(tm1892)* 2x outcrossed, NM204 *snt-1(md290)*, SY1297 *snt-1(md290);snpn-1(tm1892)*, GH19 *glo-2(zu455)*, ZM1462 *nuls94[Pacr-2::SNB-1::GFP]*, SY1368 *snpn-1(tm1892);nuls94[Pacr-2::SNB-1::GFP]*, SY1361 *snt-1(md290);[Pacr-2::SNB-1::GFP]*, SY1449 *snpn-1(tm1982);jals1092(integrated Punc-17::snpn-1; 6x outcrossed)*, SY1498 *jaEx1058[Psnpn-1::GFP-snpn-1::snpn-1utr(pSY1); Prab-3::mCherry::unc-54utr(pGH8)]; snpn-1(tm1892)*.

Standard cloning procedures were used to generate a SNPN-1 over-expression vector in cholinergic neurons [*Punc-17::snpn-1*]. Genomic DNA for the *C. elegans snpn-1* gene was amplified from hermaphrodites using the following primers, primer 1: 5'- ACGGATCCATGTCGTCAACTGCTGGAGGCGAAGTG and primer 2: 5'- CAGGATCCGAAAATAGACAAACAGCTGCCG. The primers contain a BamHI restriction site used to ligate this product into a vector containing the *Punc-17 promoter*.

The multisite gateway three-fragment vector construction protocol (Invitrogen cat. 12537-023) was implemented to generate the SNPN-1 expression vector, *jaEx1058[Psnpn-1::GFP-snpn-1::snpn-1utr]*. Primer 3: 5'- AAAACGTAATTGGCTGCC GATTTTGAG and primer 4: 5'- GAAAAATGAAGGAAGTTGGCTTCAGAG were used to amplify the region spanning 675 base pairs upstream of the *snpn-1* start codon, the *snpn-1* gene, and its 3'UTR from hermaphrodite genomic DNA with HotStarTaq Plus Master Mix kit (Qiagen, cat. 203643). The PCR product was cloned into the pCRII-Blunt-TOPO vector using a Zero Blunt TOPO PCR Cloning Kit. From this PCR product the *snpn-1* promoter, the *snpn-1* coding region and the 3'UTR were separately amplified using the following gateway primer pairs: (primer 5: 5'-GGGGACAACTTTG TATAGAAAAGTTGCCAAAACGTAATTGGCTGCCGATT and primer 6: 5'- GGGGAC TGCTTTTTTTGTACAAACTTGTCAATTTAGCTGTAAGAAAGAAGA for the *snpn-1* promoter, primer 7: 5'- GGGGACAGCTTTCTTGTACAAAGTGGCCATGTCGTCAAC TGCTGGAGGCG, primer 8: 5'-GGGGACAACTTTGTATAATAAAGTTGTGAAAAA TGAAGGAAGTTGGCTTC) for the *snpn-1* coding region plus 3'UTR). Then the *snpn-1* promoter region was cloned into the pDONR221 P4-P1r vector. The GFP sequence without a stop codon was cloned into vector pDONR221 and the genomic *snpn-1*

sequence plus 848 base pairs of downstream sequence following the stop codon was cloned into pDONR221 P2r-P3. A ligation reaction was then performed to insert all three sequences in the donor vectors into the destination vector, pDEST R4-R3 Vector II resulting in an N-terminally GFP-tagged SNPN-1 under the *snpn-1* promoter.

Quantitative RT-PCR

Total mRNA was isolated from 8 plates of worms for each strain using TRIzol (Invitrogen) extraction. Genomic DNA was removed using a TURBO-DNAFree Kit (Ambion). Reverse transcription was done from purified mRNA using SuperScript III First-Strand Synthesis System (Invitrogen) with oligo(dT) primers. qRT-PCR was quantified by fluorescent detection of SYBR green-labeled PCR product using an MJResearch Opticon2 real-time thermocycler. The cycle threshold [C(t)] value for Snapin was normalized to a dynamin (*dyn-1*) control using the equation: $\Delta C(t)_{\text{sample}} = C(t)_{\text{snpn-1}} - C(t)_{\text{dyn-1}}$. Normalized C(t) values for the *snpn-1* mutant (tm1892) were then referenced to the wild type (calibrator) to determine relative amounts of *snpn-1* mRNA using the equation: $\Delta\Delta C(t)_{\text{sample}} = \Delta C(t)_{\text{sample}} - \Delta C(t)_{\text{calibrator}}$. Primers for RT-PCR were: primer 9: 5'-CTGTGGACTTGCTCCCCTAC and primer 10: 5'-TTTTGTGAGACGTTTCGAGGA.

Behavioral assay

Behavioral analysis was conducted on N2, *snpn-1(tm1892)*, *snt-1(md290)*, and *snt-1(md290);snpn-1(tm1892)* mutants. Thrashing behavior for individual worms placed in M9 medium was quantified over a 3-minute period. Head tap assays were performed on worms acclimated for 1 minute on agar plates. The total number of

elicited body bends to a single head tap, were counted. A body bend is described as the execution of a full sinusoidal turn of the worm's head.

Electrophysiology

Standard worm dissection and electrophysiological methods were used as previously described (Richmond, 2009; Richmond et al., 1999). Briefly, animals were immobilized with Histoacryl glue, and a cuticle incision was made with a glass needle, to expose the ventral medial body wall muscles. Muscle recordings were made in the whole-cell patch-clamp configuration (holding potential, -60 mV) using an EPC-10 patch-clamp amplifier digitized at 1 kHz. Standard 5 mM Ca²⁺ extracellular solution consisted of 150 mM NaCl, 5 mM KCl, 5 mM CaCl₂, 4 mM MgCl₂, 10 mM glucose, 5 mM sucrose, 15 mM HEPES, pH'd to 7.3 and ~340 mOsm. Ca²⁺ was replaced with NaCl in the 1mM Ca²⁺ extracellular solution. The patch pipette solution contained 120 mM KCl, 20 mM KOH, 4 mM MgCl₂, 5 mM (N-tris[Hydroxymethyl] methyl-2-aminoethane-sulfonic acid), 0.25 mM CaCl₂, 4 mM Na²ATP, 36 mM sucrose with 5 mM EGTA, pH 7.2 and ~315 mOsm. Data were acquired using Pulse software (HEKA, Southboro, Massachusetts, United States) run on a PC computer. Subsequent analysis and graphing was performed using Pulsefit (HEKA), Mini analysis (Synaptosoft Inc., Decatur, Georgia, United States) and Igor Pro (Wavemetrics, Lake Oswego, Oregon, United States).

Confocal imaging and analysis

Puncta/10mm for each strain expressing SNB-1::GFP was quantified as described previously (Kim *et al* 2007). In brief, young adults were mounted on 2% agarose pads and immobilized with 10% sodium azide (Sigma) in M9 buffer. Images

were obtained with a 60x objective using an Olympus Optical FV-500 laser scanning confocal microscope. Dorsal nerve cord synapses were analyzed using the 'Punctaanalyser' program in Matlab (Kim et al., 2008).

Electron microscopy

N2, *snpn-1(tm1892)*, *snt-1(md290)* and *snt-1(md290)snpn-1(tm1892)* young adult hermaphrodites were prepared for high-pressure freezing (HPF) as described previously (Rostaing et al., 2004). Briefly, 10–15 animals were loaded in a specimen chamber filled with OP50 and immobilized by HPF at -180°C in a Bal-Tec HPM010 and moved to liquid nitrogen.

Freeze substitution was performed in a Reichert AFS machine (Leica, Oberkochen, Germany) as described previously, using tannic acid (0.1%) and 0.5% glutaraldehyde fixative infused over 96 hours, followed by 2% osmium oxide (OsO₄) (Weimer et al., 2006). Fixed specimens were embedded in Araldite 502 over a 48 h period at 65°C. Serial sections were cut at 40 nm thickness, collected on formvar-coated copper grids (EMS, FCF2010-Cu), and counterstained with 2.5% aqueous uranyl acetate for 4 min, followed by 2 min Reynolds lead citrate. Images were collected on a Jeol JEM-1220 (Tokyo, Japan) transmission electron microscope operating at 80 kV. Micrographs were obtained on a Gatan digital camera (Pleasanton, CA) at a 100x magnification.

Morphometric analysis of ventral nerve cord sections was scored blind. Images were quantified using NIH ImageJ software. A synapse is defined as a set of serial sections containing a presynaptic specialization plus two flanking sections on either side without a presynaptic specialization.

Statistical analysis

All data were plotted as mean and S.E.M, and significance was assessed using the Mann-Whitney test. Statistically significant values were: of $p > 0.05$ not significant, $p \leq 0.05$ *, $p \leq 0.01$ **, $p \leq 0.001$ ***.

2.4 Results

***snpn-1* mutants exhibit locomotory defects**

The *C. elegans* Snapin homolog (*snpn-1*), which encodes a 122 amino acid protein spanning three exons is 29% identical (59% similar) to mouse Snapin. We obtained a deletion mutant from the CGC, *snpn-1(tm1892)*, which deletes 520 genomic base pairs, spanning the presumptive upstream regulatory sequence, the start codon, first exon and intron, and half of the second exon of the *snpn-1* coding region (Figure 2.1A). Based on the extent of the *snpn-1* deletion and the absence of detectable transcripts following qRT-PCR (data not shown), this mutant is likely to be a molecular null (Hermann et al., 2012). Unlike mouse Snapin mutants which die shortly after birth, *C. elegans snpn-1(tm1892)* mutants are viable and produce off-spring, allowing us to assess the behavioral consequences of freely moving adult *snpn-1* null mutants. As shown in Figure 1B, *snpn-1(tm1892)* mutants produced significantly fewer body bend reversals in response to a gentle head tap when compared to wild-type worms ($p=0.0008$). Thrashing responses of *snpn-1(tm1892)* mutants in M9 medium, was also significantly depressed when compared to the wild type over a 3-minute scoring period ($p<0.0001$) (Figure 2.1C). Given that the interaction between Snapin and Synaptotagmin suggests a functional link between these two proteins, we next assessed the behavior of both *C. elegans snt-1* and *snpn-1:snt-1* double mutants.

Where as the head tap responses and thrashing measurements of *snt-1(md290)* null mutants were more severe than *snpn-1* mutants (Figure 2.1B,C), the *snt-1;snpn-1* double mutants showed no further reduction, with the exception of the third minute of thrashing ($P=0.016$), suggesting that any additive functions of SNT-1 and SNPN-1 are minimal and require prolonged activity.

Since the behavioral defects in *snpn-1* mutants are indicative of altered neuromuscular function, we assessed whether SNPN-1 acts pre or post-synaptically at neuromuscular junctions (NMJs) by generating an extrachromosomal GFP-tagged *snpn-1* transgene under its own promoter. GFP::SNPN-1 expression was expressed throughout the nervous system based on a high-degree of colocalization with the panneuronal reporter *pRab-3::mCherry* (Figure 2.1D), but was absent from body wall muscles suggesting that SNPN-1 plays a presynaptic role.

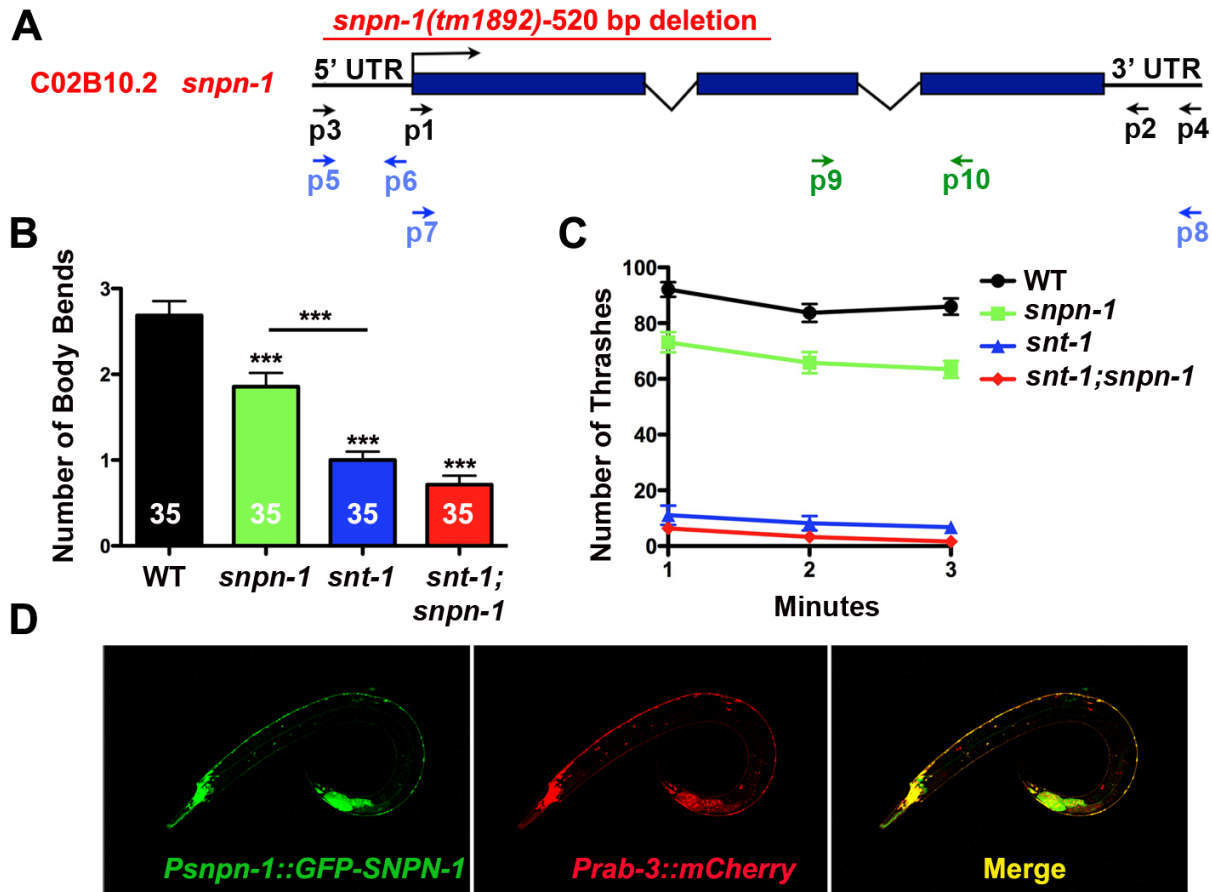


Figure 2.1. Neuronally expressed *C. elegans* Snapin and Synaptotagmin regulate locomotion. (A) Schematic of the Snapin (*snpn-1*) gene structure and location of the *snpn-1(tm1892)* deletion. (B) The number of body bend reversals triggered by a single head tap was significantly reduced in *snpn-1(tm1892)*, *snt-1(md290)* and the double mutants (mean ± SEM, Behavioral data collected by Ashley Martin). (C) The mean ± SEM values for thrashing responses of *snpn-1* mutants placed in M9 showed a modest decrease compared to *snt-1* and *snt-1;snpn-1* double mutants. N.B. The subtle differences between *snt-1* single and double mutants would be difficult to discern in this assay, given the already low thrashing rates observed in *snt-1* mutants. Significance values for all mutants were ≤ 0.0001 relative to wild type. (D) Expression of GFP::SNPN-1 under the presumptive *snpn-1* promoter co-localized with mCherry driven panneuronally using the *pRab-3* promoter. This figure was previously published in PLoS One 2013:8(2).

***snpn-1* mutants exhibit synaptic defects**

To directly assay synaptic transmission in *snpn-1* mutants, recordings were made from the cholinergic NMJs of dissected worms. *In situ* recordings, initially performed in 5mM Ca^{2+} Ringer, revealed a trend toward reduced evoked junctional current (EJC) amplitudes and evoked charge integrals in *snpn-1* mutants, although not significant ($p=0.0635$ and $p=0.174$, respectively) (Figure 2.2A-C). The frequency of endogenous synaptic events in *snpn-1* mutants was also wild type ($p=0.953$) (Figure 2.2E). On contrast and consistent with the more severe behavioral deficits, *snt-1* mutants showed a significant reduction in both EJC amplitude ($p=0.0014$) and charge integral ($p=0.0019$) as well as endogenous event frequency in 5mM Ca^{2+} Ringer ($p=0.0007$) (Figure 2.2A-C,E). Neither EJCs nor endogenous synaptic events in the *snt-1;snpn-1* double mutants were more severe than *snt-1* alone, indicating that loss of SNPN-1 in the *snt-1* background has no additional effect on these release parameters (Figure 2.2A-C,E).

Given the role of Synaptotagmin as a calcium-sensor for exocytosis, and the proposed functional interaction between SNT-1 and SNPN-1, we next examined EJCs in *snpn-1* and *snt-1* mutants under reduced Ca^{2+} conditions (1mM), where changes in the Ca^{2+} -sensitivity of release would be more apparent. Under these recording conditions, both the EJC amplitude and charge integral of *snpn-1* mutants were significantly reduced compared to wild-type ($p=0.0027$ and $p=0.02$, respectively), although these defects were much less severe than those of *snt-1* mutants ($p=0.0016$ and $p=0.0016$) (Figure 2.2F-H). A trend towards fewer endogenous minis was also observed in 1mM Ca^{2+} (*snt-1* $p=0.0007$), although this was not significant for *snpn-1*

mutants ($p=0.414$) (Figure 2.2K). As seen in 5mM Ca^{2+} Ringer, evoked and endogenous synaptic events of *snt-1;snpn-1* doubles were not more severe than *snt-1* alone.

Unlike cultured neurons from mouse Snapin mutants, we saw no evidence of asynchronous release as a result of deleting *C. elegans snpn-1* or slower EJC decay kinetics in either 5mM or 1mM Ca^{2+} (Figure 2.2D,I). However, strains with the *snt-1* mutation did show significantly faster decay kinetics in all but the low calcium *snt-1;snpn-1* double mutant. This effect could be due to more efficient neurotransmitter clearance from the synaptic cleft resulting from greatly reduced acetylcholine (ACh) release levels. Alternatively, the faster decay kinetics of *snt-1* mutants could be a reflection of the release properties of the remaining unidentified calcium-sensor(s) in the absence of SNT-1.

SNPN-1 acts presynaptically to regulate release

To determine whether the release defects of *snpn-1* mutants is due to loss of neuronal SNPN-1, we integrated a non-tagged genomic *snpn-1* transgene driven by the cholinergic neuronal promoter *Punc-17* into *snpn-1* mutants and assessed rescue of the cholinergic EJC in 1mM Ca^{2+} Ringer. As shown (Figure 2.2F-H), *Punc-17::snpn-1* rescued the evoked response (EJC amplitude $p=0.21$ relative to wild-type, EJC charge integral slightly exceeding wild-type ($p=0.028$)) (Figure 2.2F-H). These data indicate that the synaptic defect is specific to the *snpn-1* gene deletion rather than a background mutation, and that SNPN-1 is required presynaptically for normal synaptic transmission.

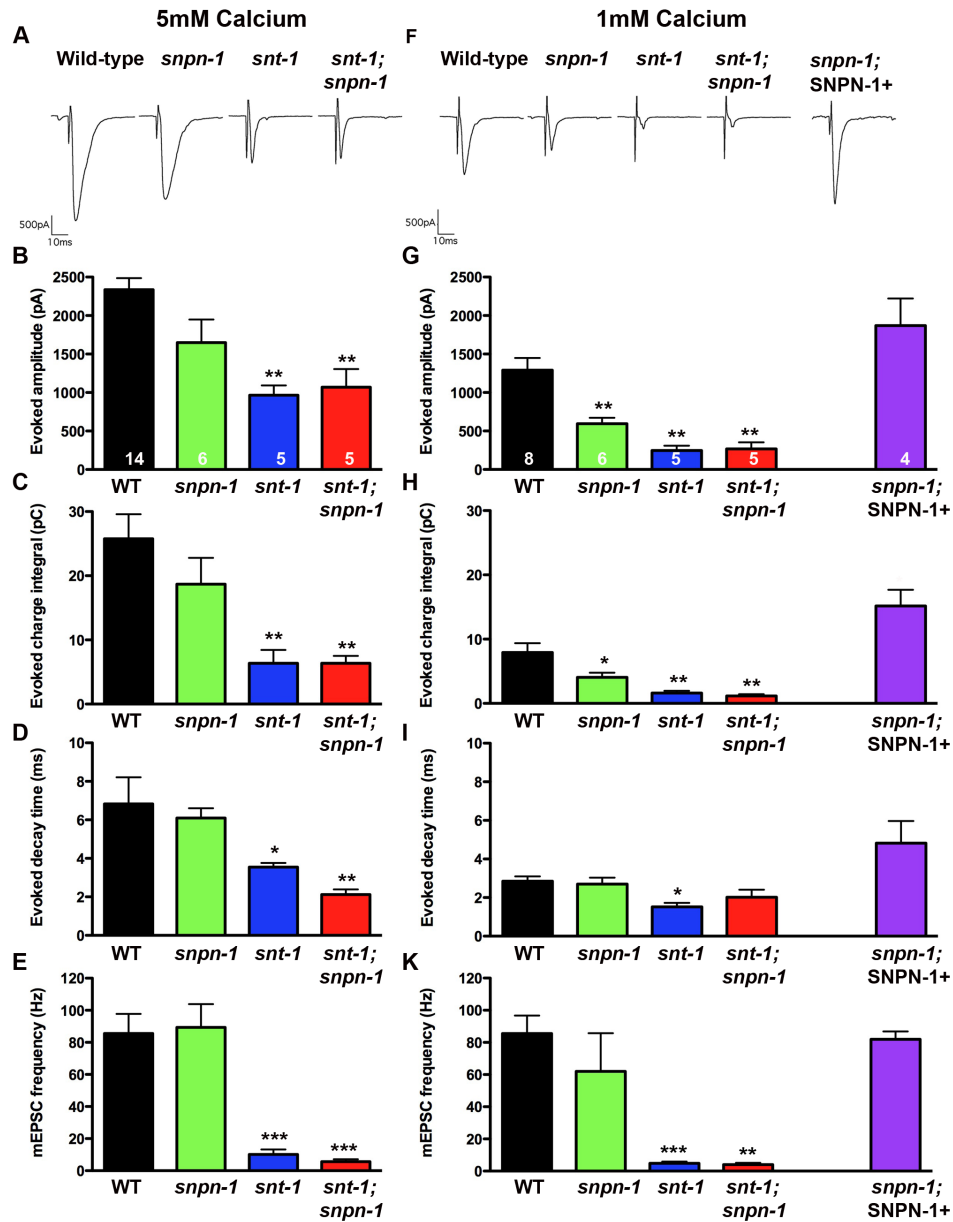


Figure 2.2. Synaptic defects of *snpn-1* and *snt-1* mutants. (A,F) Evoked post-synaptic responses from voltage-clamped body wall muscles to nerve cord stimulation in acutely dissected worms bathed in 5mM Ca²⁺ (A) and 1mM Ca²⁺ saline (B). Plots of evoked amplitude (B,G), evoked charge integral (C,H) evoked decay (D,I) and endogenous mini frequency (E,K) expressed as mean \pm SEM demonstrate that both *snpn-1* and *snt-1* mutants have release defects, although more severe in *snt-1* mutants. The synaptic defects of *snpn-1* mutants observed in 1mM Ca²⁺ conditions are fully rescued by expressing *SNPN-1* under the cholinergic neuronal promoter *Punc-17* (F-K). For all parameters plotted, *snt-1;snpn-1* double mutants do not exhibit additivity. Data collected by Dr. Richmond, and previously published PLoS One 2013;8(2).

In addition to its SNT-1/SNAP-25 interactions, Snapin is also known to be a component of BLOC-1 (biogenesis of lysosome-related organelle complex) (Hermann et al., 2012). To address the possibility that the synaptic phenotype of *snpn-1* mutants is the result of BLOC-1 disruption, we recorded the NMJ evoked responses from another mutant of the BLOC-1 protein complex, Pallidin(*glo-2*) (Hermann et al., 2012). Unlike *snpn-1* mutants, in 1mM external calcium *glo-2(zu455)* mutants exhibited wild-type response amplitudes (wild-type 1291 +/-159 pA, n=8, *glo-2* 1285+/-135 pA, n=5, p=0.94) indicating that the *snpn-1* synaptic phenotype is not due to disruption of BLOC-1 function.

SNPN-1 does not affect synaptic density in C. elegans

Cultured hippocampal neurons from Snapin mutant mice have significantly fewer synapses (Pan et al., 2009). If conserved, this phenotype could explain the behavioral and electrophysiological defects observed in *C. elegans snpn-1* mutants. To test whether *snpn-1* mutants have altered synaptic density, a transgenic line expressing GFP-tagged Synaptobrevin under the cholinergic neuronal promoter *Pacr-2* was crossed into the *snpn-1* mutant background. GFP puncta along the dorsal nerve cord were imaged and scored to provide a measure of synaptic density (Figure 2.3). Since neither the density (p=0.51) nor average fluorescence intensity (p=0.061) of puncta was altered in *snpn-1* mutants compared to the wild type, we concluded that the observed locomotory and electrophysiological defects of these mutants were not due to altered synaptic number (Figure 2.3B,C). Similarly, *snt-1* mutants showed normal synaptic density (p = 0.57) and puncta intensity (p = 0.22) (Figure 2.3B,C).

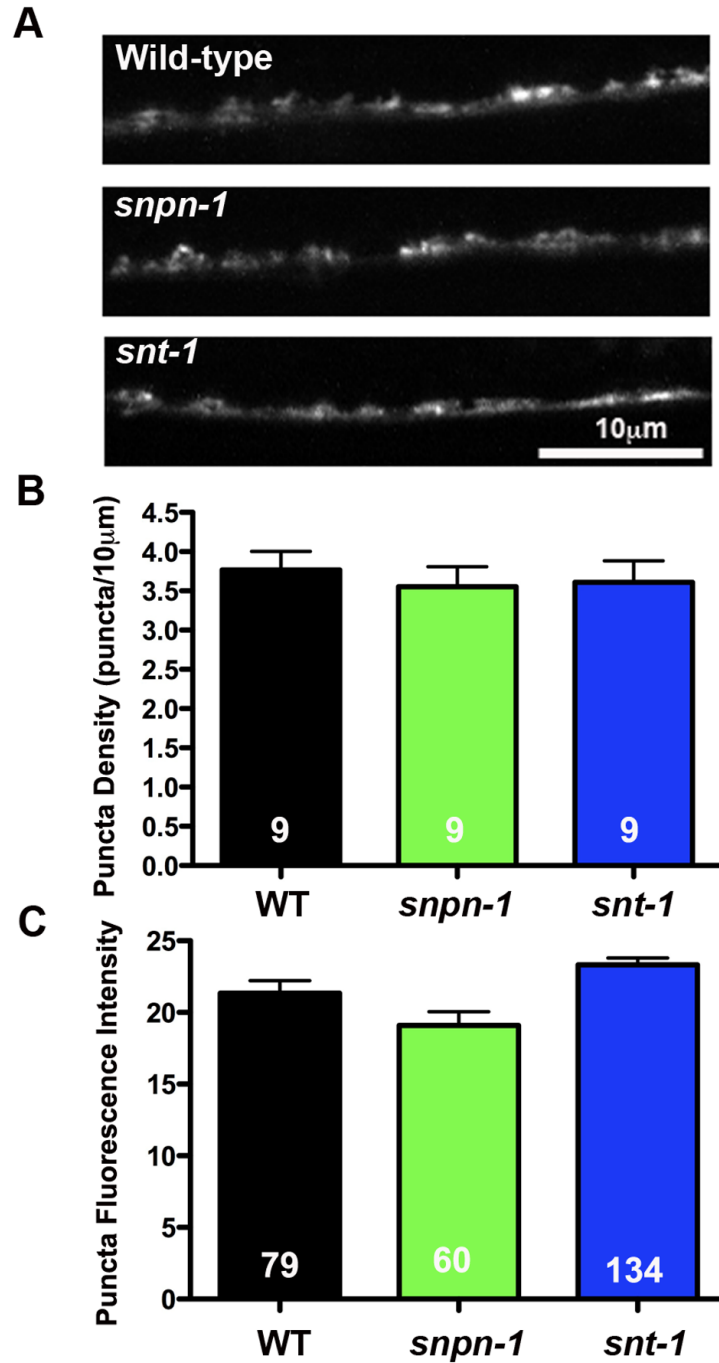


Figure 2.3. *snpn-1* and *snt-1* mutants have normal synaptic density. (A) Representative confocal images of dorsal cord synapses labeled with the GFP tagged synaptic vesicle protein, Synaptobrevin (SNB-1::GFP). (B-C) Quantification of the mean \pm SEM puncta density and fluorescence show no significant differences between the *snpn-1* and *snt-1* mutants relative to wild-type. Data collected by Susan Klosterman and previously published in PloS One 2013:8(2).

SNPN-1 functions in synaptic vesicle docking

To determine which step of the vesicle cycle is impacted in *snpn-1* mutants and the degree of functional overlap between SNPN-1 and SNT-1, *snpn-1*, *snt-1* and *snt-1;snpn-1* double mutants were prepared for EM analysis using HPF and freeze substitution. 40nm serial sections were collected anterior to the vulva to obtain NMJ micrographs from the same region where electrophysiological recordings were made (Figure 2.4A). Morphometric analysis of NMJ profiles containing a visible presynaptic density was then performed. The total number of synaptic vesicles per NMJ profile was normal in *snpn-1* mutants compared to wild-type ($p = 0.28$), whereas the vesicle density of *snt-1* mutants was significantly reduced ($p < 0.0001$), a phenotype previously been linked to an endocytic defect attributed to the loss of SNT-1 (Figure 2.4B) (Jorgensen et al., 1995). The presence of large irregular cisternae in *snt-1* mutants provided another indication of abnormal endocytosis ($p < 0.0001$) (Figure 2.4A,C). On contrast, the lack of cisternae ($p = 0.77$ relative to wild-type) and normal vesicle density of *snpn-1* mutants indicates that SNPN-1 does not play a direct role in vesicle recycling or impact the function of SNT-1 in this process. Consistent with these conclusions *snt-1;snpn-1* double mutants had similar vesicle numbers and cisternae to the *snt-1* single mutant (Figure 2.4C).

Although synaptic vesicle density was normal in *snpn-1* mutants, the number of vesicles morphologically docked on the plasma membrane was significantly reduced ($p = 0.0005$) (Figure 2.4D). Although *snt-1* mutants also showed a reduction in the absolute number of docked vesicles ($p < 0.0001$) (Figure 2.4D), in this case, the docking defect appeared to be a consequence of reduced vesicle density, since the fraction of

docked vesicles plotted as a function of total vesicles per profile was not significantly reduced in *snt-1* mutants when compared to wild-type ($p = 0.17$) (Figure 2.4E). The fact that the 50% reduction in absolute docked vesicles in *snt-1* mutants produced a more pronounced reduction in EJC charge integral (75%) suggests that SNT-1 has additional roles beyond endocytosis, such as its well-documented role as a calcium sensor for vesicle fusion. In contrast to *snt-1*, the vesicle-docking defect of *snpn-1* mutants was not due to reduced vesicle density ($p = 0.0016$ for the fraction of docked vesicles relative to wild-type) and therefore implicates SNPN-1 in vesicle docking. The additivity of absolute docking defects observed in the *snt-1;snpn-1* double mutants compared to *snt-1* alone ($p < 0.0001$ relative to *snpn-1* and $p = 0.0001$ relative to *snt-1*) further suggests that the SNPN-1 docking function is independent of SNT-1 (Figure 2.4D).

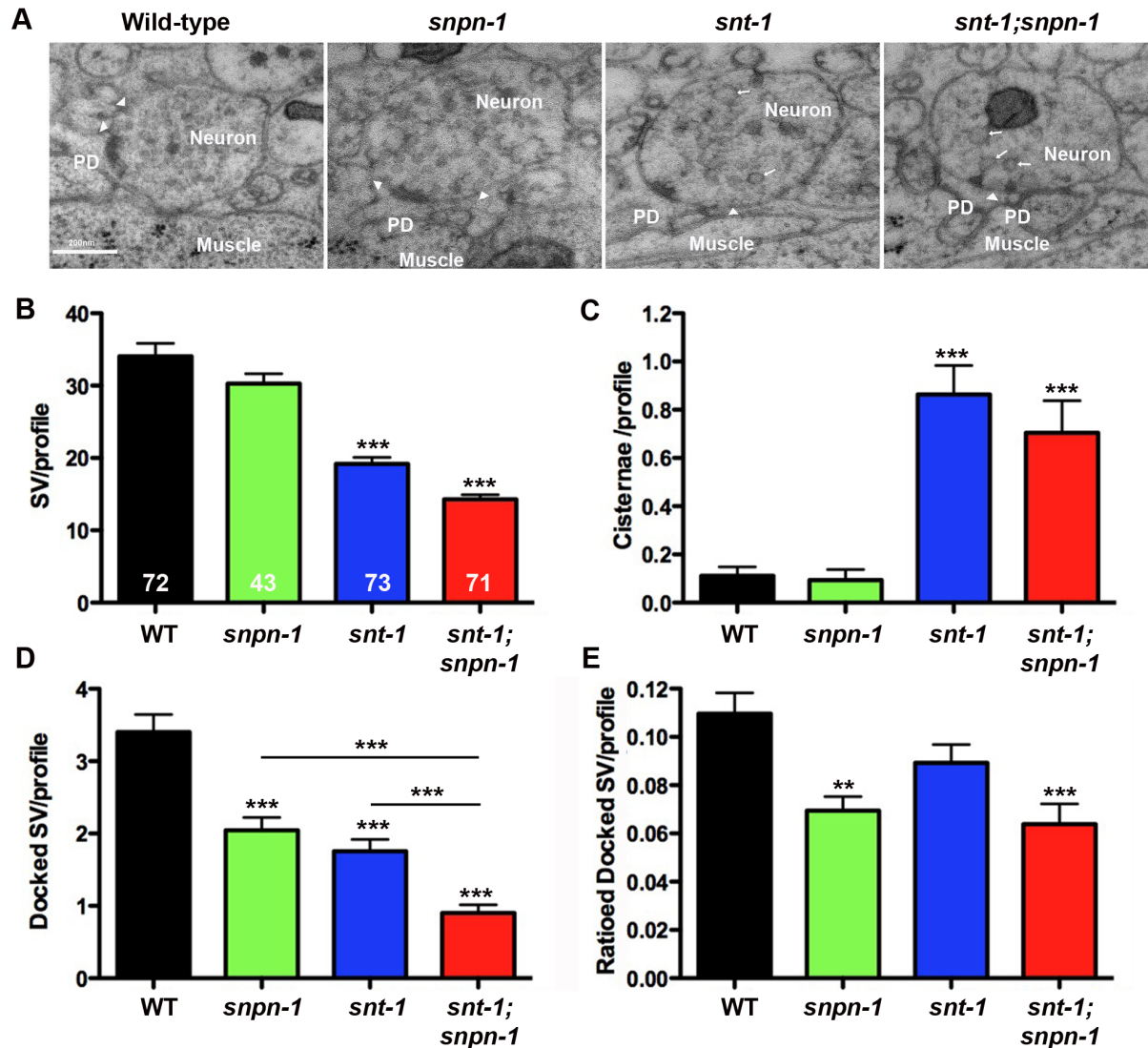


Figure 2.4. The additive ultrastructural phenotypes of *snpn-1* and *snt-1* mutants suggest independent roles in the vesicle cycle. (A) Representative micrographs of NMJs from 40nm sections prepared by HPF/FS. Labels show the neuronal presynaptic density (PD), docked synaptic vesicles are indicated with an arrowhead and an arrow indicates cisternae. Graphed data show the mean \pm SEM value for the absolute number of synaptic vesicles per synaptic profile is reduced in *snt-1* but not *snpn-1* mutants (B) and that both *snt-1* single and *snt-1;snpn-1* double mutants exhibit increased numbers of cisternae, but not *snpn-1* mutants (C). Both *snt-1* mutant phenotypes shown in B and C are indicative of an endocytic defect. The number of SVs docked at the plasma membrane show reductions in both *snpn-1* and *snt-1* mutants which are additive in the *snt-1;snpn-1* double (D). However, when the docking defect is plotted as a ratio of SV number in each profile, the docking defect only persists in the presence of the *snpn-1* mutant (E). Scale bar 200 nm. This data was previously published in PLoS One 2013:8(2).

There is an apparent disparity between the additive docking defect in the *snt-1;snpn-1* double mutant relative to the *snt-1* mutant alone ($p = 0.0001$) (Figure 2.4D), and the lack of additivity of the EJC deficit in the double mutant when compared to the *snt-1* single mutant (EJC amplitude $p = 1.0$, charge integral $p = 0.55$) (Figure 2.2G,H). To address this issue, the distribution of docked vesicles relative to the presynaptic density (Figure 2.5A), which is the presumptive Ca^{2+} entry and release site of the NMJ, was examined in the *snpn-1* and *snt-1* single and double mutants. This analysis showed that the number of docked vesicles near the presynaptic density was reduced to similar levels in *snt-1* and *snt-1;snpn-1* double mutants (Figure 2.5C,D), both being more severe than *snpn-1* alone (Figure 2.5B). Thus, the similar extent of the electrophysiological deficits observed in *snt-1* single and *snt-1;snpn-1* double mutants may reflect the similar degree to which releasable docked vesicles near the presynaptic density are reduced.

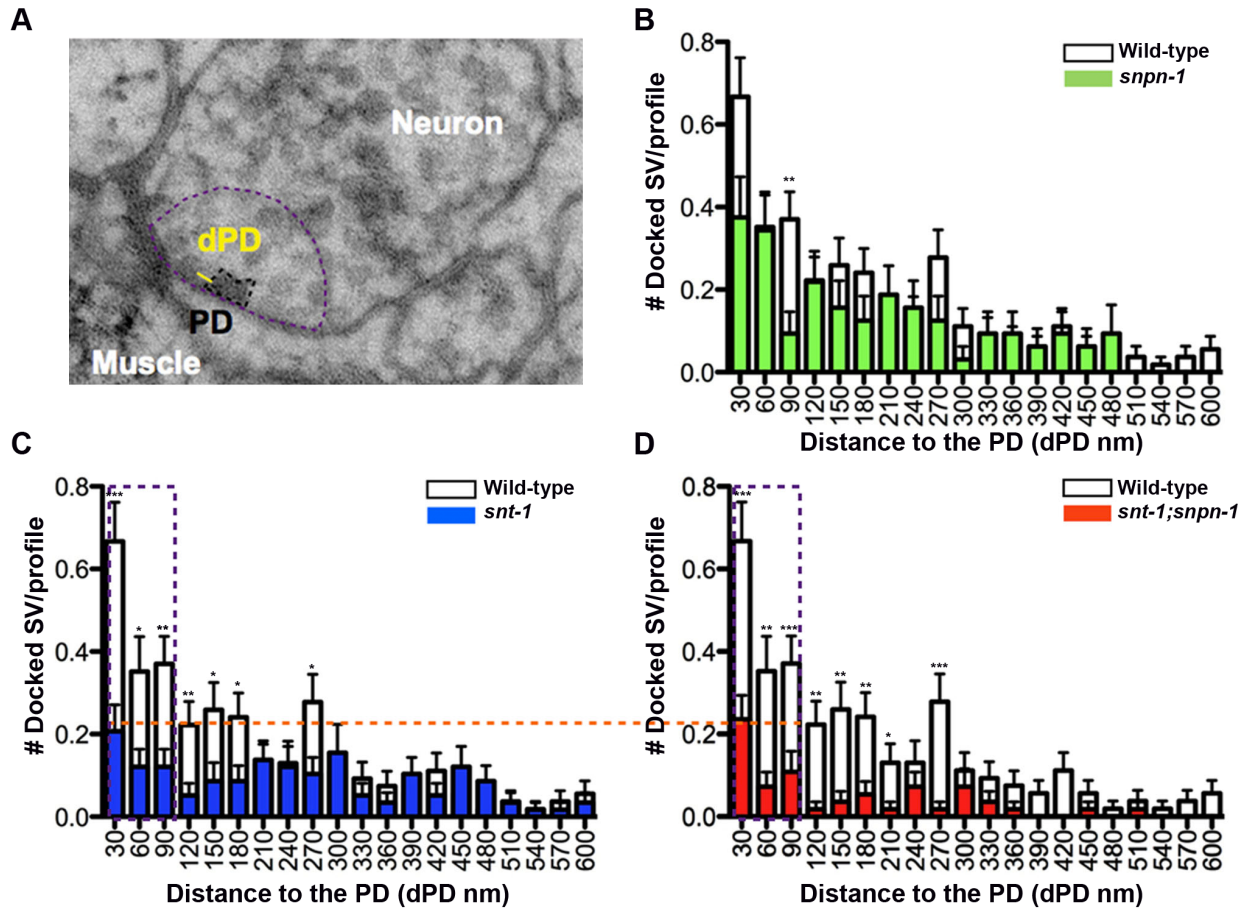


Figure 2.5. PD proximal docked vesicle numbers in *snt-1* and *snt-1;snpn-1* mutants correlate with their release defects. (A) The distance from a docked synaptic vesicle membrane to the closest PD referred to as dPD is used to plot the distribution of docked vesicles relative to the PD, in graphs (B-D). The vesicle docking defect (highlighted by the horizontal dashed line) within 90 nm of the PD (shown as a vertical rectangular box in graphs C and D) is similar in *snt-1* (C) and *snt-1;snpn-1* double mutants (D). All statistically significant values for dPD plotted as mean and SEM for mutants when compared to the wild type are shown. This data was previously published in PLoS One 2013:8(2).

2.5 Discussion

Ultrastructural and electrophysiological analyses of *snpn-1* mutant NMJs demonstrate a role for Snapin in synaptic vesicle docking and exocytosis. Specifically, *snpn-1* mutants exhibit fewer docked vesicles and a concomitant reduction in evoked release, evident in low calcium recording conditions. A similar vesicle docking defect is reported for cultured cortical neurons from mouse Snapin mutants at the EM level, however this defect is accompanied by a corresponding reduction in total vesicle density, which is not seen in *C. elegans snpn-1* mutant synapses (Pan et al., 2009). Thus, in mouse Snapin mutants the ratio of docked vesicles is not impacted, suggesting that docking in mouse Snapin mutants is likely to be a secondary consequence of vesicle depletion rather than a primary docking defect.

Under the HPF fixation conditions used here to analyze *C. elegans* NMJs, morphological vesicle docking has been shown in recent studies to require both the priming factor UNC-13(Munc13) and the plasma membrane SNARE, UNC-64(Syntaxin), which establish morphological docking as a correlate of vesicle priming (Gracheva et al., 2007; Hammarlund et al., 2007; Weimer et al., 2006). Although it should be noted that there is a small residual docked vesicle pool near the presynaptic density that are unprimed in these mutants, that require interactions between vesicle-associated Rab-3(RAB-3) with integral components of the presynaptic density, Rim(UNC-10) and Liprin(SYD-2). This appears to be a tethering step that precedes and promotes vesicle priming at release sites (Gracheva et al., 2007; Gracheva et al., 2008; Stigloher et al., 2011). This hypothesis is supported by observations that vertebrate Rab-3 and Rim interact with Munc13 in a trimeric complex (Dulubova et al., 2005), thus

these two processes (Rab-3/Rim dependent tethering and UNC-13/SNARE-dependent priming) are thought to act in concert to maintain a superprimed vesicle pool close to the presynaptic density at which voltage gated Ca^{2+} channels are enriched. The existence of a Rab3-dependent superprimed vesicle pool was first established in mouse hippocampal neurons from Rab3 quadruple knockouts (Schluter et al., 2006). These mutants have an exocytic defect that is due to loss of a subpopulation of vesicles with higher release probabilities, possibly due to proximity to Ca^{2+} entry points. Consistent with this model, *C. elegans rab-3*, *unc-10(Rim)* and *syd-2(Liprin)* mutants all exhibit more profound evoked release defects under low Ca^{2+} recording conditions which correspond with fewer proximally docked vesicles (Gracheva et al., 2008; Stigloher et al., 2011). The observation that SNPN-1 also promotes vesicle docking near presynaptic densities may explain the fact that the release deficit observed in *C. elegans snpn-1* mutants is only seen under low Ca^{2+} conditions, which should favor fusion of proximal, superprimed vesicles. Given that Snapin is an established SNAP-25 binding partner, the docking defect that we observe is most consistent with evidence implicating the Snapin/SNAP-25 interaction in the stabilization of assembled SNARE complexes, promoting priming (Ilardi et al., 1999; Pan et al., 2009).

The extent to which Snapin regulates synapses appears to be species specific. In both *C. elegans snpn-1* mutants and *Drosophila* Snapin knock-down by RNAi (Dickman et al., 2012) evoked release defects are mild. In contrast, cortical neurons from Snapin knockout mice exhibit severe evoked release defects, still evident at synapses from heterozygotes (Pan et al., 2009). Similarly, there are no Snapin-dependent defects in synaptic development or density in either *C. elegans* or

Drosophila, whereas Snapin-null mutants exhibit reduced brain cell density, and reduced cell viability and synaptic density in cultured cortical neurons (Pan et al., 2009; Zhou et al., 2012). These mammalian neuronal growth and survival defects appear to be associated with loss of BDNF/TrkB retrograde signaling that leads to the disruption of a Snapin/dynein interaction (Zhou et al., 2012). This growth factor pathway may be responsible for exacerbating the synaptic function defects in mouse Snapin mutant synapses to a greater extent than that observed *in situ* at fly and worm NMJs.

Biochemical evidence demonstrates that dimerized vertebrate Snapin can interact simultaneously with SNAP-25 and Synaptotagmin (Pan et al., 2009), which could promote the interaction between the calcium sensor and the SNARE complex, improving the efficacy of primed vesicle release. Consistent with this model, cultured neurons from Snapin mutant mice have severe defects in the frequency of endogenous release and evoked release amplitude attributable to a reduced primed vesicle pool based on sucrose responses (Pan et al., 2009). A similar reduction in the readily releasable vesicle pool has been recorded in chromaffin cells from Snapin knockout mice, suggesting Snapin may also promote dense core vesicle priming (Tian et al., 2005). Furthermore, a single amino acid substitution in vertebrate Snapin that reduces Snapin dimerization, weakens binding to both SNAP-25 and Synaptotagmin and fails to restore the vesicle priming defect of neurons from Snapin null mutants (Pan et al., 2009). However, this latter result does not establish whether it is the reduction in SNAP-25 binding, Synaptotagmin binding or both which fail to rescue Snapin function. While our results are consistent with a priming function for Snapin in *C. elegans*, our data do not support a requirement for the simultaneous binding of Snapin to SNAP-25

and Synaptotagmin. Specifically, our analyses of *snt-1* and *snt-1;snpn-1* double mutants suggest that in *C. elegans* Snapin mutants the docking defect persists in the absence of Synaptotagmin. Thus in *C. elegans*, Snapin's role in synaptic vesicle docking/priming appears to be Synaptotagmin-independent and therefore likely reflects the specific disruption of Snapin interaction with SNAP-25, resulting in the destabilization of SNARE complexes. A similar conclusion was reached for the role of *Drosophila* Snapin in synaptic homeostasis, a process that requires genetic interactions between Snapin and SNAP-25, but is Synaptotagmin independent (Dickman et al., 2012).

Here we showed that *C. elegans snt-1* mutants exhibit an endocytic defect, consistent with a previously established interaction of Synaptotagmin-1 with the AP-2 complex, required for clathrin-mediated endocytosis (Jorgensen et al., 1995; Poskanzer et al., 2003; Yao et al., 2012; Zhang et al., 1994). Specifically, we showed that *snt-1* mutants accumulate abnormal levels of cisternae and exhibit synaptic vesicle depletion (Jorgensen et al., 1995). This reduction in vesicle recycling correlates with a pronounced reduction in endogenous mini frequency in *C. elegans snt-1* mutants, suggesting that vesicle depletion compromises endogenous release as well as evoked release. This observation contrasts with increases in mini frequency observed in Synaptotagmin mutant *Drosophila* larvae and in most mouse cultures, changes attributed to loss of a fusion clamp normally provided by Synaptotagmin (Broadie et al., 1994; Littleton et al., 1994; Pang et al., 2006). Possibly, this fusion clamp effect is masked in adult *C. elegans* as a result of a lifetime of vesicle depletion coupled with the worm's extremely high endogenous release rate at NMJs, that may emphasize the

endocytosis defect rather than loss of a fusion clamp. In contrast to *snt-1* mutants, *C. elegans snpn-1* mutants show no evidence of a vesicle replenishment defect, based on similar vesicle density and number of cisternae compared to wild-type. This observation again supports the main conclusion of this study that the impact of Snapin on synaptic transmission in *C. elegans* appears to be independent of Synaptotagmin function.

2.6 Acknowledgements

Anna Burdina and Hetal Patel for development of reagents. Mei Zhen and Taizo Kawana for in house Matlab software (Punctaanalyzer). Greg Herman and Daniel Saxton for *snpn-1* primer design and Marc Hammarlund for plasmids. . Some strains were provided by the CGC, which is funded by NIH Office of Research Infrastructure Programs (P40 OD010440).

III. VPS-39 promotes fusion competent vesicles in *C. elegans*

Susan M. Klosterman, Szi-Chieh Yu, Anna O Burdina, and Janet Richmond

3.1 Introduction

Effective neuronal communication requires the exquisite control of neurotransmitter release at presynaptic terminals, which ultimately governs the cognitive and behavioral output of the nervous system. This process is critically dependent on the SNARE fusion machinery, a trimeric complex comprised of the highly conserved SNARE proteins Synaptobrevin, Syntaxin, and SNAP-25. Multiple studies have demonstrated that SNARE complex assembly is required during the priming process to render synaptic vesicles docked on the plasma membrane in a fusion competent state. In addition, several SNARE interacting proteins including: (Munc13)UNC-13, (Munc18)UNC-18, Complexin, Tomosyn and Synaptotagmin are known to play important regulatory roles prior to membrane fusion. Of these, the Syntaxin binding protein (Munc18)UNC-18 has been implicated in one of the earliest events in the synaptic vesicle cycle, forming heterodimers that are thought to protect Syntaxin during axonal transport to the synapse by maintaining Syntaxin in a folded closed conformation. Precisely, how Syntaxin then transitions to an open configuration, to reveal the H3 alpha helical domain that is subsequently incorporated into the core SNARE complex remains unknown. Recent biochemical evidence suggests that members of the homotypic fusion and vacuole protein sorting (HOPS) complex could serve such a function (Kim et al., 2006).

The HOPS complex is composed of six functionally conserved proteins (Vps18, 11, 16, 33, 39 and 41) belonging to the vacuolar protein sorting (Vps) family (Wurmser

et al., 2000), first identified in screens for yeast mutants exhibiting defective vacuolar morphologies (Raymond et al., 1992). Members of the yeast HOPS complex are known to interact with the yeast Syntaxin homolog (Vam3p) (Sato et al., 2000) implicating the complex in both yeast vacuole docking and SNARE-mediated vacuole fusion (Eitzen et al., 2000; Price et al., 2000; Sato et al., 2000; Wurmser et al., 2000). Similarly, over-expression of the human HOPS complex Vps39 homolog (hVam6) results in extensive clustering and fusion of lysosomes and late endosomes in HeLa cells (Caplan et al., 2001). The mammalian HOPS complex is expressed throughout the nervous system, and colocalizes with the synaptically enriched vesicle-associated protein Synapsin (Kim et al., 2006). Furthermore components of the mammalian HOPS complex (hVps-11, 16 and 18) can co-immunoprecipitate Syntaxin1A and Munc18 from rat brain homogenate, while leaving the other SNAREs, SNAP-25 and Synaptobrevin behind. The incorporation of Munc18 and Syntaxin into large heterooligomeric complexes with the HOPS complex occurs at the expense of Munc18/Syntaxin dimers (Kim et al., 2006). These large complexes were found in synaptosomal fractions enriched for the synaptic vesicle protein Synaptophysin, but excluded from fractions enriched for the postsynaptic protein PSD-95. Together these data suggest the HOPS complex may have a synaptic role through Munc18/Syntaxin interactions. The potentiation of Ca^{2+} -dependent hormone release from PC12 cells by overexpression of hVps 11, 16 and 18 supports this concept. While the precise role of the HOPS complex in neurons remains to be determined, the fact that this complex binds to Syntaxin and Munc18 and promotes release has given rise to the hypothesis that it may regulate vesicle fusion (Kim et al., 2006). To address this question *in vivo*

we obtained a putative null mutant of the *C. elegans* HOPS complex gene *vps-39*, and performed a detailed characterization.

3.2 Materials and Methods

Genetics

All strains were maintained at 20 °C on agar plates seeded with OP50 bacteria using standard methods (Brenner, 1974). The following genotypes were used: the wild-type reference strain Bristol N2, the *vps-39* (*tm2253*) loss of function allele out-crossed and balanced with pF25B3.3::GFP due to maternal-effect sterility (SY1245) and the VPS-39 over-expression lines: *Pvps-39::vps-39::mCherry::unc-54* 3'UTR, *vps-39* (*tm2253*) (*jaEx1056*, SY1455), *Prab-3::vps-39::mCherry::unc-54* 3'UTR, *vps-39* (*tm2253*), *str-1::GFP* (*jals1096*, SY1517) and *Prab-3::vps-39::unc-54* 3'UTR, *vps-39* (*tm2253*), *str-1::GFP* (*jals1099*, SY1540). The reference strain used for coelomocyte GFP uptake analysis was KG1640 (*unc-129::CTNS-1a-RFP*, *unc-129::nlp-21-Venus*, *ttx-3::RFP*). This strain was crossed into the balanced *vps-39* loss-of-function strain (SY1245) and the VPS-39::mCherry over-expression line (SY1517) to generate SY1409 and SY1524, respectively. EG1985 *oxIs34[openSYX, Pmyo-2:GFP];unc-64(js115)* was used and then crossed into a balanced *vps-39* mutant(SY1245) and the VPS-39::mCherry over-expression line (SY1517) to generate SY1549 and SY1550 respectively. SY1540 was also crossed into *unc-13* (e51) to generate SY1557.

Molecular Biology

VPS-39 expression constructs were generated using the MultiSite Gateway Three-Fragment Vector Construction Kit (Invitrogen) using High Fidelity Phusion

Polymerase (Finnzymes) for amplification. 1.6kb upstream of VPS-39 was amplified and cloned into pDONR P4-P1R (Invitrogen) using the following primers (grey base pairs indicate the homologous recombination sites compatible with the gateway vector): GGGGACAACCTTTGTATAGAAAAGTTGCGCTTTCTTCAGCACAGGGTTCTTC and GG GACTGCTTTTTTTGTACAAACTTGCCATTTTGCTTTGGTGGGTCGAAG. Genomic *vps-39* was amplified without its stop codon and cloned into pDONR 221 using: GGGGACAAGTTTGTACAAAAAAGCAGGCTCGATGTACGATGCATACACGCCTTGC and GGGGACCACTTTGTACAAGAAAGCTGGGTCATTTCTGTTTCCTCCTTGAGA ATC. After final recombination into pDEST R4-R3 Vector II, constructs were injected at 10ng/ml using STR-1::GFP as the co-injection marker. Stable extra-chromosomal transgenic lines were integrated using 4,5',8-trimethylpsoralen (TMP) mutagenesis and then out-crossed a minimum of 4x.

Confocal Microscopy

All fluorescently labeled strains were mounted on 2% agarose pads with 10% sodium azide, and imaged using an Olympus Fluoview laser-scanning confocal system (40x or 60x objective-oil immersion). For immunohistochemistry, worms were dissected along their longitudinal axis to expose the nerve cord as previously described (Richmond et al., 1999) and fixed with 4% paraformaldehyde in PBS for 30 minutes. Preparations were then washed 3x with TBS-Tween(TBST) for 10 minutes before blocking with 5% BSA for 1 hour. Primary antibody incubation was performed overnight at a 1:100 dilution, and secondary antibody incubation was done at a 1:500 dilution for 1 hour the next day. Images were obtained with the same system described above but using the 60x water objective. ImageJ was used to generate z

projections, which were analyzed using ImageJ by measuring the fluorescence intensity for regions of interest spanning 10 μm long sections of the nerve cord anterior to the vulva, or within the circumference of coelomocytes, following background subtraction. The numbers of discernable puncta per coelomocyte and axon commissures were counted manually.

Pharmacology

Acute sensitivity to the acetylcholine esterase trichlorfon/dylox (Chem Services) was tested by time-dependent paralysis. Worms were placed on dylox treated plates and examined every ten minutes for 130 mins. Dylox was used at a final concentration of 5mM on standard NGM plates seeded with OP50. For each strain, 10 young adults were used per test, and tests were replicated a minimum of three times. Animals were considered paralyzed if they failed to respond to touch with a platinum wire. All pharmacological assays were performed blind.

Electrophysiology

Electrophysiological methods were as previously described (Richmond, 2009). In short, animals were immobilized with Histoacryl Blue glue, and incisions were made anterior to the vulva using a glass needle to expose NMJs. Recordings were made in the whole-cell voltage-clamp mode at a holding potential of -60mV using an EPC-10 HEKA amplifier, digitized at 1 kHz. The 5 mM Ca^{2+} extracellular solution contained; 150 mM NaCl, 5 mM KCl, 5 mM CaCl_2 , 4 mM MgCl_2 , 10 mM glucose, 5 mM sucrose, and 15 mM HEPES (pH 7.3, ~340 mOsm), Ca^{2+} was replaced with NaCl in the 0.5 mM Ca^{2+} extracellular solution. The patch pipette contained; 120 mM KCl, 20 mM KOH, 4 mM MgCl_2 , 5 mM (N-tris[Hydroxymethyl] methyl-2-aminoethane-sulfonic acid), 0.25 mM

CaCl₂, 4 mM Na²ATP, 36 mM sucrose, and 5 mM EGTA (pH 7.4, ~315 mOsm). Data were acquired using Pulse software (HEKA, Southboro, Massachusetts, United States) on a Dell computer. Subsequent analysis and graphing was performed with Pulsefit (HEKA), Mini analysis (Synaptosoft Inc., Decatur, Georgia, United States) and Igor Pro (Wavemetrics, Lake Oswego, Oregon, United States).

Electron Microscopy

Young-adult hermaphrodites were fixed by high-pressure freeze (HPF) fixation as previously described (Weimer et al., 2006). Briefly, ~20 animals were loaded into specimen chambers filled with *Escherichia coli* and immobilized by high-pressure freezing to -180°C in a Bal-Tec HPM010 and stored in liquid nitrogen until freeze substituted.

Freeze substitution was performed in a Reichert AFS (Leica, Oberkochen, Germany) as described previously, using tannic acid (0.1%) fixative introduced over 24 hours, followed by 2% osmium oxide (OsO₄). Fixed specimens were embedded in Araldite 502 over 48 h period at 65°C. 40 nm thick serial sections were collected on formvar-covered carbon coated copper grids (EMS, FCF2010-Cu), and counterstained with 2.5% aqueous uranyl acetate for 4 min, followed by Reynolds lead citrate for 2 min. Images were obtained on a Jeol JEM-1220 (Tokyo, Japan) transmission electron microscope operating at 80 kV. Micrographs were imaged using a Gatan digital camera (Pleasanton, CA).

Unbiased morphometric analysis of ventral nerve cord serial sections was achieved by blinding strain identities until analysis was complete. Images were quantified using NIH ImageJ software. A synapse was defined as a set of serial

sections containing a presynaptic specialization plus two flanking sections on either side without presynaptic specialization.

Statistical analysis

All data are expressed as mean \pm SEM. The Mann Whitney T-test was used to determine significance values. * indicates a p value from 0.01-0.05, **0.001-0.01, and ***<0.001.

3.3 Results

vps-39 encodes a component of the HOPS complex

In order to study the potential role of the HOPS complex in neuronal function, we obtained a *vps-39 (tm2253)* mutant from the CGC. VPS-39 is a highly conserved component of the HOPS complex and contains three known protein domains, a Rab binding domain (RBD), a clathrin heavy chain repeat (CHCR) and a membrane localization domain (MLD) (Figure 3.1A). *C. elegans* VPS-39 shares 30% identity and 50% homology with the human homolog, hVam6, mediating interactions between Rab7 and the SNARE complex (Figure 3.1B).

The *vps-39 (tm2253)* allele contains a 1045bp deletion and a 4bp insertion spanning exons 7-9 as indicated (Figure 3.1C). Although the number of eggs laid by this mutant was normal, they failed to hatch (Figure 3.2C). However, when balanced over a GFP marker, homozygous progeny survived to adulthood, demonstrating that this is a recessive mutation with maternal-effect embryonic lethality.

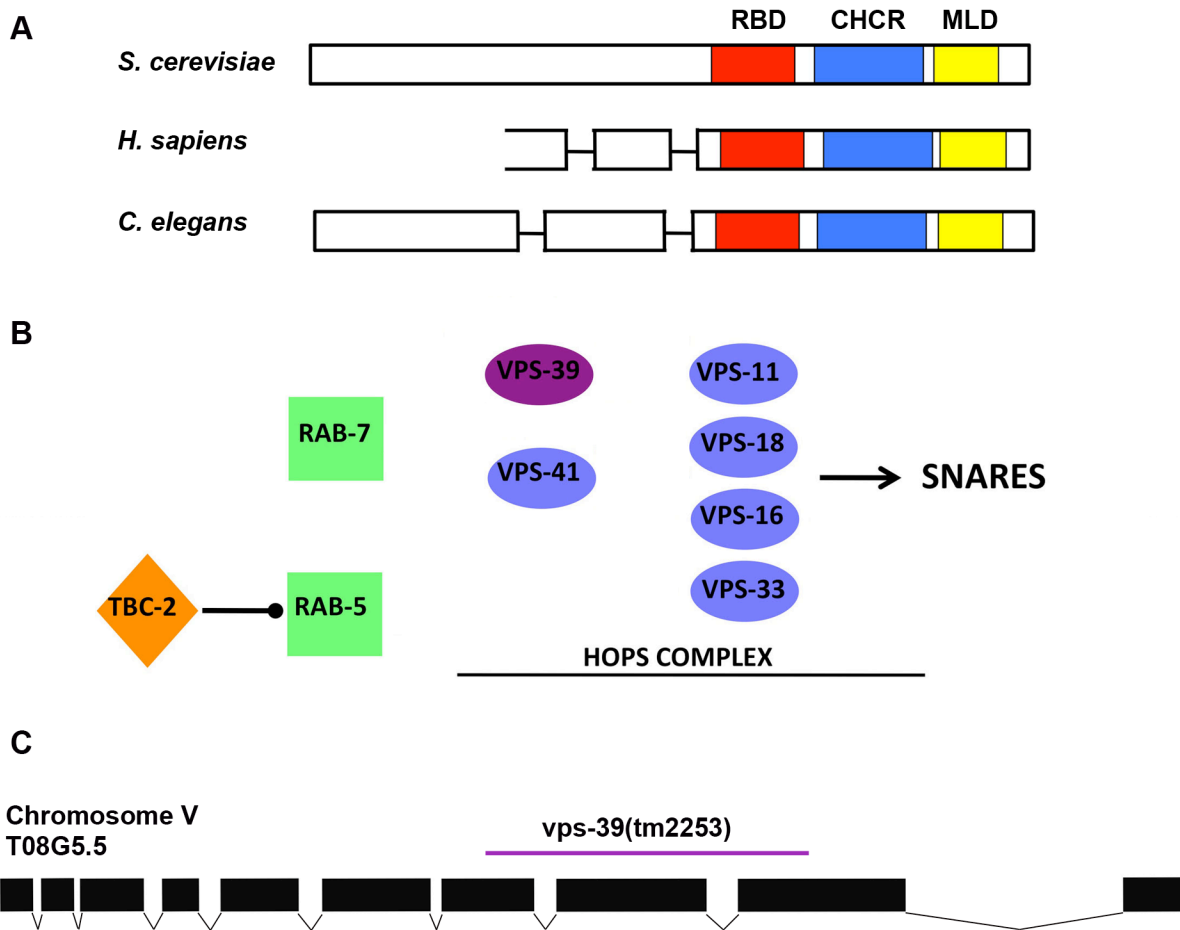


Figure 3.1. VPS-39 is a member of the HOPS complex. (A) VPS-39 is well conserved among species and contains three motifs: a Rab binding domain (RBD), a clathrin heavy chain repeat domain (CHCR), and a membrane localization domain (MLD). (B) VPS-39 is a conserved member of the HOPS complex that is regulated by a TBC-2, RAB-5, RAB-7 upstream signaling cascade, and in turn mediates interactions with SNARE proteins via the HOPS complex. (C) The *vps-39* gene structure consists of 10 exons. The *tm2253* allele impacts exons 7-9 and consists of a 1045bp deletion and a 4bp insertion. Data collected by Susan Klosterman.

Neuronal expression of VPS-39 is required for early development

To determine the expression pattern of VPS-39 a full-length transgene with a C-terminal mCherry tag driven by 1.6kb of upstream sequence was generated. A transgenic line expressing this construct revealed VPS-39 expression in many tissue types including neurons, muscles, and the six *C. elegans* scavenger cells, known as coelomocytes (Figure 3.2A). Expression of VPS-39 in neurons using the pan-neuronal *rab-3* promoter (*Prab-3*) (Figure 3.2B) partially rescued the embryonic lethality of *vps-39* (*tm2253*) (Figure 3.2C), indicating that neuronal VPS-39 plays an essential role during embryonic developmental.

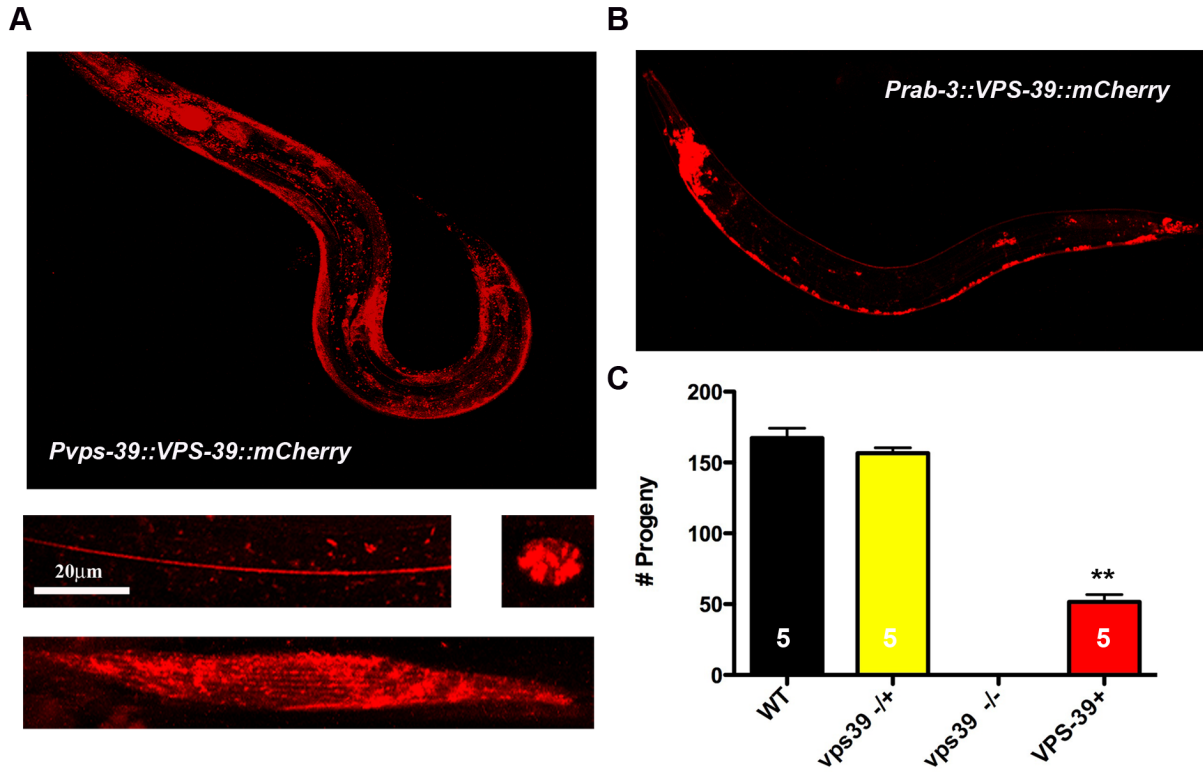


Figure 3.2. VPS-39 expression and rescue of *vps-39* mutant embryonic lethality. (A) An extrachromosomal *VPS-39::mCherry* construct driven by 1.6kb of upstream sequence shows expression in many tissues of an intact worm. Lower enlarged images show *VPS-39::mCherry* labeled neurons, a coelomocyte, and body wall muscle. (B) Expression of an integrated *pRab-3::VPS-39::mCherry* line which was used for all rescue experiments. (C) Quantification of progeny number, after 4 days plating of individual worms, sample size indicated in each bar. Panneuronal expression of *VPS-39* partially rescues the *vps-39* mutant phenotype. Data collected by Susan Klosterman.

VPS-39 is required for GFP processing in the coelomocytes

TBC-2, an upstream inhibitor of HOPS complex function (Figure 3.1B) has been reported to impact endosomal processing in *C. elegans* coelomocytes, resulting in the accumulation of abnormally large lysosomes, visualized through coelomocyte uptake of signal secreted GFP (Chotard et al., 2010). VPS-39 is also expressed in coelomocytes and would be predicted to display the opposite phenotype to *tbc-2* mutants. We therefore examined the coelomocyte expression of a neuronally secreted ectopic peptide, NLP-21::GFP as depicted in Figure 3.3A. In direct contrast to *tbc-2* mutants, coelomocytes in *vps-39* mutants exhibited a significant increase in the number of abnormally small GFP puncta when compared to wild type (Figure 3.3B,C). This phenotype was not rescued by expression of VPS-39 in neurons, consistent with a cell autonomous requirement for VPS-39 in coelomocyte GFP processing (Figure 3.3B,C).

The overall GFP fluorescence intensity per coelomocyte has also been used as an indirect assay of neuronal peptide release (Sieburth et al., 2007). As shown in Figure 3D, the average GFP fluorescence intensity in *vps-39* mutants was not significantly different from wild-type, suggesting that peptide release from neurons may be unaffected with the caveat that the *vps-39* mutant coelomocyte processing defects may affect GFP turnover and therefore GFP intensity.

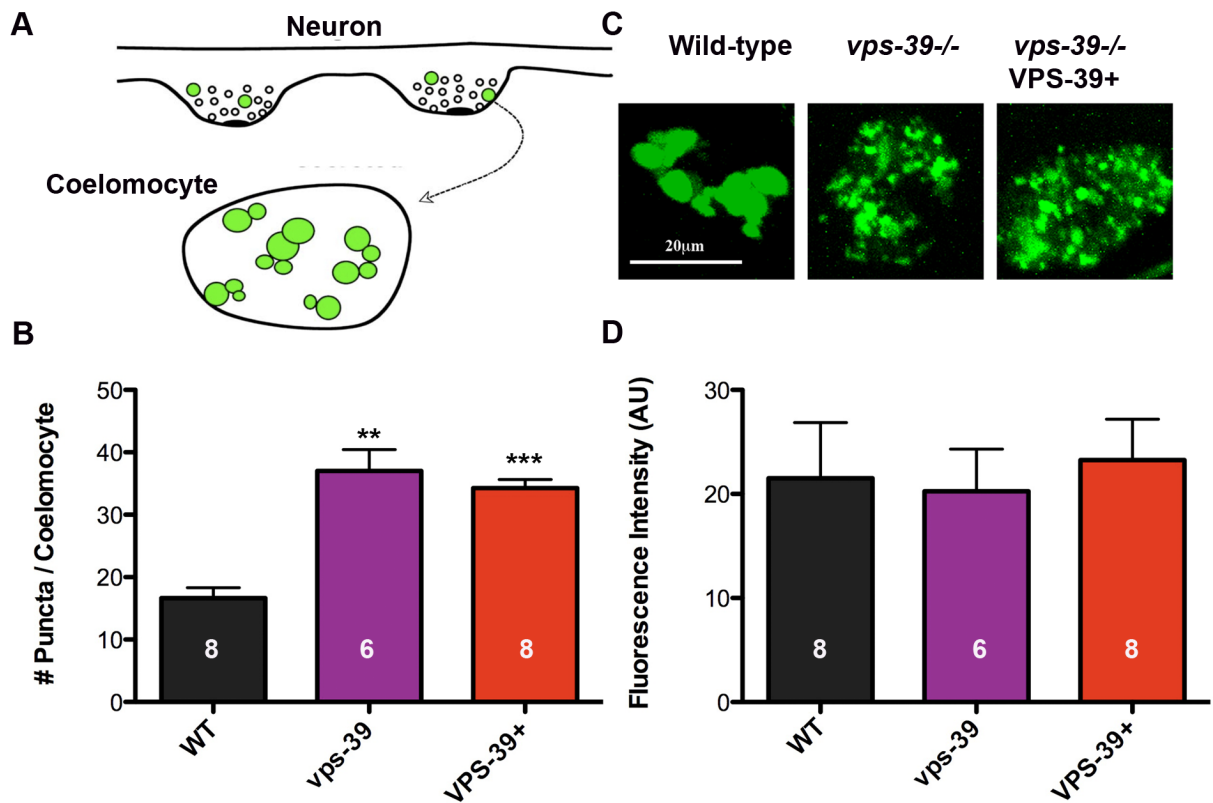


Figure 3.3. VPS-39 is required for coelomocyte processing. (A) Schematic of the assay in which GFP is secreted from neurons into the pseudocoelom prior to endocytosis by the coelomocytes, adapted from (Gracheva et al., 2007). (B) Loss of VPS-39 significantly increases the number of puncta/coelomocyte, which cannot be rescued by neuronal re-expression of VPS-39 in the *vps-39* mutant background. (C) Representative images of GFP expression in coelomocytes in *vps-39* mutants alone (*vps-39*^{-/-}) and with neuronal VPS-39 expression (VPS-39+), relative to wild-type. (D) There is no significant difference in total GFP fluorescence intensity among the three genotypes. Data collected by Susan Klosterman.

VPS-39 transport is kinesin-dependent

In mammalian cultures, HOPS complex components are found to colocalize with the synaptic vesicle marker Synapsin at presynaptic terminals (Kim et al., 2006). Synaptic vesicle transport to synapses in *C. elegans* requires the microtubule associated Kinesin motor (UNC-104). Therefore, to test whether the synaptic localization of *C. elegans* VPS-39 is dependent on vesicle transport for synaptic localization, we examined VPS-39::mCherry expression in an *unc-104* mutant background (Figure 3.4). This resulted in an accumulation of VPS-39 in the motor neuron cell bodies of *unc-104* mutants, and a corresponding decrease in labeling at distal synapses. These results are consistent with a physical interaction between VPS-39 and vesicles transported via microtubule transport, resulting in synaptic enrichment of this HOPS complex component.

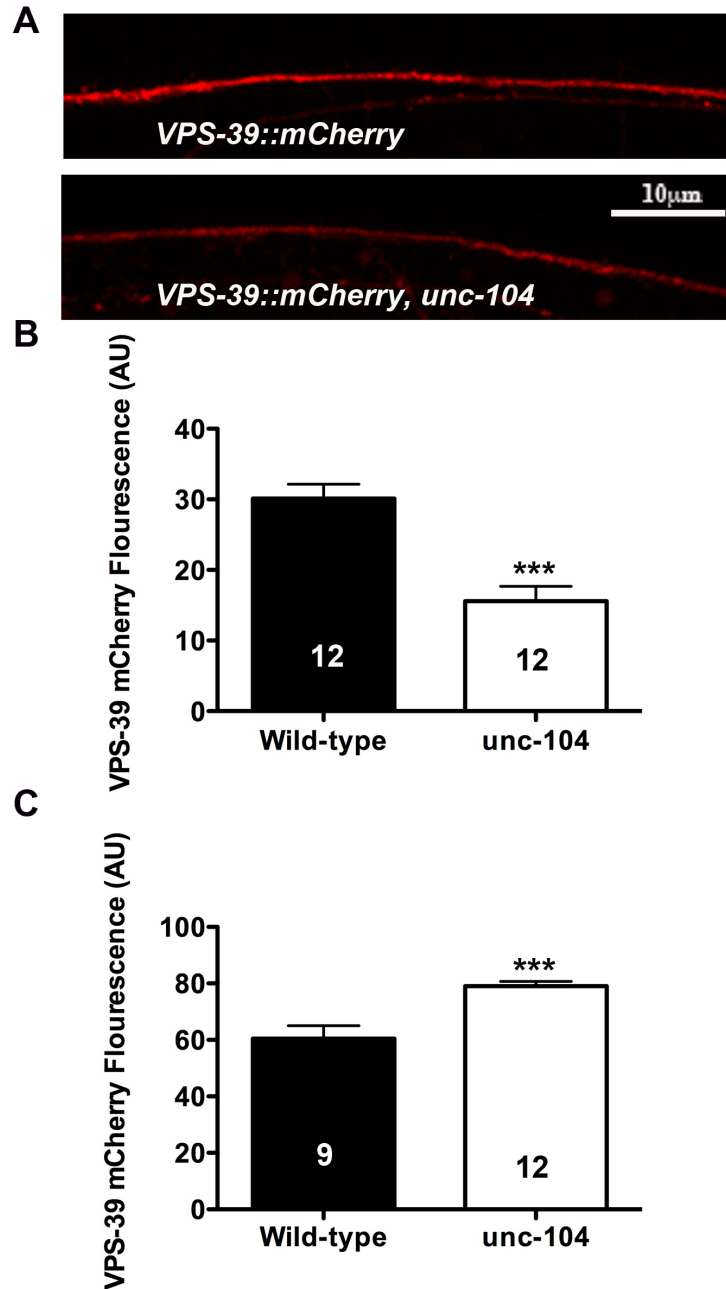


Figure 3.4. Axonal expression of *VPS-39::mCherry* is *UNC-104*/Kinesin-dependent. (A) Representative images from the dorsal nerve cord of *VPS-39::mCherry*, showing a reduction in an *unc-104* mutant when compared to the wild-type background. (B) Quantification of nerve cord *VPS-39::mCherry* fluorescence indicates a significant reduction in *VPS-39::mCherry* expression in the *unc-104* mutant and (C) a concomitant increase in cell soma expression. Data collected by Susan Klosterman.

VPS-39 functions in neurons to promote cholinergic synaptic transmission

Given that VPS-39 is expressed in neurons and has an essential role in early viability we next assayed synaptic function in intact *vps-39* mutant worms. Exposure to the acetylcholinesterase inhibitor, trichlorfon (dylox) can be used to indirectly measure acetylcholine release at the NMJ, as the resulting buildup of ACh in the synaptic cleft leads to hypercontracted body-wall muscles resulting in complete paralysis (Figure 3.5A,B). Mutants defective in ACh release take longer to paralyze in this assay. In *vps-39* mutants we observed a dylox-resistant phenotype that could be reversed by re-expressing VPS-39 specifically in neurons using two separately integrated transgenic lines, one containing an mCherry tag (Figure 3.5C,D). The use of two independent VPS-39 integrants indicates that the rescue of dylox sensitivity in *vps-39* mutants is not due to a positional effect of the VPS-39 insertion site and confirms the functionality of the VPS-39::mCherry construct used in subsequent experiments. The rescue of dylox resistance by reintroduction of VPS-39, indicates that this phenotype is due to disruption of the *vps-39* locus in *vps-39(tm2253)* mutant, rather than a background mutation.

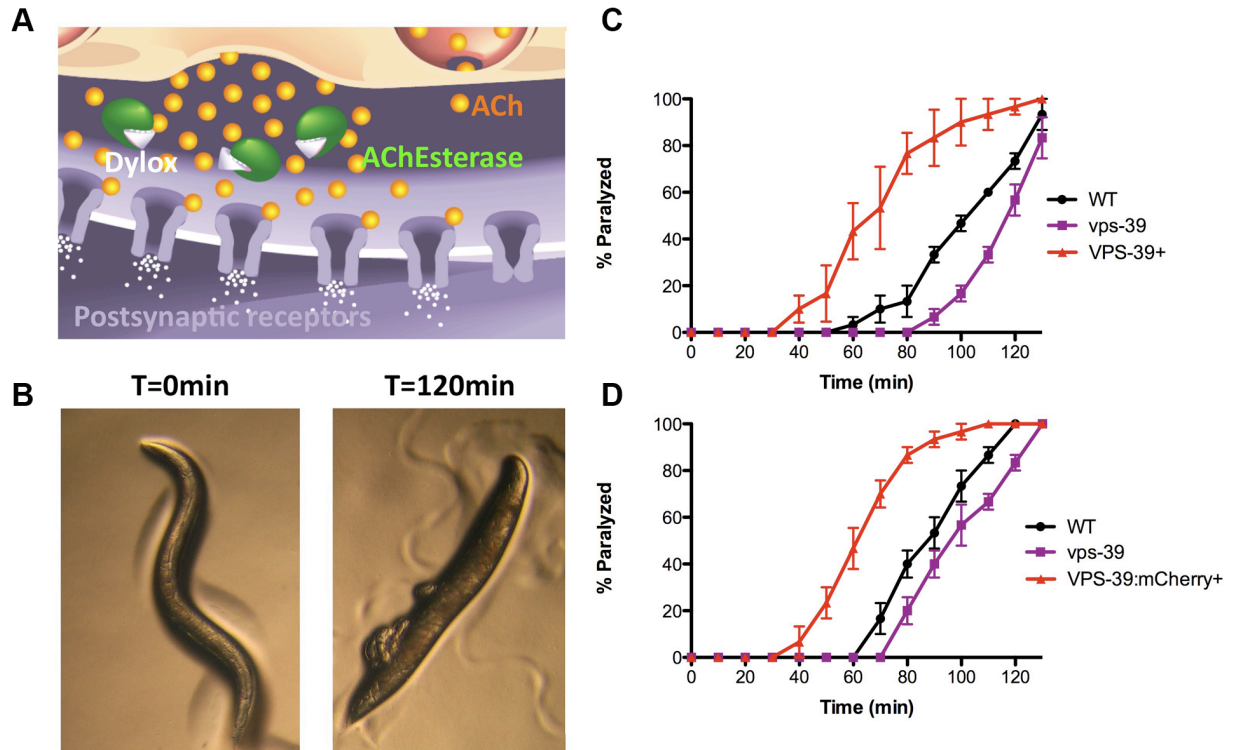


Figure 3.5. VPS-39 regulates ACh release in intact worms. (A) Schematic of the assay in which AChEsterase activity is blocked by dylox. This leads to an accumulation of ACh in the synaptic cleft resulting in the gradual onset of hypercontracted paralysis as exemplified in (B). A wild-type worm initially exposed to 5mM dylox (T=0min) exhibits locomotory activity and deep body bends, where as a worm after 120 minutes of dylox exposure is hypercontracted and paralyzed due to ACh buildup in the synaptic cleft. (C) The delayed time course of dylox-induced paralysis in *vps-39* mutants is reversed by re-expressing VPS-39 in neurons. (D) Same as (C) but an independent VPS-39 expressing line tagged with mCherry. Each experiment was repeated three times, each time using 10 worms per strain. Data collected by Susan Klosterman.

Neuronal cytoarchitecture is normal in vps-39 mutants

Dylox resistance in *vps-39* mutants could be due to defects in neurite outgrowth or synaptogenesis. To address these possibilities we first examined neuronal architecture using pACR-2::GFP, which labels cholinergic motor neurons in *vps-39* mutants. Both axon fasciculation and axon targeting were unaffected (Figure 3.6A-C). We next examined expression of the post-synaptic nicotinic receptor ACR-16::GFP as a proxy for cholinergic synaptic density. ACR-16 receptor fluorescence intensity was unaltered suggesting that synaptogenesis and receptor localization were normal in *vps-39* mutants (Figure 3.6D, E). These results, in conjunction with neuronal rescue of the *vps-39* mutant dylox sensitivity suggest that VPS-39 functions presynaptically to regulate ACh release.

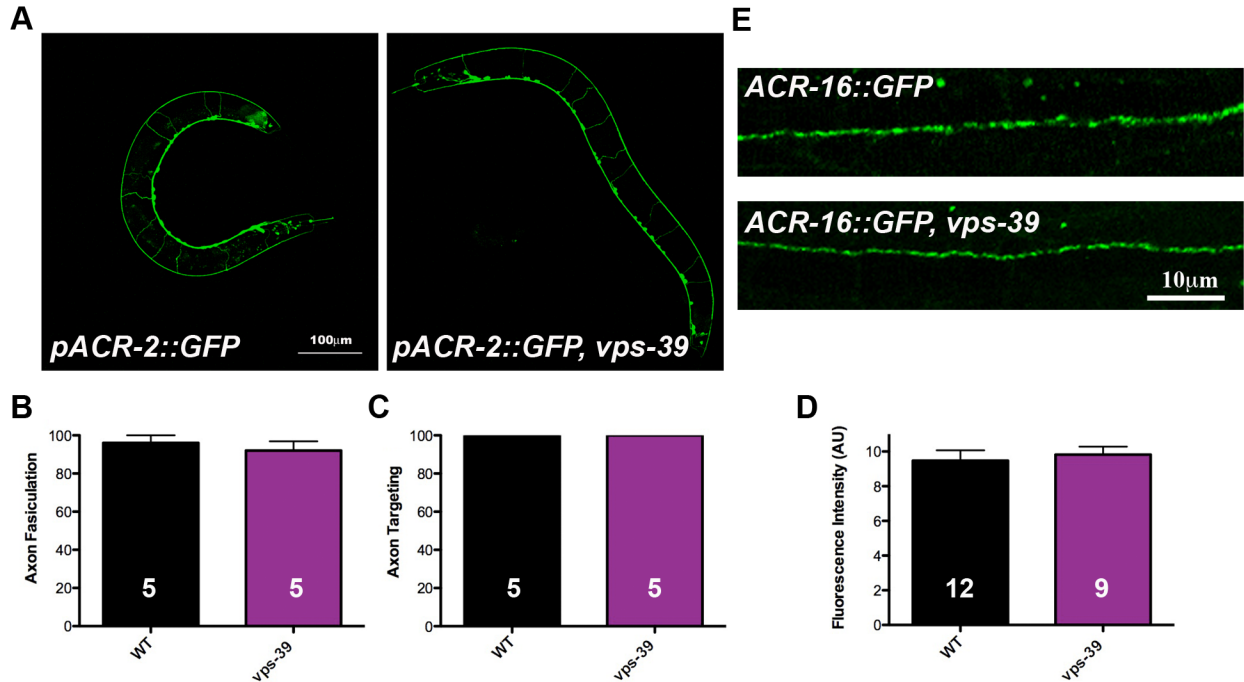


Figure 3.6. VPS-39 is not required for synaptic development. (A) Representative images of *pACR-2::GFP* in a wild type and *vps-39* mutant, show reciprocal commissures extending between the brighter ventral nerve cord and the dorsal nerve cord. No significant difference in axon fasciculation (B) or axon targeting (C) was observed in *vps-39* mutants relative to control. (D) Representative images of *ACR-16::GFP* staining in the ventral nerve cord in wild-type and the *vps-39* mutant background. (E) No significant difference in *ACR-16* expression was observed in the *vps-39* mutant. Number of measurements indicated in each bar (3 measurements/worm) (C), # of worms examined, indicated in bars. Data collected by Susan Klosterman.

VPS-39 regulates synaptic transmission

To determine the precise nature of the presynaptic defect in *vps-39* mutants, evoked synaptic responses to nerve stimulation were recorded from voltage-clamped body wall muscles of dissected worms. The average NMJ evoked response in *vps-39* mutants was significantly reduced as evidenced by a smaller, more rapidly decaying EPSC leading to a pronounced reduction in total charge transfer (Figure 3.7A-D). Under 5 mM extracellular calcium recording conditions expression of VPS-39 restored the evoked response to wild-type levels (Figure 3.7A-D).

To determine whether *vps-39* mutants impact the calcium-dependence of release we measured evoked responses in lower extracellular calcium conditions (0.5mM) (Figure 3.7E-F). In 0.5 mM calcium, the extent of the evoked EPSC defect in *vps-39* mutants (57% reduction in the charge integral) was identical to the reduction observed in 5 mM calcium (57%) and the evoked defect was again fully rescued by neuronal re-expression of VPS-39. These data suggest that VPS-39 does not impact the calcium-dependence of release.

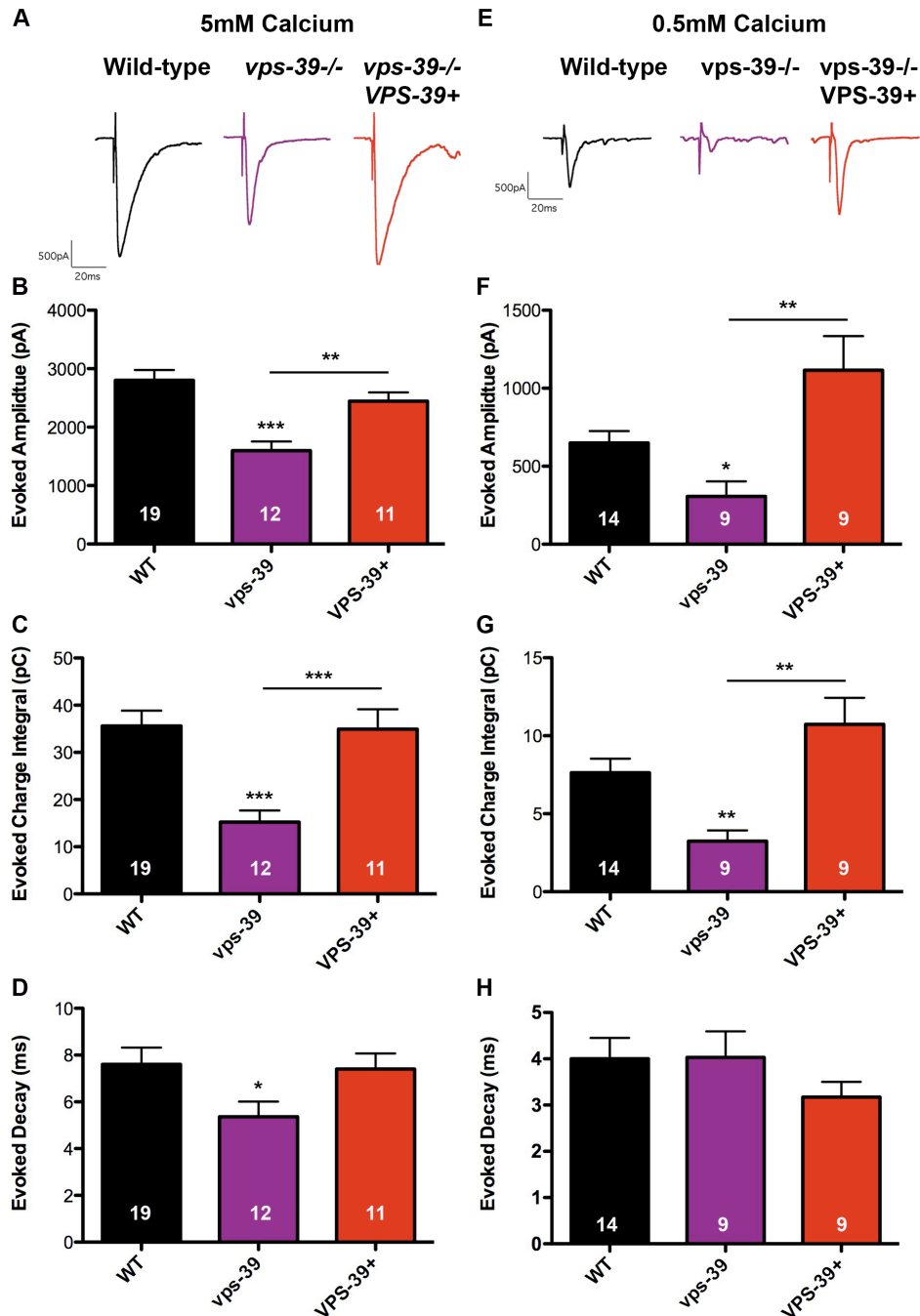


Figure 3.7. VPS-39 promotes evoked release at the NMJ. (A) Representative evoked traces in 5 mM extracellular calcium. (B) Evoked amplitude, (C) evoked charge integral and (D) evoked decay in 5 mM calcium all display a significant reduction in *vps-39* mutants, which is rescued to wild-type levels upon VPS-39 re-expression in neurons. (E) Representative evoked traces in 0.5 mM extracellular calcium. (F) Evoked amplitude and (G) evoked charge integral are also significantly reduced in the *vps-39* mutant at 0.5 calcium and restored to wild-type levels upon expression of VPS-39. (H) There are no significant differences in evoked decay for these strains in 0.5 mM calcium. Sample size indicated in each bar. Data collected by Dr. Richmond

VPS-39 functions to dock synaptic vesicles

The reduced evoked release in *vps-39* mutants could be the result of changes in synaptic vesicle biogenesis or synaptic delivery. To address this question, worms were immobilized by high-pressure freeze fixation/freeze substitution and EM images of cholinergic NMJs from ultra-thin sections (40 nm) were acquired. Both *vps-39* mutants and the rescuing VPS-39 transgenic line displayed wild-type numbers of synaptic vesicles (WT = 30.97 ± 1.64 vesicles/profile n = 66 profiles, *vps-39* mutant = 27.7 ± 0.93 vesicles/profile n = 54 profiles, VPS-39+ = 27.9 ± 1.01 vesicles/profile n = 56). These results indicate that changes in vesicle density do not account for the release defect in *vps-39* mutants or the neuronal rescue.

Several recent studies of HPF/FS worm specimens have established that the number of morphologically docked vesicles in presynaptic terminals correlates with the number of primed, fusion competent vesicles (Weimer et al., 2006, Hammarlund et al., 2007a, Gracheva et al., 2008). Therefore, to determine whether VPS-39 regulates synaptic vesicle priming, we quantified the number and distribution of docked vesicles in *vps-39* mutants (Figure 3.8). The docked synaptic vesicle distribution relative to the presynaptic density (PD) was reduced throughout the terminal suggesting that *vps-39* mutants have fewer primed vesicles (Figure 3.8B). However, VPS-39 expression in the mutant background only slightly restored the docked vesicle pool, while exhibiting functional rescue of release (Figure 3.8C).

Recent evidence suggests that docked vesicles represent two spatially and functionally distinct primed vesicle pools (Hu et al., 2013). Specifically, vesicles docked <100nm from the PD through interactions with the PD proteins Rim and the long

isoform of UNC-13 (L) mediate fast, EGTA-resistant release. Vesicles docked further away, which require both UNC-13(L) and the more diffusely distributed short UNC-13(S) isoform for priming, exhibit slower, EGTA-sensitive release. These data suggest that proximally docked synaptic vesicles (i.e. EGTA-resistant) have enhanced calcium-sensitivity, which reflects proximity to PD enriched voltage-gated calcium channels as well as the calmodulin-binding domain found only in the UNC-13(L) isoform.

When we grouped the docking data for *vps-39* mutants and the VPS-39 rescuing line into these two spatially distinct primed pools (proximal < 90 nm from the PD, distal >90 nm from the PD), we observed docking defects in both proximal and distal vesicle pools in the mutant, but rescue of only the proximal vesicle pool upon VPS-39 re-expression (Fig. 3.8D,E). The rescue of the PD proximal docked vesicle pool by neuronal VPS-39 expression corresponds with the rescue of evoked release under both high and low calcium conditions (Fig 3.7). Together these data suggest that VPS-39 promotes the docking of fusion competent synaptic vesicles.

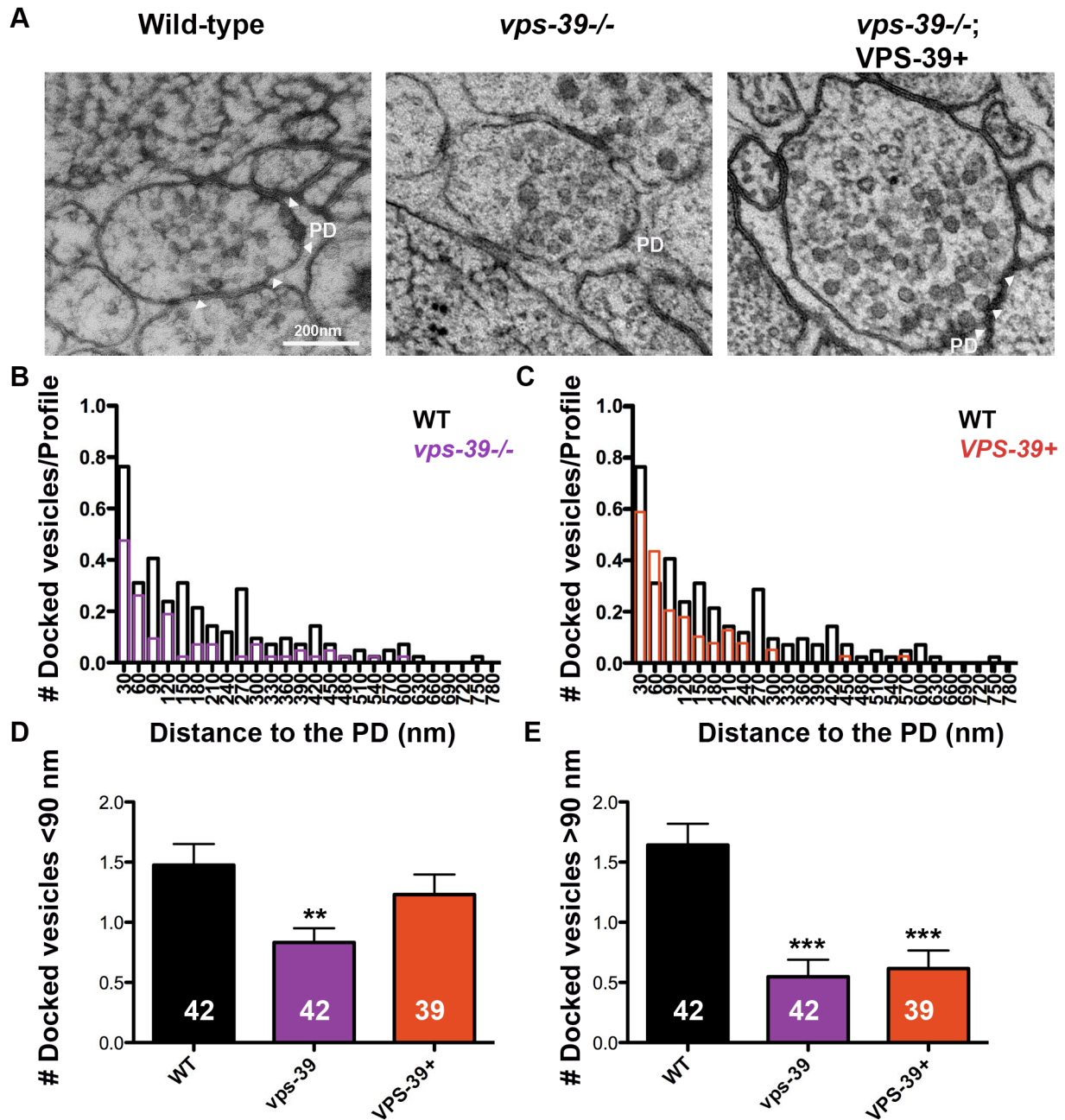


Figure 3.8. VPS-39 is required for vesicle docking/priming. (A) Representative electron micrographs. (B) Distribution of docked vesicles with respect to the PD showing *vps-39* mutants (purple) has a reduced number. (C) Neuronal VPS-39 expression profiles (red) display slightly increased docking near the PD. (D) Docked vesicles/profile within 90 nm of the PD are reduced in *vps-39* mutants (E) >90 nm from the PD, docked vesicle/profile remain significantly reduced in both *vps-39*^{-/-} and the VPS-39 rescue line. Number of profiles for each strain shown in white.

VPS-39/HOPS does not bypass UNC-13 function

Syntaxin adopts a default closed conformation in solution, which occludes its H3 SNARE binding domain. UNC-13 interacts with the N-terminus of Syntaxin and is thought to promote priming by binding and stabilizing Syntaxin in an open configuration compatible with SNARE complex assembly (Betz et al., 1997; Dulubova et al., 1999; Richmond et al., 2001). Consistent with this model, previous studies have shown that priming defective *unc-13* mutants are partially rescued by expression of a mutated Syntaxin construct that adopts a constitutively open configuration in which the H3 domain is exposed (Richmond et al., 2001). If VPS-39 functions upstream of UNC-13 to trigger the dissociation or rearrangement of UNC-18/Syntaxin dimers, as previous biochemical data imply (Kim et al., 2006a), VPS-39 may render Syntaxin available but in its default closed state. In this closed configuration with the H3 domain occluded, priming would then require UNC-13 interactions to stabilize the Syntaxin open state. We therefore, predicted that VPS-39 overexpression would not bypass the severe priming defect of *unc-13* mutants. Consistent with this model, VPS-39 overexpression failed to rescue the evoked synaptic response of *unc-13(e51)* mutants which specifically disrupts the UNC-13(L) isoform (Kohn et al., 2000) (Figure 3.9A,B).

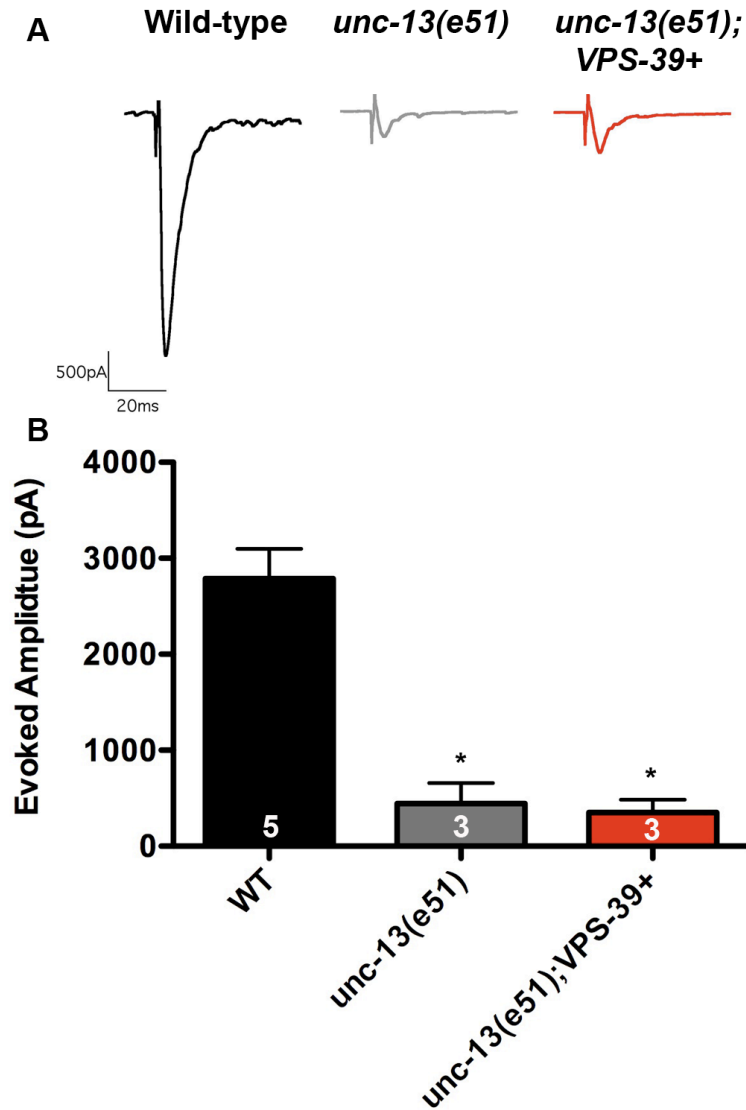


Figure 3.9. Expression of VPS-39 in neurons does not rescue *unc-13(L)* mutants. (A) Representative traces of *unc-13(e51)* mutants with and without VPS-39 expression. (B) Evoked amplitudes of the *unc-13(e51)* mutant alone and in the *unc-13* mutant expressing VPS-39 are significantly reduced when compared to wild-type. Sample size indicated in each bar. Data collected by Dr. Richmond

Open Syntaxin partially bypasses vps-39 mutants

The efficient trafficking of Syntaxin to synaptic terminals is dependent on the chaperone function of Munc18. The molecular events that transition Munc18/Syntaxin dimers, once they reach the synapse, to enable Syntaxin to bind to UNC-13 and participate in SNARE complex assembly are unknown. Several lines of evidence implicate VPS-39 and the HOPS complex in this process: 1) HOPS proteins are enriched at synapses. 2) The HOPS components, Vps16 and Vps18 bind to both Munc18 and Syntaxin. 3) Over-expression of hVPS18 in PC12 cells promotes evoked release (Kim et al., 2006). 4) *vps-39/vam6* loss of function mutants in yeast, mouse and as shown here in *C. elegans*, exhibit vesicle fusion defects (Kramer and Ungermann, 2011). Based on this evidence, we hypothesized that VPS-39 may regulate *C. elegans* homologs of Munc18 (UNC-18) and Syntaxin (UNC-64) to promote vesicle priming. If VPS-39 is required to promote a molecular transition of Munc18/Syntaxin dimers to a conformation that allows Syntaxin to participate in priming, we predicted that constitutively open Syntaxin should by-pass the requirement for VPS-39.

To test this hypothesis we generated *vps-39* mutants expressing the constitutively open form of *C. elegans* Syntaxin (UNC-64(LE-AA) (Richmond et al., 2001). Expression of open Syntaxin enhanced the dylox sensitivity of *vps-39* mutants beyond that of wild-type worms, although not to the extent observed in open Syntaxin alone suggesting that open Syntaxin partially bypasses the requirement for VPS-39 (Figure 3.10A). Furthermore, neuronal expression of VPS-39 showed no additivity with open Syntaxin consistent with these two manipulations acting in the same pathway to promote release (Figure 3.10B).

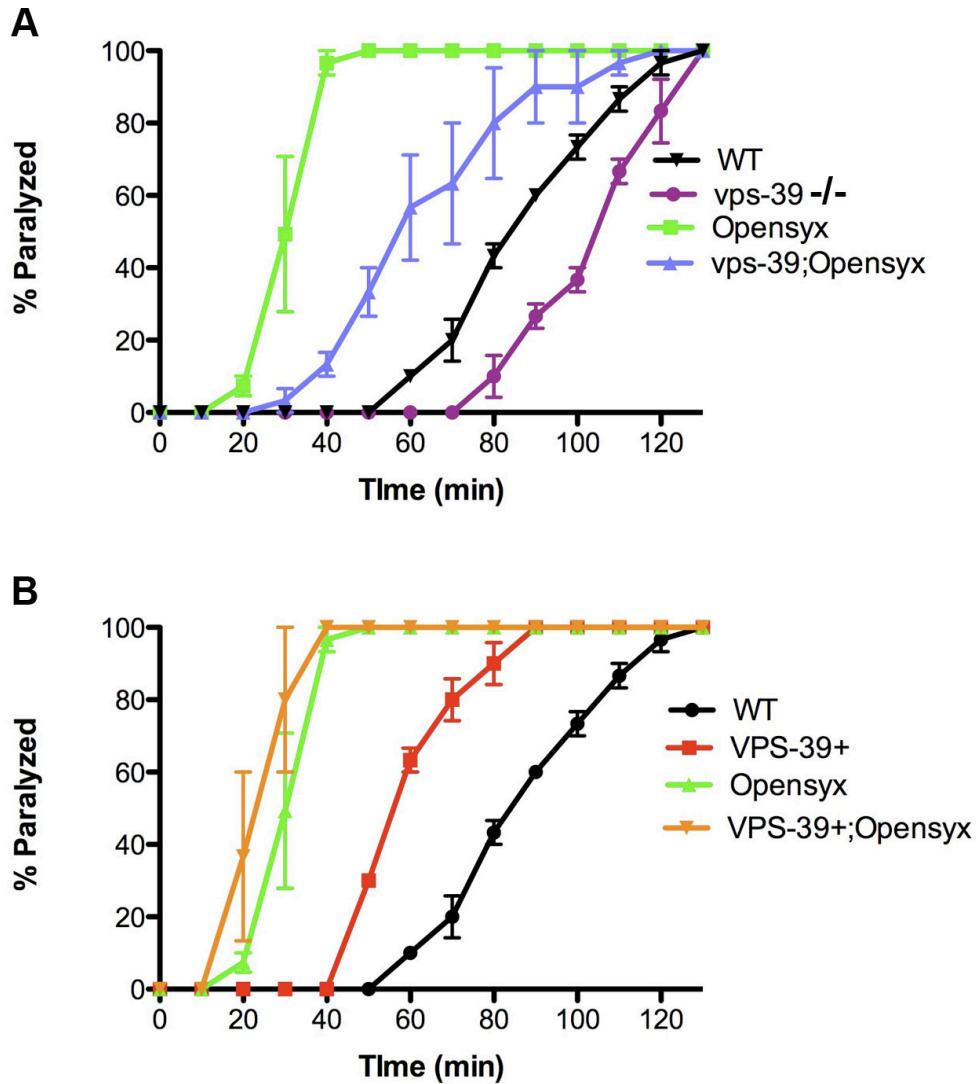


Figure 3.10. Open Syntaxin rescues the dylox resistance of *vps-39* mutants. (A) Dylox sensitivity of *vps-39* mutants with and without open Syntaxin. (B) Dylox sensitivity of VPS-39 neuronal expression with and without open Syntaxin. Both graphs plotted with WT and open Syntaxin alone. Each experiment was repeated three times, each time using 10 worms/strain. Data collected by Susan Klosterman.

Consistent with these behavioral data, open Syntaxin rescued the evoked release amplitude of *vps-39* mutants to wild-type levels in 5 mM extracellular calcium (Figure 3.11A,B). The faster decay kinetics of *vps-39* mutants were also restored, whereas open Syntaxin alone significantly prolonged the evoked response relative to wild-type. Together these observations suggest that open Syntaxin rescues the *vps-39* synaptic phenotype (Figure 3.11C,D).

The prolonged duration of the open Syntaxin evoked response correlates with a previously observed increase in the number of docked vesicles distributed further from the PD (Hammarlund et al., 2007). We hypothesized that the delayed release due to open Syntaxin may reflect an increase in the slow, EGTA-sensitive pool of primed vesicles, not associated with the PD proteins Rim and UNC-13(L). To test this model, we recorded EJC's in low calcium conditions, which should reduce calcium entry, restricting the fusion of vesicles to those that are EGTA-resistant associated with the PD. Consistent with our interpretation, the EJC duration of open Syntaxin expressing worms in low calcium was no longer increased when compared to wild-type (Figure 3.11E,H). Furthermore, in low calcium, open Syntaxin failed to rescue *vps-39* mutants (Figure 3.11E-H). These data imply that open Syntaxin partially ameliorates the release defect of *vps-39* mutants primarily by restoring primed vesicles that are uncoupled from UNC-13(L). Consistent with this interpretation, EM analysis of docked vesicles confirmed an increase in distally docked vesicles in open Syntaxin mutants (Figure 3.12A), which partially rescued the docking defect of *vps-39* mutants (Figure 3.12B,C).

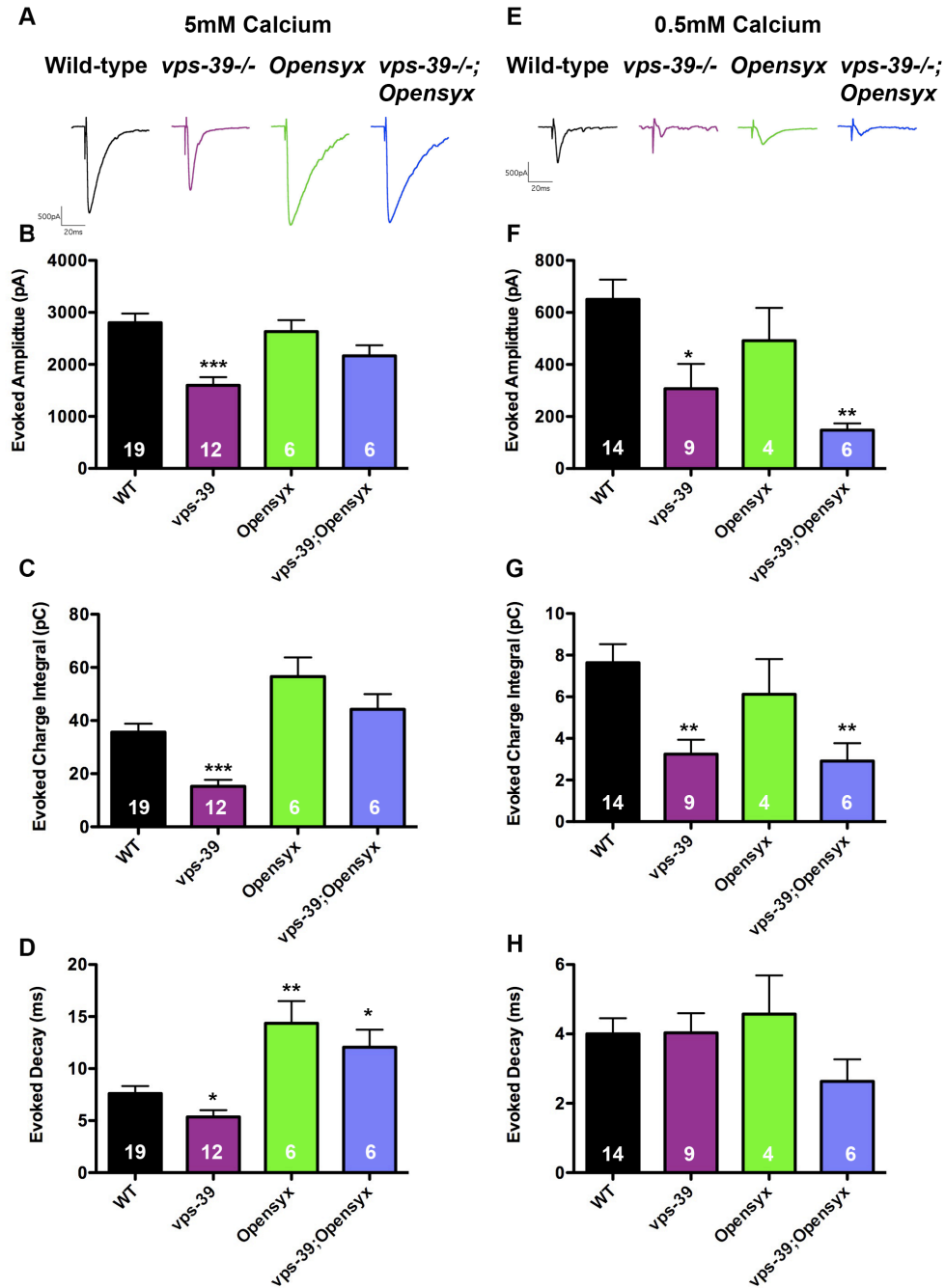


Figure 3.11. Open Syntaxin partially rescues the *vps-39* mutant evoked defect. (A) Representative evoked NMJ traces of *vps-39* mutant with and without open Syntaxin at 5mM calcium. (B) Evoked amplitude, (C) evoked charge integral and (D) evoked decay defects observed in the *vps-39* mutant are all significantly rescued to wild-type levels at 5mM calcium. (E) Representative evoked NMJ traces for the same strains in 0.5 mM calcium. (F) Evoked amplitude and (G) evoked charge integral *vps-39* mutant defects are not rescued in 0.5mM calcium. (H) None of the evoked decays are significantly different from each other. Data collected by Dr. Richmond

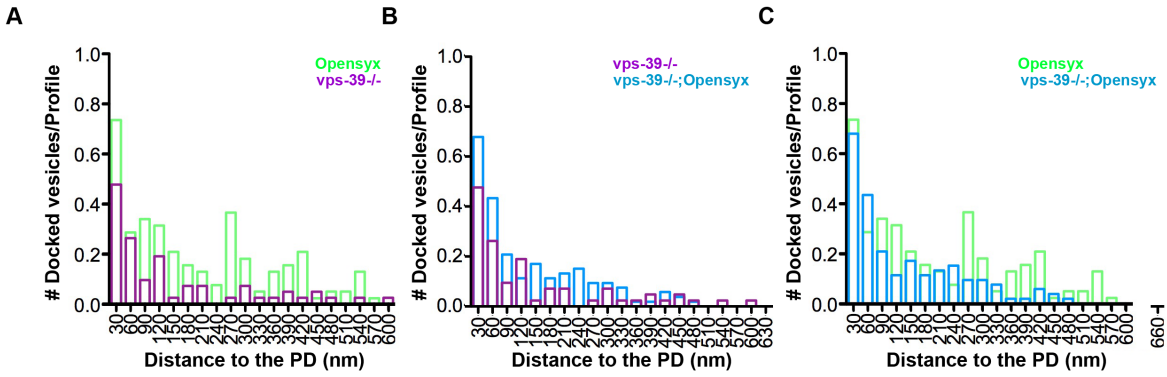


Figure 3.12. Open Syntaxin partially rescues *vps-39* mutant docking defects. (A) Distribution of docked vesicles with respect to the PD comparing *vps-39* mutants (purple) to open Syntaxin expressed in *unc-64* mutants (green). (B) Open Syntaxin partially rescues the docking defect of *vps-39* mutants, although not to the level of open Syntaxin alone (C).

Neuronal VPS-39 compensates for open Syntaxin evoked defects in low calcium

We have established that neuronal expression of VPS-39 in the *vps-39* mutant background rescues both high and low calcium evoked release which corresponds to a concomitant rescue of the docked vesicle pool proximal to the PD (Figure 3.8). In contrast, open Syntaxin exhibits an evoked defect in low calcium, despite similar levels of proximally docked vesicles to the VPS-39 rescuing line (Figure 3.14A). These data suggest that VPS-39 promotes the calcium sensitivity of release.

To determine whether VPS-39+ can rescue the calcium sensitivity of release in the presence of open Syntaxin, we recorded evoked release in VPS-39+;open Syntaxin double transgenics. In high calcium, increased release due to longer decay rates was observed in both the open syntaxin and double transgenics (Figure 3.13A-D). While in low calcium, the VPS-39+ phenotype prevailed, enhancing the open Syntaxin release defect in the double transgenics (Figure 3.13E-H).

EM analysis of open syntaxin and VPS-39+ single and double transgenics mirrored these electrophysiological results, open Syntaxin promoting distally docked vesicles in the VPS-39+ line (Figure 3.14C), while the presence of VPS-39+ promoted proximally docked vesicles at the expense of a larger distally docked pool in open Syntaxin alone (Figure 3.14B).

Together these results are consistent with the hypothesis that VPS-39 promotes the formation of fusion competent vesicles near the PD that have higher calcium sensitivity than those of open Syntaxin.

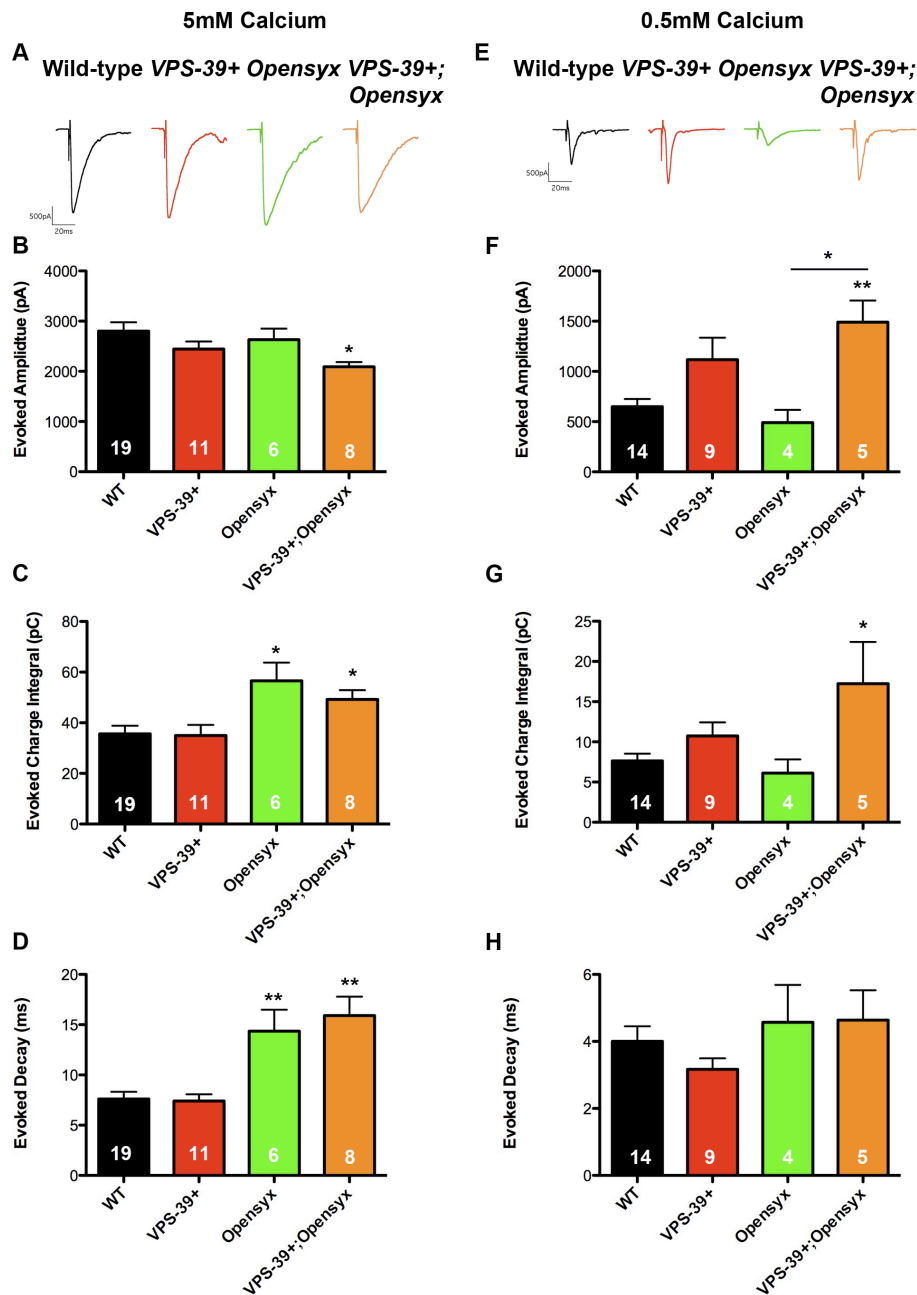


Figure 3.13. VPS-39/open Syntaxin co-expression enhances release at low calcium. (A) Representative traces of VPS-39 expression with and without open Syntaxin at 5mM calcium. (B) Evoked amplitude, (C) evoked charge integral, and (D) evoked decay are indicative of a prolonged response whenever open Syntaxin is present at 5 mM calcium. (E) Representative traces of VPS-39 expression with and without open Syntaxin at 0.5mM calcium. (F) Evoked amplitude, (G) evoked charge integral, and (H) evoked decay at 0.5mM calcium. VPS-39+ can significantly enhance the evoked amplitude of open Syntaxin at 0.5mM calcium (F). Data collected by Dr. Richmond

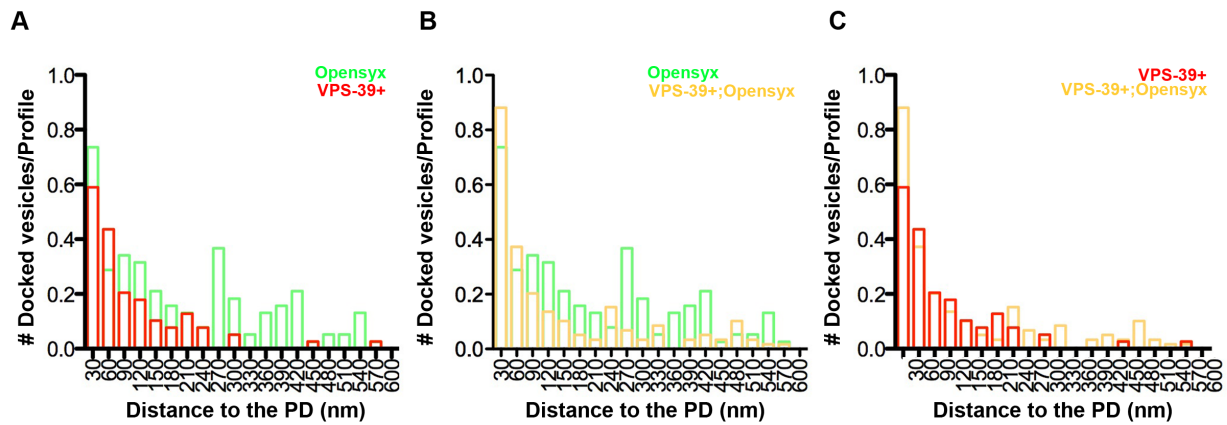


Figure 3.14. VPS-39 and open Syntaxin exhibit differential docked vesicle distributions. (A) Distribution of docked vesicles with respect to the PD comparing VPS-39+ (red) to open Syntaxin (green). Open Syntaxin exhibits more proximally docked vesicles. In the VPS-39+:open Syntaxin doubles, the proximal docked vesicle pool is similar to that of open Syntaxin alone (B) as well as VPS-39+ alone.

3.4 Discussion

Recent data demonstrating potential biochemical and functional interactions between the HOPS complex and the exocytic proteins, Syntaxin and Munc18 prompted us to examine a *C. elegans* mutant of the HOPS complex component, VPS-39. The phenotypes associated with loss of VPS-39 included a reduction in GFP processing within coelomocytes, neuronal-dependent embryonic lethality and cholinergic release defects associated with reduced vesicle docking.

GFP containing vesicles within the coelomocytes of *vps-39* mutants were smaller and more abundant, in direct contrast to mutants lacking TBC-2, which exhibit abnormally large GFP vesicles (Chotard et al., 2010). TBC-2 acts upstream of the HOPS complex and negatively regulates a sequential RAB-5, RAB-7 signaling pathway which normally activates VPS-39 (Figure 3.1B). The abnormally large coelomocyte vesicles in *tbc-2* mutants reflect increased homotypic fusion within the coelomocytes. Similarly, *tbc-2* mutants exhibit larger intestinal endosomes again suggestive of exuberant fusion (Chotard et al., 2010). Furthermore, *rab-5(RNAi)*, *rab-7(ok511)* deletion mutants and *vps-39(RNAi)* or *vps-41(RNAi)* all strongly suppress the enlarged endosomal vesicle phenotype observed in *tbc-2(tm2241)* mutant intestines (Chotard et al., 2010). Together these observations support the notion that TBC-2 inhibits fusion while RAB-5, RAB-7, and the HOPS complex components VPS-39, and VPS-41 promote fusion in *C. elegans* coelomocytes and intestinal cells.

Our present data also implicate VPS-39 in the regulation of synaptic vesicle fusion, although it is unclear whether this VPS-39 function requires the other HOPS complex members. However, *C. elegans* mutants impacting the HOPS complex

components, VPS-16 and VPS-33, exhibit the same maternal embryonic lethality observed in *vps-39* mutants. The fact that neuronal expression of VPS-39 rescues both synaptic transmission defects and embryonic lethality, suggests that the HOPS complex is involved.

Together the available data support a generalized fusion role for the VPS-39-dependent pathway in multiple tissues, consistent with its ubiquitous expression pattern in *C. elegans*. Furthermore, this function appears to be highly conserved based on the following observations from other organisms. In yeast, deletion of Vps39 results in the cytoplasmic accumulation of vesicles due to failure to fuse with the vacuole (Raymond et al., 1992). Zebra fish that lack the Vps39 homolog (*lbc*) display an accumulation of vesicles in their retinal pigment epithelium, indicative of a fusion defect of endocytic vesicles (Schonthaler et al., 2008). In contrast, overexpression of the human homolog Vam6p, induces abnormal clustering and fusion of lysosomes. This latter observation suggests that hVam6p may function as a tethering/docking factor (Caplan et al., 2001).

Although we cannot absolutely rule out indirect actions of VPS-39 through endosomal or lysosomal sorting of synaptic components rather than direct actions of VPS-39 on synaptic function, we propose the following mechanism of action. Our data support a role for VPS-39, possibly in conjunction with the HOPS complex, to promote a Syntaxin/Munc18 conformational change that when stabilized by UNC-13, allows SNARE complex formation to proceed (Figure 3.15). This model is based on the following experimental evidence. We have excluded neuronal developmental abnormalities as the underlying causes of the presynaptic defect in *vps-39* mutants. Our ultrastructural data instead, place VPS-39 function in the docking/priming process

of the synaptic vesicle cycle, a stage that is dependent on the Syntaxin binding protein, UNC-13. Evidence suggests that UNC-13 is required to stabilize Syntaxin in an open configuration compatible with SNARE complex formation near the PD, where the long isoform of UNC-13(L) is enriched (Betz et al., 1997; Dulubova et al., 1999; Richmond et al., 2001). The observation that constitutively open Syntaxin partially rescues both *unc-13* and *vps-39* mutants places both proteins in this pathway. However, VPS-39 overexpression fails to rescue *unc-13* mutants suggesting the HOPS complex likely acts upstream of UNC-13. Based on these data and previous biochemical evidence (Kim et al., 2006), we propose that VPS-39 promotes the transition of UNC-18/closed Syntaxin to the open Syntaxin configuration that can then be stabilized by UNC-13.

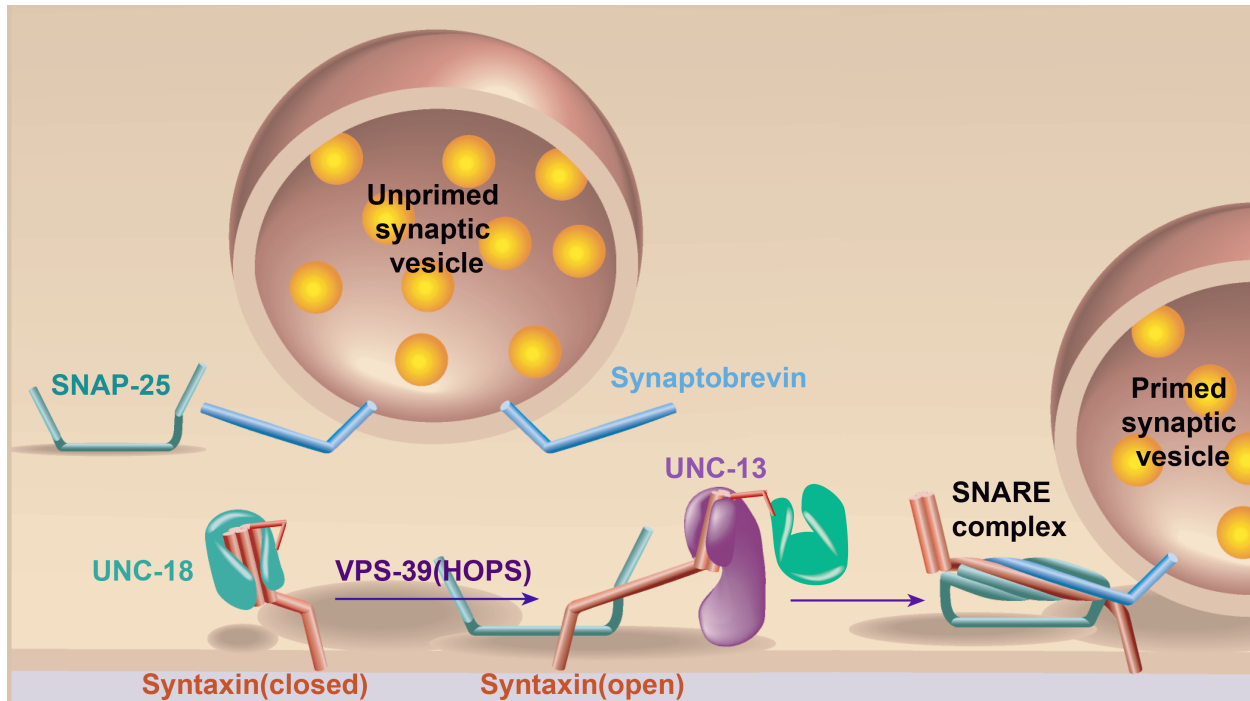


Figure 3.15. Model of VPS-39 function. VPS-39, likely in conjunction with the HOPS complex interacts with UNC-18 and Syntaxin, forming a heterologous complex that promotes a Syntaxin conformational transition that can then be stabilized by UNC-13. Since UNC-13(L) is enriched at the presynaptic density, this process promotes formation of primed vesicles through SNARE complex assembly at sites enriched for calcium entry.

3.5 Acknowledgements

We would like to thank Marc Hammarlund for kindly providing Gateway donor vectors, Denis Touroutine for an expression vector, and the *C. elegans* knockout consortium for strains.

VI. Photoactivation of adenylate cyclase promotes synaptic vesicle docking and release in a Tomosyn-dependent pathway

Szi-chieh Yu, Kaiyun Chen, Carolin Wichmann, Martin Schwärzel, David E Featherstone, and Janet E. Richmond

4.1 Introduction

Synaptic vesicle release is critically dependent on three conserved synaptic proteins, the vesicle-associated protein Synaptobrevin, and the plasma membrane associated proteins, Syntaxin and SNAP-25 (synaptosomal-associated protein 25 kDa) (Bennett et al., 1992; Fasshauer et al., 1998; Oyler et al., 1989; Trimble et al., 1988). These three proteins zipper together via coiled-coil domains to form SNARE (soluble N-ethylmaleimide sensitive factor adaptor protein receptor) complexes. This step is thought to bring the vesicle membrane into close apposition with the plasma membrane, developing a fusion competent primed state prior to calcium-triggered fusion (Jahn et al., 2003; Matos et al., 2003; Sollner et al., 1993; Sutton et al., 1998). Treatment with clostridial toxins and loss of functional SNARE proteins have established that all three SNARE proteins are essential and comprise the minimal vesicle fusion machinery for neurotransmission (Augustine et al., 1996; Blasi et al., 1993a; Blasi et al., 1993b; Schiavo et al., 1992; Schoch et al., 2001).

Tomosyn, first identified in a Syntaxin pull-down assay, contains a C-terminal coiled-coil domain that is able to substitute for Synaptobrevin and form a ternary complex with Syntaxin and SNAP-25, known as the Tomosyn complex, whose biochemical properties (heat-stability, NSF-disassembly) are similar to the fusogenic SNARE complex (Cheviet et al., 2006; Hatsuzawa et al., 2003; Pobbati et al., 2004).

However, unlike Synaptobrevin, Tomosyn is not an integral vesicle protein and *in vitro* data suggest that Tomosyn complex formation occurs at the expense of SNARE complex assembly and vesicle priming (Fujita et al., 1998; Masuda et al., 1998). Consistent with this hypothesis, overexpression of Tomosyn in both chromaffin and PC12 cells as well as *C. elegans* reduced the readily releasable vesicle pool (Gracheva et al., 2006; Hatsuzawa et al., 2003; Yizhar et al., 2004). Conversely, loss of Tomosyn in *C. elegans*, *Drosophila* and mice exhibited enhanced evoked responses, due to increased vesicle priming and prolonged decay time (Chen et al., 2011; Gracheva et al., 2006; McEwen et al., 2006; Sakisaka et al., 2008). Taken together these observations demonstrate that Tomosyn has a conserved inhibitory role in neurotransmission, although the reasons for the altered kinetics in Tomosyn mutants remain unclear.

A similar prolonged evoked response has been observed at the fly neuromuscular junction (NMJ) under conditions which increase cAMP (cyclic adenosine monophosphate) signaling, specifically in *Dunce* mutants defective in cAMP phosphodiesterase activity, as well as upon forskolin activation of adenylate cyclase (Chen et al., 2011; Renger et al., 2000). cAMP signaling through protein Kinase A (PKA) has previously been implicated in the regulation of Tomosyn. Specifically, biochemical data have demonstrated that PKA phosphorylation within the rat Tomosyn N-terminal WD40 repeats reduces its interaction with Syntaxin-1. Precisely, how the phosphorylation of Tomosyn distal to the SNARE motif reduces its Syntaxin affinity is unknown. However, studies from cultured superior cervical ganglion (SCG) neurons have shown that intramolecular interactions within Tomosyn can interfere with the binding of the Tomosyn SNARE domain to Syntaxin and SNAP-25 (Yamamoto et al.,

2009). The PKA phosphorylation of Tomosyn is postulated to regulate this Tomosyn intramolecular switch. Based on these data we hypothesize that Tomosyn may be a target of cAMP signaling in the regulation of synaptic strength *in vivo*.

To test this hypothesis and determine the underlying functional changes associated with enhanced cAMP signaling, we obtained a recently developed optogenetic tool, photoactivatable adenylate cyclase, derived from soil bacterium *Beggiatoa* (bPAC) (Stierl et al., 2011). bPAC contains a blue light sensing BLUF (blue light receptor using FAD) domain linked C-terminal to an adenylate cyclase. Upon blue light activation, bPAC is able to generate cAMP acutely and reversibly (Stierl et al., 2011). This tool allows us to study the effects of up-regulated cAMP in dissected fly larvae using electrophysiology and also importantly in intact larvae using high pressure freeze electron microscopy (HPF EM) immediately following blue light activation. Compared to forskolin application and *Dunce* mutants, bPAC allows tissue specific up-regulation of cAMP and avoids developmental defects resulting from chronic accumulation of cAMP (Bellen et al., 1987; Guan et al., 2011). Therefore, the manipulation of intracellular cAMP levels in live animals using bPAC provides a feasible and powerful method to study short-term synaptic plasticity in the cAMP-signaling pathway.

In this study, we used a combination of neuronally expressed bPAC and Tomosyn RNA interference (RNAi) in *Drosophila* larvae to determine whether the synaptic modulation of Tomosyn functions in a cAMP/PKA-dependent manner at the NMJ. We show that neuronal bPAC activation phenocopies Tomosyn knockdown, resulting in prolonged evoked synaptic responses, and that both conditions are

associated with increased numbers of plasma membrane docked vesicles. Following blue light activation of bPAC expressing synapses, we also observed translocation of Tomosyn from the synaptic plasma membrane to the lumen. This result suggests that the inhibitory interaction of Tomosyn with plasma membrane SNAREs (Syntaxin and SNAP-25) is reduced following up-regulated cAMP signaling. Furthermore, ultrastructural analysis showed no additivity in bPAC activation combined with Tomosyn RNAi, compared with activated bPAC alone, implying that Tomosyn functions as an important effector in the cAMP signaling pathway. Based on these results we postulate that the cAMP-dependent phosphorylation of Tomosyn promotes the assembly of fusogenic SNARE complexes resulting in increased vesicle docking and enhanced release.

4.2 Materials and Methods

Electrophysiology

Two-electrode voltage clamp was performed as previously described (Chen et al., 2005). Briefly, third-instar larvae were dissected under red-filtered light. Ventral longitudinal muscles 6 and 7 in abdominal segments 3–4 larvae were voltage-clamped at -60 mV using an MDS Analytical Technologies GeneClamp 500B amplifier, in standard *Drosophila* saline (135 mM NaCl, 5 mM KCl, 4 mM MgCl₂, 1.8 mM CaCl₂, 5 mM TES, and 72 mM sucrose). Electrodes (resistance 10–20 M Ω) were filled with 3 M KCl. Segmental nerves innervating muscles 6 and 7 were stimulated using a Grass S48 stimulator via a suction electrode. bPAC was activated using 5 minutes blue light illumination (470nm, M470L2 high-power LED driven by LED driver, LEDD1B, Thorlabs). All electrophysiological recordings were digitized and analyzed using a

Digidata 1322A digitizer (Axon Instruments) with PClamp 10 software. Statistical significance was determined using the unpaired Student t test. Asterisks in figures indicate statistical significance values of *** $P \leq 0.001$, ** $P \leq 0.01$, * $P \leq 0.05$.

Confocal Microscopy

Wandering third instar larvae were manually dissected under dim light to expose ventral NMJs. Dissected larvae were then exposed to LED blue light stimulation for 5 minutes and fixed 30 minutes in 4% paraformaldehyde. Following fixation, tissues were rinsed in PBTX and stained overnight using an anti-Tomosyn rabbit antibody (1:2000), then treated 2-4hr with Atto-labeled anti-rabbit secondary antibody (1:100). Image acquisition was performed using a Leica TCS STED microscope in confocal mode (for analysis of luminal:cortical Tomosyn ratios). Analysis of type 1B motor terminals on ventral muscles was performed using NIH ImageJ.

Electron Microscopy

Late second/early third instar larvae were prepared by HPF fixation, based on methods previously described (Weimer et al., 2006). Briefly, one to three animals were loaded in a 200 μm deep specimen chamber filled with yeast paste and immobilized by high-pressure freezing at -180°C under high pressure in a Bal-Tec HPM010 machine and stored in liquid nitrogen. For bPAC photostimulation, *Drosophila* larvae were selected under low-intensity, red-filtered light and illuminated with intense LED blue light for 5 minutes, followed by immediate high-pressure freezing.

Freeze substitution (FS) was performed in a Reichert AFS machine (Leica, Oberkochen, Germany) as described previously for morphological specimen preparation, using tannic acid (0.1% in dry acetone) fixative incubated at -90°C for 100

hr, then substituting with dry acetone and incubating for 39.5 h in 2% OsO₄ (w/v in dry acetone) while slowly increasing temperature up to room temperature (Weimer and Richmond, 2005). Fixed specimens were then embedded in Epoxy resin (Agar Scientific, AGAR 100 Premix kit hard) at room temperature with increasing concentrations from 50% to 90% and 100% at 65°C over 48h. Serial sections were cut at a thickness of 45 nm, collected on formvar-covered carbon coated copper grids (EMS, FCF2010-Cu) and counterstained in 2.5% aqueous uranyl acetate for 30 min, followed by Reynolds lead citrate for 2 min. Images were obtained with a 3608 x 2672 CCD camera (Gatan ES1000W Erlangshen CCD camera, model 785) on a Jeol JEM-1220 (Tokyo, Japan) transmission electron microscope operating at 80 kV. Morphometric analysis of NMJ sections were scored blind and images were quantified using NIH ImageJ software. Statistical significance was determined using the Mann-Whitney test. Statistically significant values were: *p ≤ 0.05, **p ≤ 0.01, ***p ≤ 0.001

4.3 Results

Photoactivatable adenylate cyclase (PAC) regulates synaptic transmission at the fly NMJ

In order to test the hypothesis that cAMP-regulation of Tomosyn impacts synaptic strength, we needed a molecular tool to acutely activate cAMP in motor neurons. Pharmacological reagents such as the adenylate cyclase activator, forskolin and *Dunce* (phosphodiesterase) mutants are known to enhance neurotransmission in *Drosophila* by increasing cAMP signaling (Chen et al., 2011; Renger et al., 2000). However, these manipulations are not neuron-specific and chronic up-regulation of intracellular cAMP in *Drosophila Dunce* mutants is associated with synaptic connectivity defects, complicating

the interpretation of functional changes (Guan et al, 2011). Therefore, we obtained the bPAC to up-regulate intracellular cAMP levels upon blue light activation (Stierl et al., 2011). This tool allowed us to study neuron-specific functional changes resulting from acute elevation of cAMP signaling while recording from neuromuscular synapses. This also provided a means of performing ultrastructural analyses from intact larvae fixed by HPF immediately following enhanced cAMP signaling (Figure 4.1).

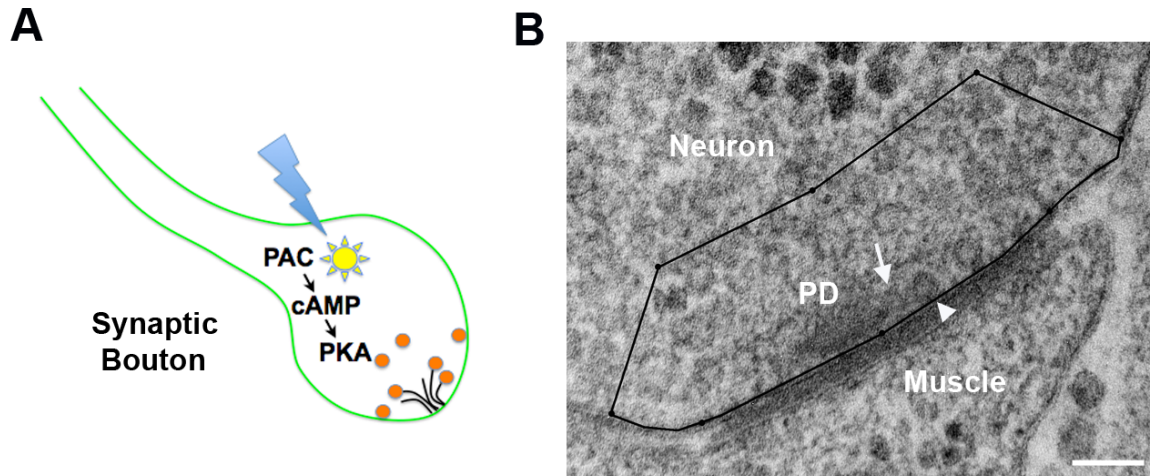


Figure 4.1. The optogenetic tool bPAC acutely and reversibly increases spacial cAMP level. (A) Schematic pathway of blue light stimulated bPAC enhancing intracellular cAMP followed by PKA activation at NMJs. (B) Example of a high pressure frozen *Drosophila* larvae neuromuscular junction from a control larvae. A standardized area of quantification is defined as 400 nm along the plasma membrane on each side of the presynaptic density (PD) midpoint and extending 200 nm into cytoplasm. The arrow shows a PD tethered synaptic vesicle and arrowhead shows a plasma membrane docked synaptic vesicle. Scale bar represents 100nm.

The electrophysiological and ultrastructural consequences of activating bPAC were examined in third instar larvae, the latest stage at which larvae could be successfully fixed by HPF due to size restrictions. Data were collected from transgenic flies using the motor neuron specific D42Gal4 line to drive expression of UAS-bPAC.

We first examined the electrophysiological properties of miniature excitatory junctional currents (miniEJCs) in dissected larva, recorded from voltage-clamped postsynaptic ventral longitudinal muscles 6 and 7 (Figure 4.2A,C-E). Although the miniEJC amplitude was slightly increased upon bPAC activation ($p = 0.03$, $n = 8$) (Figure 4.2C), the miniEJC decay time (decay half-width, $p > 0.4$, $n = 8$) was not affected within 5 minutes of blue light exposure in either the bPAC transgenics without the D42Gal4 driver, used as controls, or bPAC expressed under the D42Gal4 driver (Figure 4.2D). The small increase in miniEJC amplitude following D42Gal4:bPAC activation may represent overlapping minis resulting from the significant increase in miniEJC frequency observed ($p < 0.01$, $n = 8$) (Figure 4.2E), an effect previously documented following forskolin application to *Drosophila* NMJs (Yoshihara et al., 2000).

To test whether increased cAMP signaling impacted evoked synaptic transmission, EJCs from bPAC expressing third-instar NMJs were elicited by stimulating the motor nerves (Figure 4.2B,F-H). The EJC area of activated bPAC larvae increased by 52% after 5 minutes blue light activation ($p < 0.001$, $n = 10$) whereas the control bPAC expressing larvae without the D42Gal4 driver showed no change upon blue light activation ($p > 0.5$, $n = 8$) (Figure 4.2H). The enhanced EJC area primarily reflected increased EJC decay time in bPAC-activated larvae ($p < 0.001$, $n = 10$), although EJC amplitude was also slightly but significantly increased ($p = 0.007$, $n = 10$) (Figure

4.2F,G). This result was consistent with the sustained enhancement in EJC duration previously observed following forskolin application (Chen et al., 2011), further confirming that the broadening effect of the EJC in activated bPAC larvae reflects cAMP signaling. Additionally, this effect was similar to the enhanced EJC area reflecting increased decay time resulting from Tomosyn RNAi (Chen et al., 2011). Together these observations support the hypothesis that cAMP signaling and Tomosyn may function in the same pathway.

To examine the timing of the bPAC activation over time, the normalized EJC area for all recordings was plotted for 5 minutes before and after blue light activation. The increase in EJC area was found within one minute of blue light activation of bPAC expressing larvae (Figure 4.2I), indicating that the synaptic response of the blue light activated bPAC is relatively rapid,

Together, these data demonstrated that blue light activation of bPAC in larvae phenocopies Tomosyn RNAi knockdown as well as the application of forskolin, suggesting that bPAC is a useful tool with which to explore the underlying changes associated with acute cAMP signaling in intact larvae as well as the relationship between cAMP signaling and Tomosyn regulation.

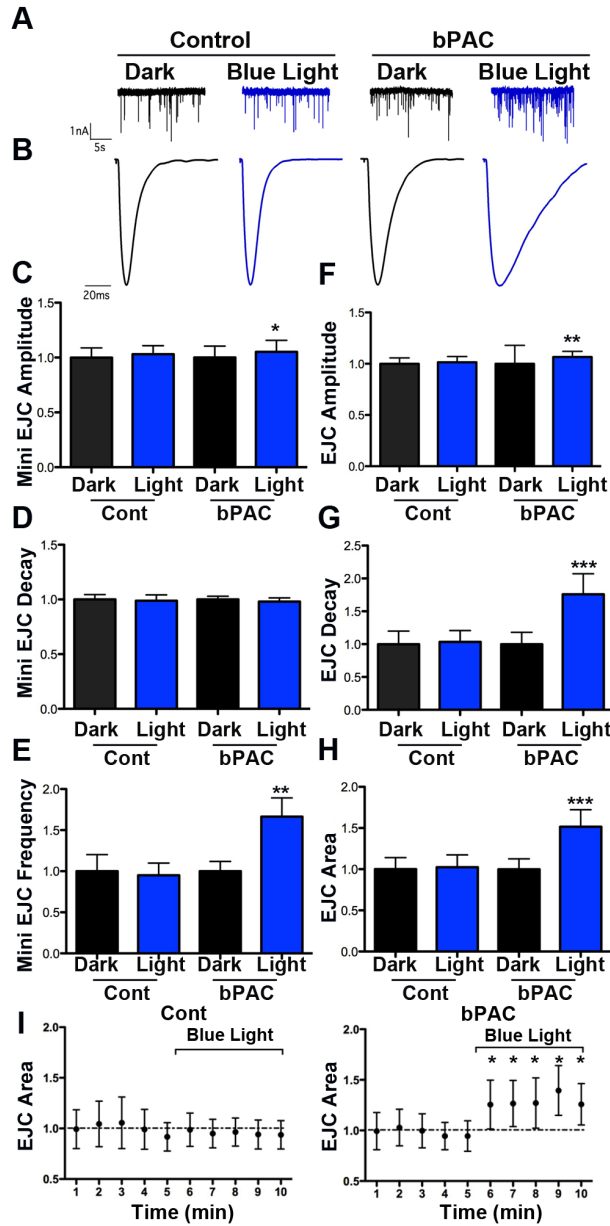


Figure 4.2 bPAC activation enhances synaptic release at NMJs. (A-B) Representative miniEJCs and EJCs recorded from larval NMJs after motor neuron expression of USA-bPAC transgene using the D42Gal4 driver and control (UAS-bPAC alone) in the dark or during 5 minutes blue light activation. (C-E) Neuronally expressed bPAC activation significantly but slightly affected miniEJC amplitude (C). Additionally, miniEJC frequency (E) was significantly increased. However, decay time (D) was not changed if compared to control. (F-H) EJC amplitude was significantly but slightly altered by bPAC activation. However, EJC decay time (G) and EJC area (H) were significantly enhanced in bPAC transgenics upon blue light activation. (I) bPAC activation increased EJC area within 1 minute of blue-light activation. EJC area of each time point during blue light activation was compared to the one before blue light (at 5 minutes time point) by paired t-test. All data presented were normalized to control.

bPAC activation of fly larvae increases synaptic vesicle docking

To better understand the cause of the enhanced electrophysiological response observed upon blue light activation of bPAC, we performed HPF/FS on late second/early third-instar larvae to examine the distribution of synaptic vesicles at the EM level. The advantage of these techniques over conventional chemical fixation is that the instantaneous freezing and gradual substitution of amorphous ice with fixatives in the fly larvae prevents fixation-induced osmotic shock that can result in cell shrinkage as well as the possible redistribution of synaptic vesicles. Thus the ultrastructural analysis is predicted to be representative of the close-to-native state of the synapse.

To standardize the quantification of synaptic vesicles a roughly rectangular area within each synaptic profile was defined, that extended 400nm along the plasma membrane on each side of the presynaptic density mid-point and extended 200nm into the cytoplasm (Figure 4.1B). We found that the average number of vesicles per 100nm² within this defined synaptic profile region was unchanged (1.62 ± 0.03 vesicles/100nm²/profile, $n = 47$ for control;ElavGal-4 and 1.63 ± 0.03 vesicles/100nm²/profile, $n = 35$ for control;UAS-bPAC vs. 1.67 ± 0.025 vesicles/100nm²/profile, $n = 65$ for ElavGal-4;UAS-bPAC. $p = 0.24$ and $p = 0.43$) (Figure 4.3B), but the number of vesicles contacting the plasma membrane in ElavGal-4;bPAC transgenics was significantly increased by 50% after 5 minutes blue light activation, relative to the two control conditions (1.40 ± 0.15 vesicles/profile $n = 47$, for control;ElavGal-4 and 1.46 ± 0.17 vesicles/profile, $n = 35$, for control;UAS-bPAC vs. 2.11 ± 0.16 vesicles/profile, $n = 65$, for ElavGal-4;UAS-bPAC. $p < 0.01$ and $p = 0.018$) (Figure 4.3D). Moreover, the number of synaptic dense projection tethered vesicles

was not altered, when comparing the two controls to activated bPAC transgenics (2.09 ± 0.17 vesicles/profile $n = 23$, for control;ElavGal-4 and 1.45 ± 0.27 vesicles/profile, $n = 20$, for control;UAS-bPAC vs. 1.46 ± 0.27 vesicles/profile, $n = 24$, for ElavGal-4;UAS-bPAC. $p = 0.09$ and $p = 0.98$) (Figure 4.3C). These data suggest that the prolonged response in bPAC activated fly larvae is associated with increased vesicle docking and that the increased docking does not deplete the synaptic vesicles tethered to *Drosophila* dense projections.

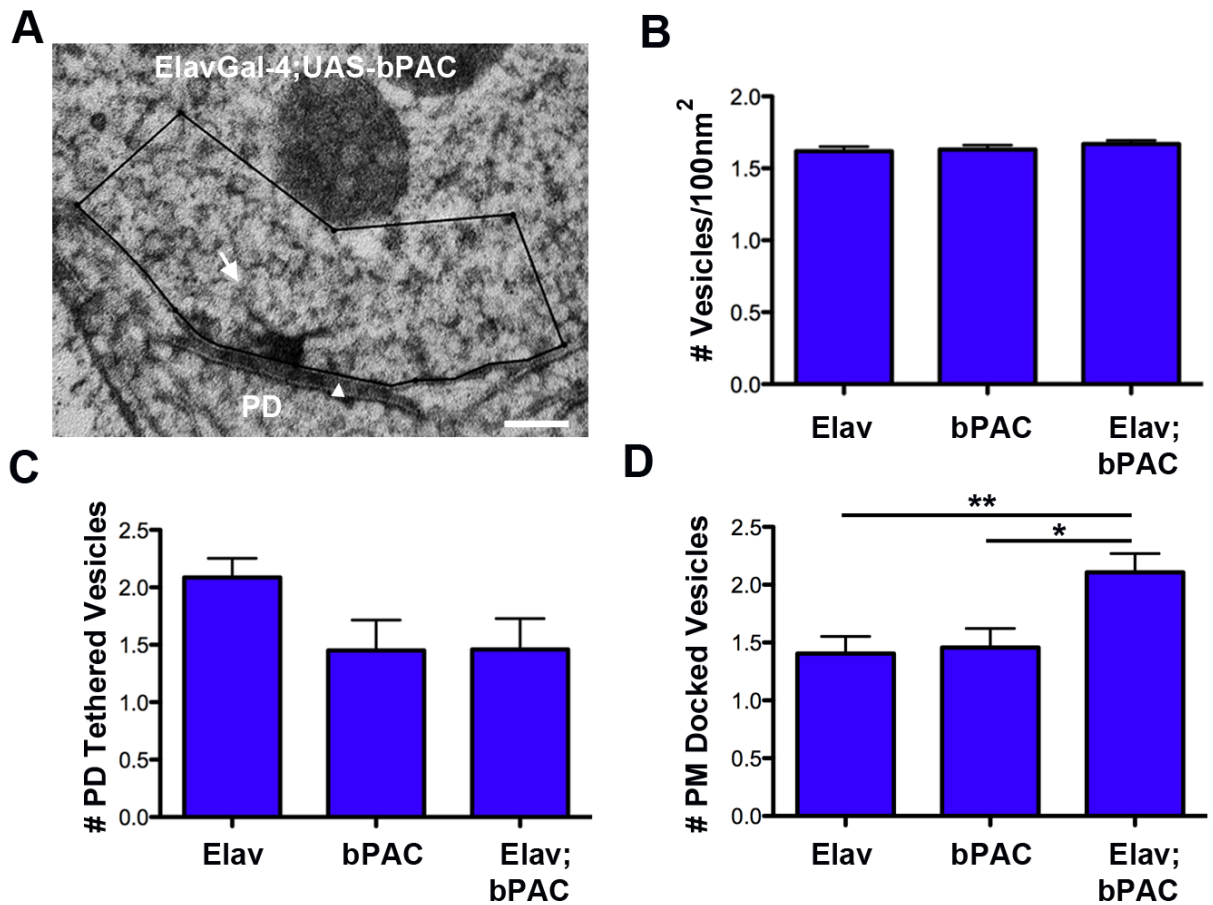


Figure 4.3. bPAC activation increases plasma membrane synaptic vesicle docking. (A) *Drosophila* NMJ representative micrograph of 5 minute blue light activation of neuronally expressed bPAC, using the panneuronal Gal-4 driver, Elav followed by HPF fixation. The presynaptic density is labeled PD, the plasma membrane contacting vesicles are indicated with an arrowhead, and the PD tethered vesicles are indicated with arrows. (B) The average number of synaptic vesicles per NMJ profile within the quantified area (~800nm x 200nm) was not significantly different among controls (ElavGal-4 or UAS-bPAC) and activated bPAC transgenics following 5 minutes blue light activation. (C) The number of vesicles tethered to the dense projection was not significantly different between activated bPAC as well as ElavGal-4 and UAS-bPAC controls. (D) The number of synaptic vesicles docked at the plasma membrane was significantly increased following bPAC activation, compared to ElavGal-4 and UAS-bPAC expression alone.

Increased synaptic vesicle docking is observed following Tomosyn RNAi

Previous electrophysiological analyses of fly larvae following Tomosyn RNAi showed an increased EJC charge integral (Chen et al., 2011), similar to that observed upon bPAC activation. If Tomosyn function is regulated by the cAMP pathway, we would expect vesicle docking following Tomosyn knockdown to phenocopy that of activated bPAC. To test this hypothesis we compared the synaptic ultrastructure in HPF/FS prepared larvae with a panneuronal ElavGal-4 driven Tomosyn RNAi construct to that of the ElavGal-4 driver alone. The vesicle density of Tomosyn RNAi NMJs was not altered when compared to the control larvae (1.88 ± 0.05 vesicles/100nm²/profile, n = 70 for control;ElavGal-4 vs. 1.76 ± 0.07 vesicles/100nm²/profile, n = 34 for ElavGal-4;TomRNAi, p = 0.19) (Figure 4.4A,B). Similarly, Tomosyn RNAi did not change the number of dense projection tethered vesicles compared to the control ElavGal-4 driver alone (2.02 ± 0.19 vesicles/profile, n = 43 for control;ElavGal-4 vs. 2.42 ± 0.35 vesicles/profile, n = 19 for ElavGal-4;TomRNAi, p = 0.53) (Figure 4.4C). However, vesicle localization was affected. Specifically, Tomosyn RNAi knockdown significantly increased the number of plasma membrane docked vesicles by 52% (1.56 ± 0.13 vesicles/profile, n = 70, for control;ElavGal-4 vs. 2.21 ± 0.26 vesicles/profile, n = 34, for ElavGal-4;TomRNAi, p = 0.04) (Figure 4.4D). These observations are consistent with the hypothesis that Tomosyn may suppress vesicle docking in a cAMP-dependent manner.

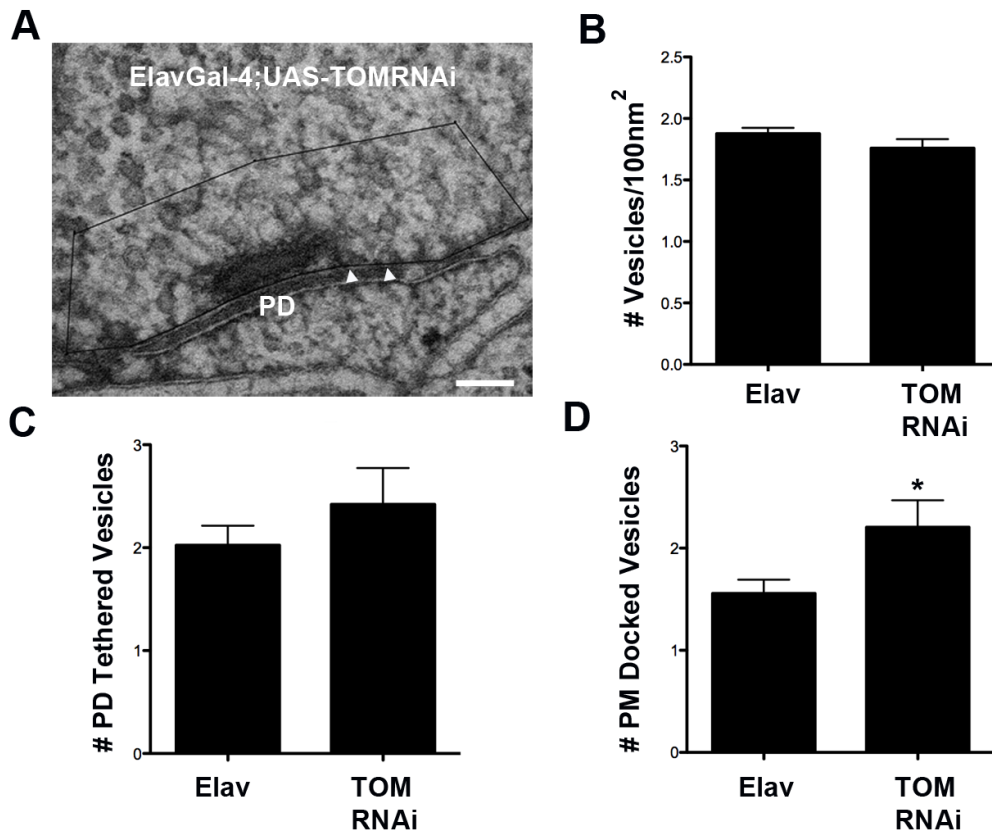


Figure 4.4. Tomosyn RNAi increases plasma membrane synaptic vesicle docking. (A) Representative micrographs of *Drosophila* NMJs prepared by HPF fixation in Elav driven Tomosyn RNAi. The presynaptic density is labeled PD, the plasma membrane contacting vesicles are indicated with arrowheads. (B) The average number of synaptic vesicles and (C) dense projection tethered vesicles per profile showed no difference between ElavGal-4 control and Tomosyn RNAi. (D) The number of docked synaptic vesicles increased in Tomosyn RNAi, compared to ElavGal-4 control.

bPAC activation results in synaptic redistribution of Tomosyn

PKA phosphorylation of recombinant Tomosyn has been shown to reduce its interaction with Syntaxin-1, allowing more fusogenic SNARE complexes to assemble (Baba et al., 2005). Since Syntaxin is an integral plasma membrane protein, disruption of the Tomosyn/Syntaxin interaction is predicted to reduce the plasma membrane association of Tomosyn (Gracheva et al., 2007). As a consequence, to test whether PKA phosphorylation of Tomosyn impacts its subcellular location, we used confocal microscopy to examine anti-Tomosyn staining with and without cAMP signaling. Larvae expressing bPAC in motor neurons were dissected and subsequently subjected to 5 minute blue light activation, prior to chemical fixation and confocal imaging. We found that fly Tomosyn staining redistributed from cortical membrane to synaptic lumen upon 5 minute blue light activation in bPAC expressing synapses (Figure 4.5). The translocation of Tomosyn supports the hypothesis that phosphorylation of Tomosyn reduces its interaction with Syntaxin *in vivo*, hence allowing vesicle-associated Synaptobrevin to form fusogenic SNARE complexes resulting vesicle docking.

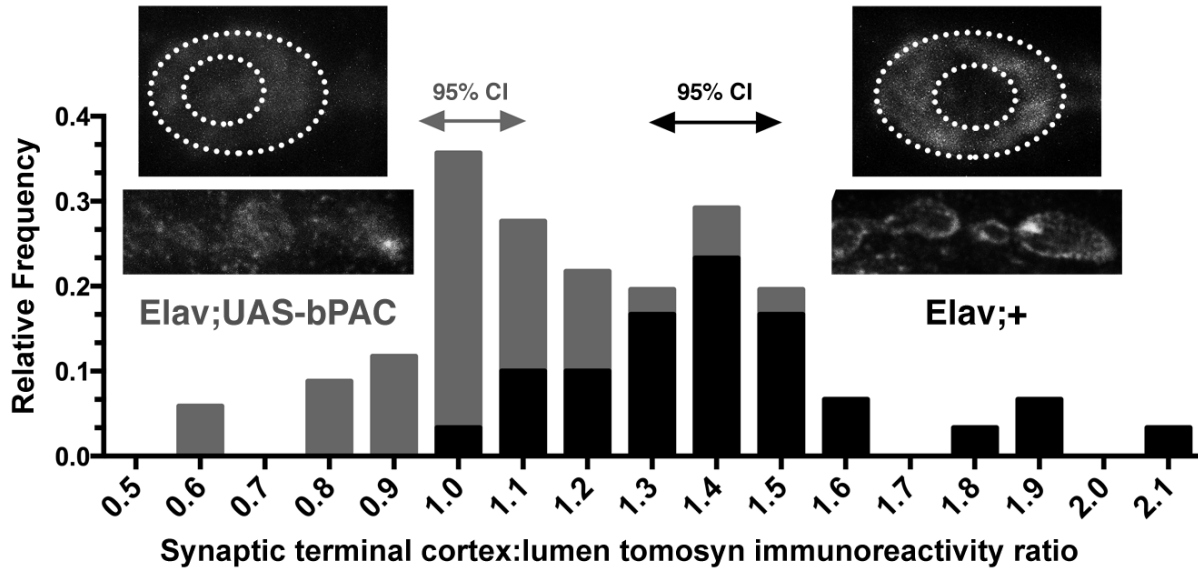


Figure 4.5. bPAC activation translocates Tomosyn from the plasma membrane to the synaptic lumen. Confocal images show the distribution of anti-Tomosyn from the NMJ of dissected larvae in ElavGal-4 control and activated ElavGal-4;bPAC. The Tomosyn immunoreactivity ratio of the synaptic bouton cortex to lumen was quantified. Following 5 minutes blue light activation, the relative frequency of bPAC activation was shifted to the left, showing cAMP-dependent redistribution of Tomosyn from the plasma membrane cortical region to the lumen.

Tomosyn functions as an important effector in the cAMP-signaling pathway

To understand if cAMP signaling acts via Tomosyn at *Drosophila* synapses, we next examined the consequences of bPAC activation in the Tomosyn RNAi background. We predicted that if Tomosyn translocation from the plasma membrane is required to enhance vesicle docking, then bPAC activation combined with Tomosyn knockdown should not show additivity at the EM level. Consistent with this model, blue light activated larvae with ElavGal-4 driving both panneuronal UAS-TomRNAi and UAS-bPAC showed no further increase in the number of docked synaptic vesicles when compared to bPAC activation alone (2.11 ± 0.16 vesicles/profile, $n = 65$, for ElavGal-4;UAS-bPAC vs. 2.28 ± 0.22 vesicles/profile, $n = 39$. $p = 0.50$) (Figure 4.6C). Although the synaptic vesicle density of ElavGal-4;TomRNAi;bPAC larvae exhibited a small but significant decrease compared to bPAC activation alone (1.67 ± 0.025 vesicles/100nm²/profile, $n = 65$ for ElavGal-4;UAS-bPAC vs. 1.54 ± 0.043 vesicles/100nm²/profile, $n = 39$ for ElavGal-4;TomRNAi;UAS-bPAC. $p < 0.01$) (Figure 4.6A), the slight decrease in vesicle number did not affect the ratio of docked vesicles to the total vesicle number within the quantified area for these two strains ($9.13 \pm 0.75\%$ vesicles/profile, $n = 65$, for ElavGal-4;UAS-bPAC vs. $10.66 \pm 0.99\%$ vesicles/profile, $n = 39$. $p = 0.18$) (Figure 4.6D). Additionally, the number of tethered vesicles to the dense projection showed no difference between activated bPAC alone and bPAC with Tomosyn RNAi knockdown (1.46 ± 0.27 vesicles/profile, $n = 24$, for ElavGal-4;UAS-bPAC vs. 1.32 ± 0.22 vesicles/profile, $n = 19$. $p = 0.89$) (Figure 4.6B). Therefore, these data support the hypothesis that Tomosyn may be an important effector of cAMP

signaling at *Drosophila* synapses and this pathway does not affect the tethering of synaptic vesicles to the active zone dense projection.

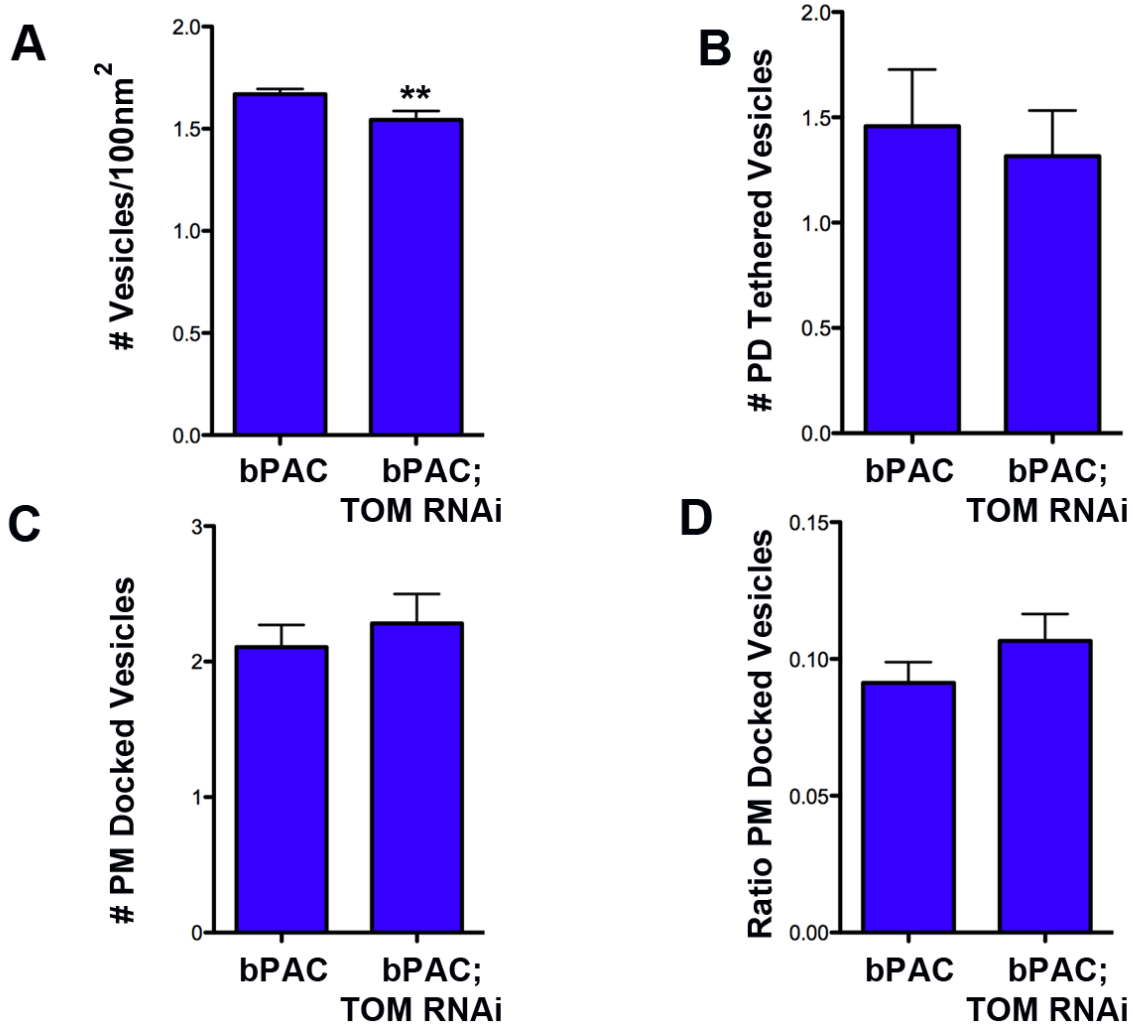


Figure 4.6. bPAC activation in the Tomosyn RNAi background shows no additivity of synaptic vesicle docking. (A) Although the synaptic vesicle density of ElavGal-4;TomRNAi;bPAC exhibited a small but significant reduction compared to activated ElavGal-4;bPAC alone, (B) there was no additivity in the number of dense projection tethered vesicles, (C) the absolute number of docked vesicles in ElavGal-4;TomRNAi;bPAC (D) nor in the ratio of docked vesicles to the total number of vesicles per profile

4.4 Discussion

In this study we used bPAC to investigate synaptic events associated with increased cAMP signaling at the fly NMJ in order to test the link between cAMP activation and Tomosyn function. This necessitated performing the first detailed characterization of bPAC actions at *Drosophila* synapses. Our electrophysiological analyses showed an increase in evoked release following bPAC activation, primarily due to slower decay kinetics. We believe this response is due to increased cAMP signaling, as we have previously observed a similar effect upon application of the adenylate cyclase activator, forskolin. Furthermore, the restricted expression of bPAC within the presynaptic terminals rules out a post-synaptic contribution to the observed increase in release.

To gain a greater understanding of the underlying cause of this prolonged response we imaged HPF fixed sections from larvae following bPAC stimulation. While synaptic vesicle density was unaffected, the number of docked vesicles increased in a bPAC-dependent manner. Both the electrophysiological and ultrastructural effects of bPAC activation mimicked the synaptic changes associated with Tomosyn RNAi, suggesting that Tomosyn may be an important downstream effector of cAMP. Consistent with this hypothesis, stimulation of bPAC caused a translocation of Tomosyn away from the plasma membrane, providing a mechanistic link between cAMP-signaling and reduced Tomosyn function at the membrane. We envision that raised cAMP levels, leads to the PKA-dependent phosphorylation of Tomosyn, which has previously been shown to reduce its binding affinity for the plasma membrane SNARE, Syntaxin, leading to its redistribution away from the plasma membrane. As a consequence of

this signaling cascade, the formation of inhibitory Tomosyn complexes should be suppressed allowing more vesicles to become docked as a result of enhanced priming. In support of this model, we observed no additivity in terms of the number of synaptic vesicles docked when bPAC was activated along with Tomosyn RNAi.

bPAC as an optogenetic tool to acutely and reversibly increase intracellular cAMP

In this study we used a newly developed variant (bPAC) of the photoactivatable adenylate cyclases of which *Euglena gracilis* PAC α was the founding member (Iseki et al., 2002). Previous studies have shown that blue-light activation of PAC α results in action potential broadening in *Aplysia* sensory neurons, due in large part to the previously established PKA-dependent closure of potassium channels (Nagahama et al., 2007). Neuronally expressed PAC α has also been shown to enhance spontaneous neurotransmitter release at both *Drosophila* as well as *C. elegans* NMJs (Bucher and Buchner, 2009; Weissenberger et al., 2011), however the effects on evoked neurotransmission have never been studied. Since PAC α is known to exhibit considerable basal activity levels in the dark, in the present study we used the more efficient and less leaky bPAC construct to examine the acute effects of cAMP signaling at *Drosophila* synapses (Stierl et al., 2011). We observed no significant difference between EJC's in control larvae (D42Gal4) and those expressing neuronal bPAC under dark conditions, confirming previous *in situ* data that the levels of bPAC activity in the dark is low and does not significantly impact these synaptic properties. Following bPAC activation, we also observed an increase in miniEJC frequency. In addition we observed a prolongation of the EJC response, similar to that previously observed

following forskolin application, suggesting that this effect is also due to enhanced cAMP signaling (Chen et al., 2011).

The use of this optogenetic tool also allowed us to perform the first ultrastructural analysis of synapses in intact larvae preserved by HPF at a similar time point after bPAC photoactivation. Blue-light activation of bPAC produced a pronounced and correlative increase in EJC charge integral and docked vesicles, that phenocopies Tomosyn RNAi.

The enhanced release associated with Tomosyn and cAMP correlates with an increase in vesicle docking at Drosophila synapses

Our results indicate that Tomosyn negatively regulates synaptic vesicle docking at fly synapses and that this inhibition is relieved in a cAMP-dependent manner. Previous studies have suggested that docking at *Drosophila* synapses is an event upstream of vesicle priming and SNARE complex formation. Specifically at NMJs of priming-defective *Dunc-13* mutants as well as loss of Syntaxin or Synaptobrevin function, the number of docked vesicles actually appeared to accumulate (Aravamudan et al., 1999; Broadie et al., 1995). However, increasing evidence suggests that the mode of chemical fixation used to prepare samples in these studies may have deleteriously impacted ultrastructural morphology leading to non-physiological vesicle association with the membrane. A strong argument in support of this notion comes from a comparison of ultrastructural results obtained for *C. elegans unc-13* as well as mouse Munc13 mutants, following either classical chemical fixation or HPF. Specifically, docking defects were not observed following chemical fixation in mutants of either species, but were very prominent following HPF preparation (Augustin et al.,

1999; Richmond et al., 1999; Siksou et al., 2009; Weimer et al., 2006). A similar dramatic reduction in docked vesicles has been observed at *C. elegans* Syntaxin mutant NMJs following HPF fixation (Hammarlund et al., 2007). Thus, a growing body of evidence indicates that synaptic vesicle docking at the HPF ultrastructural level is a morphological correlate of SNARE complex assembly, which brings the vesicle into close apposition with the plasma membrane. This result is consistent with our previous analysis of *C. elegans* Tomosyn mutants, which also exhibit prolonged release and enhanced synaptic vesicle docking (Gracheva et al., 2006). Furthermore, in *C. elegans* we have shown that Tomosyn and the priming factor, UNC-13 play antagonistic roles in vesicle priming (Gracheva et al., 2010; McEwen et al., 2006). Therefore, the appearance of more docked synaptic vesicles following bPAC activation and/or Tomosyn RNAi at fly NMJs is most likely a reflection of increased synaptic vesicle priming. Interestingly, the number of vesicles tethered to the dense projection at the fly NMJ was unaffected by either treatment, suggesting that cAMP and Tomosyn are not involved in vesicle tethering, a process that is dependent on the integral dense-projection protein, Bruchpilot (Hallermann et al., 2010). The fact that the number of tethered vesicles is normal, suggests that vesicle tethering is sustainable under these conditions of increased vesicle priming.

Whether the enhanced number of docked vesicles observed following bPAC activation also accounts for the increase in miniEJC frequency in addition to the evoked responses, is less clear. Since neither *C. elegans* or Mouse Tomosyn mutants, nor *Drosophila* Tomosyn knock-down result in obvious increased minis, we suspect that this

effect may be due to an alternative cAMP target, such as cAMP-gated channels or the cAMP activated GEF, EPAC that regulates Rim (de Rooij et al., 1998; Zufall, 1993).

cAMP signaling regulates Tomosyn membrane localization and leads to enhanced synaptic strength in vivo

cAMP has long been recognized to play an important role in the facilitation of synaptic strength, both in terms of basal release and during synaptic plasticity associated with certain forms of learning (Byrne and Kandel, 1996; Weiskopf et al., 1994). Critical research in this area has involved the study of *Drosophila* olfactory learning and has identified a number of learning defective mutants that disrupt the cAMP signaling pathway in mushroom body Kenyon cells (Benzer, 1971; Dudai et al., 1976). Although these mutants have provided important insights into the pathway and mechanisms underlying this form of associative learning, the downstream effectors of cAMP beyond PKA and CREB during intermediate and late stages of memory consolidation have yet to be fully realized. Recently, we uncovered a role for Tomosyn in PKA-dependent fly olfactory learning (Chen et al., 2011). Specifically, we demonstrated that Tomosyn RNAi in Kenyon cells eliminated the anesthesia-sensitive phase of memory that is known to require PKA-signaling (Schwaerzel et al., 2007). The impetus to examine Tomosyn in fly learning arose from a previous study that established vertebrate Tomosyn as a PKA-effector, phosphorylation resulting in a decreased ability for Tomosyn to form complexes with Syntaxin and SNAP-25 *in vitro* (Baba et al., 2005).

By acutely stimulating cAMP production with bPAC in the present study, we were able to establish that Tomosyn undergoes a subcellular translocation away from the

plasma membrane, consistent with a reduction in Tomosyn complex assembly, a predicted result of PKA-dependent phosphorylation. This compliments previous work, in which the membrane association of Tomosyn was found to be promoted by the Rho-Kinase-dependent phosphorylation of Syntaxin, a condition that enhances Tomosyn complex formation and results in the inhibition of secretion (Gladycheva et al., 2007; Sakisaka et al., 2004).

Based on previous studies, disruption of Tomosyn complex assembly via PKA-dependent phosphorylation is predicted to enhance synaptic transmission by promoting fusogenic SNARE complexes and vesicle priming (Baba et al., 2005; Hatsuzawa et al., 2003). However *in vitro* studies have also documented a contradictory role for Tomosyn PKA-phosphorylation leading to SNARE complex oligomerization that inhibits vesicle priming (Sakisaka et al., 2008). In the present study, we were able to show that acute cAMP signaling not only leads to the translocation of Tomosyn away from the plasma membrane, but in the same time frame results in enhanced synaptic transmission that correlates with more docked vesicles. This suggests that the predominant effect of cAMP signaling *in vivo* is excitatory. Although, these data do not directly establish that Tomosyn phosphorylation occurs as a result of raised cAMP levels, the fact that bPAC activation translocates Tomosyn, phenocopies Tomosyn knock-down and is occluded by Tomosyn RNAi support the conclusion that Tomosyn is regulated in a cAMP-dependent manner. That Tomosyn RNAi phenocopies loss of PKA-activity in fly learning assays and that Tomosyn is a known PKA-target, further suggest that the cAMP effects uncovered in this study reflect PKA-dependent regulation of Tomosyn.

V. Future directions

The results presented in this thesis give rise to several additional questions that I have summarized in following sections.

1. To understand if VPS-39 function requires the other HOPS complex members, detailed experiments including dylox, electrophysiology and EM analysis will be performed on a *vps-33* mutant obtained from the Caenorhabditis Genetics Center (CGC).
2. (a) To determine whether Tomosyn is a direct effector of PKA in the cAMP pathway, we will first need to generate a *Drosophila* Tomosyn knockout mutant by transposase hopping of a P-element (G0294) that is inserted in the intron upstream of the Tomosyn SNARE motif encoding exon. This mutant will be outcrossed and characterized to determine the electrophysiological and ultrastructural phenotype of the mutant to confirm that it phenocopies Tomosyn RNAi.
(b) We will then establish that expression of full length *Drosophila* Tomosyn rescues the Tomosyn mutant by immunohistochemistry, electrophysiology and EM. A full-length Tomosyn construct has been synthesized with a Flag tag to aid in the assessment of expression levels.
(c) We have identified a serine at position Ser700 in the *Drosophila* Tomosyn protein sequence that has a PKA-phosphorylation probability of 0.994 compared to a score of 0.987 for rat Tomosyn Ser724, using the same algorithm. Phosphomimetic aspartate and phosphoresistant alanine substitutions of this serine have been synthesized and will be used to generate transgenic fly lines. We anticipate that Ser/Ala Tomosyn may be enriched on the plasma membrane and should fail to

translocate into the lumen upon adenylate cyclase activation. Tomosyn Ser/Asp is expected to have a luminal distribution under basal and elevated cAMP levels. Examination of the electrophysiological and ultrastructural phenotypes of Tomosyn Ser/Ala is predicted to show synaptic inhibition and decreased vesicle docking compared to expression of the Wild-type Tomosyn construct, while Ser/Asp is expected to have enhanced release due to increased vesicle docking.

(d) The ability of Tomosyn Ser/Ala and Ser/Asp expression to rescue fly learning in Tomosyn mutants will also be assessed. We anticipate that neither construct will support PKA-dependent learning, since neither can react to PKA.

(e) A scaffolding protein, A-kinase anchoring protein (AKAP), has been shown to provide a focal point for PKA signaling. Therefore, the endogenous competitor, eCOPR2 peptide which constitutes the *Drosophila* PKA-RII regulatory domain that binds AKAP, will be used to compete with PKA binding to AKAP. Electrophysiological and ultrastructural phenotypes of eCOPR2 and the control eCOPR2 Δ (13 amino acids deleted in the essential AKAP docking domain) will be studied in basal and elevated cAMP conditions to test whether the spatial regulation of PKA is important for synaptic transmission.

Reference

- Aravamudan, B., Fergestad, T., Davis, W.S., Rodesch, C.K., and Broadie, K. (1999). *Drosophila* UNC-13 is essential for synaptic transmission. *Nat Neurosci* 2, 965-971.
- Augustin, I., Rosenmund, C., Sudhof, T.C., and Brose, N. (1999). Munc13-1 is essential for fusion competence of glutamatergic synaptic vesicles. *Nature* 400, 457-461.
- Augustine, G.J., Burns, M.E., DeBello, W.M., Pettit, D.L., and Schweizer, F.E. (1996). Exocytosis: proteins and perturbations. *Annu Rev Pharmacol Toxicol* 36, 659-701.
- Baba, T., Sakisaka, T., Mochida, S., and Takai, Y. (2005). PKA-catalyzed phosphorylation of tomosyn and its implication in Ca²⁺-dependent exocytosis of neurotransmitter. *J Cell Biol* 170, 1113-1125.
- Bellen, H.J., Gregory, B.K., Olsson, C.L., and Kiger, J.A., Jr. (1987). Two *Drosophila* learning mutants, *dunce* and *rutabaga*, provide evidence of a maternal role for cAMP on embryogenesis. *Dev Biol* 121, 432-444.
- Bennett, M.K., Calakos, N., and Scheller, R.H. (1992). Syntaxin: a synaptic protein implicated in docking of synaptic vesicles at presynaptic active zones. *Science* 257, 255-259.
- Benzer, S. (1971). From the gene to behavior. *Jama* 218, 1015-1022.
- Betz, A., Ashery, U., Rickmann, M., Augustin, I., Neher, E., Sudhof, T.C., Rettig, J., and Brose, N. (1998). Munc13-1 is a presynaptic phorbol ester receptor that enhances neurotransmitter release. *Neuron* 21, 123-136.
- Betz, A., Okamoto, M., Benseler, F., and Brose, N. (1997). Direct interaction of the rat unc-13homologue Munc13-1 with the N terminus of syntaxin. *J Biol Chem* 272, 2520-2526.
- Blasi, J., Chapman, E.R., Link, E., Binz, T., Yamasaki, S., De Camilli, P., Sudhof, T.C., Niemann, H., and Jahn, R. (1993a). Botulinum neurotoxin A selectively cleaves the synaptic protein SNAP-25. *Nature* 365, 160-163.
- Blasi, J., Chapman, E.R., Yamasaki, S., Binz, T., Niemann, H., and Jahn, R. (1993b). Botulinum neurotoxin C1 blocks neurotransmitter release by means of cleaving HPC-1/syntaxin. *The EMBO journal* 12, 4821-4828.
- Brenner, S. (1974). The genetics of *Caenorhabditis elegans*. *Genetics* 77, 71-94.
- Broadie, K., Bellen, H.J., DiAntonio, A., Littleton, J.T., and Schwarz, T.L. (1994). Absence of synaptotagmin disrupts excitation-secretion coupling during synaptic transmission. *Proceedings of the National Academy of Sciences of the United States of America* 91, 10727-10731.

- Broadie, K., Prokop, A., Bellen, H.J., O'Kane, C.J., Schulze, K.L., and Sweeney, S.T. (1995). Syntaxin and synaptobrevin function downstream of vesicle docking in *Drosophila*. *Neuron* *15*, 663-673.
- Brose, N., Petrenko, A.G., Sudhof, T.C., and Jahn, R. (1992). Synaptotagmin: a calcium sensor on the synaptic vesicle surface. *Science* *256*, 1021-1025.
- Bucher, D., and Buchner, E. (2009). Stimulating PACalpha increases miniature excitatory junction potential frequency at the *Drosophila* neuromuscular junction. *J Neurogenet* *23*, 220-224.
- Byrne, J.H., and Kandel, E.R. (1996). Presynaptic facilitation revisited: state and time dependence. *The Journal of neuroscience : the official journal of the Society for Neuroscience* *16*, 425-435.
- Caplan, S., Hartnell, L.M., Aguilar, R.C., Naslavsky, N., and Bonifacino, J.S. (2001). Human Vam6p promotes lysosome clustering and fusion in vivo. *J Cell Biol* *154*, 109-122.
- Chen, K., Merino, C., Sigrist, S.J., and Featherstone, D.E. (2005). The 4.1 protein coracle mediates subunit-selective anchoring of *Drosophila* glutamate receptors to the postsynaptic actin cytoskeleton. *The Journal of neuroscience : the official journal of the Society for Neuroscience* *25*, 6667-6675.
- Chen, K., Richlitzki, A., Featherstone, D.E., Schwarzel, M., and Richmond, J.E. (2011). Tomosyn-dependent regulation of synaptic transmission is required for a late phase of associative odor memory. *Proceedings of the National Academy of Sciences of the United States of America* *108*, 18482-18487.
- Cheviet, S., Bezzi, P., Ivarsson, R., Renstrom, E., Viertl, D., Kasas, S., Catsicas, S., and Regazzi, R. (2006). Tomosyn-1 is involved in a post-docking event required for pancreatic beta-cell exocytosis. *Journal of cell science* *119*, 2912-2920.
- Chheda, M.G., Ashery, U., Thakur, P., Rettig, J., and Sheng, Z.H. (2001). Phosphorylation of Snapin by PKA modulates its interaction with the SNARE complex. *Nat Cell Biol* *3*, 331-338.
- Chotard, L., Mishra, A.K., Sylvain, M.A., Tuck, S., Lambright, D.G., and Rocheleau, C.E. (2010). TBC-2 regulates RAB-5/RAB-7-mediated endosomal trafficking in *Caenorhabditis elegans*. *Molecular biology of the cell* *21*, 2285-2296.
- Davletov, B.A., and Sudhof, T.C. (1993). A single C2 domain from synaptotagmin I is sufficient for high affinity Ca²⁺/phospholipid binding. *J Biol Chem* *268*, 26386-26390.
- de Rooij, J., Zwartkruis, F.J., Verheijen, M.H., Cool, R.H., Nijman, S.M., Wittinghofer, A., and Bos, J.L. (1998). Epac is a Rap1 guanine-nucleotide-exchange factor directly activated by cyclic AMP. *Nature* *396*, 474-477.

Deak, F., Schoch, S., Liu, X., Sudhof, T.C., and Kavalali, E.T. (2004). Synaptobrevin is essential for fast synaptic-vesicle endocytosis. *Nature cell biology* 6, 1102-1108.

Dickman, D.K., Tong, A., and Davis, G.W. (2012). Snapin is critical for presynaptic homeostatic plasticity. *The Journal of neuroscience : the official journal of the Society for Neuroscience* 32, 8716-8724.

Dudai, Y., Jan, Y.N., Byers, D., Quinn, W.G., and Benzer, S. (1976). *dunce*, a mutant of *Drosophila* deficient in learning. *Proceedings of the National Academy of Sciences of the United States of America* 73, 1684-1688.

Dulubova, I., Lou, X., Lu, J., Huryeva, I., Alam, A., Schneggenburger, R., Sudhof, T.C., and Rizo, J. (2005). A Munc13/RIM/Rab3 tripartite complex: from priming to plasticity? *The EMBO journal* 24, 2839-2850.

Dulubova, I., Sugita, S., Hill, S., Hosaka, M., Fernandez, I., Sudhof, T.C., and Rizo, J. (1999). A conformational switch in syntaxin during exocytosis: role of munc18. *The EMBO journal* 18, 4372-4382.

Eitzen, G., Will, E., Gallwitz, D., Haas, A., and Wickner, W. (2000). Sequential action of two GTPases to promote vacuole docking and fusion. *The EMBO journal* 19, 6713-6720.

Fasshauer, D., Sutton, R.B., Brunger, A.T., and Jahn, R. (1998). Conserved structural features of the synaptic fusion complex: SNARE proteins reclassified as Q- and R-SNAREs. *Proc Natl Acad Sci U S A* 95, 15781-15786.

Fernandez-Chacon, R., Konigstorfer, A., Gerber, S.H., Garcia, J., Matos, M.F., Stevens, C.F., Brose, N., Rizo, J., Rosenmund, C., and Sudhof, T.C. (2001). Synaptotagmin I functions as a calcium regulator of release probability. *Nature* 410, 41-49.

Fujita, Y., Shirataki, H., Sakisaka, T., Asakura, T., Ohya, T., Kotani, H., Yokoyama, S., Nishioka, H., Matsuura, Y., Mizoguchi, A., *et al.* (1998). Tomosyn: a syntaxin-1-binding protein that forms a novel complex in the neurotransmitter release process. *Neuron* 20, 905-915.

Geppert, M., Archer, B.T., 3rd, and Sudhof, T.C. (1991). Synaptotagmin II. A novel differentially distributed form of synaptotagmin. *The Journal of biological chemistry* 266, 13548-13552.

Geppert, M., Goda, Y., Hammer, R.E., Li, C., Rosahl, T.W., Stevens, C.F., and Sudhof, T.C. (1994). Synaptotagmin I: a major Ca²⁺ sensor for transmitter release at a central synapse. *Cell* 79, 717-727.

Gladychева, S.E., Lam, A.D., Liu, J., D'Andrea-Merrins, M., Yizhar, O., Lentz, S.I., Ashery, U., Ernst, S.A., and Stuenkel, E.L. (2007). Receptor-mediated regulation of tomosyn-syntaxin 1A interactions in bovine adrenal chromaffin cells. *The Journal of biological chemistry* 282, 22887-22899.

- Gowthaman, R., Silvester, A.J., Saranya, K., Kanya, K.S., and Archana, N.R. (2006). Modeling of the potential coiled-coil structure of snapin protein and its interaction with SNARE complex. *Bioinformation* 1, 269-275.
- Gracheva, E.O., Burdina, A.O., Holgado, A.M., Berthelot-Grosjean, M., Ackley, B.D., Hadwiger, G., Nonet, M.L., Weimer, R.M., and Richmond, J.E. (2006). Tomosyn inhibits synaptic vesicle priming in *Caenorhabditis elegans*. *PLoS Biol* 4, e261.
- Gracheva, E.O., Burdina, A.O., Touroutine, D., Berthelot-Grosjean, M., Parekh, H., and Richmond, J.E. (2007). Tomosyn negatively regulates both synaptic transmitter and neuropeptide release at the *C. elegans* neuromuscular junction. *J Physiol* 585, 705-709.
- Gracheva, E.O., Hadwiger, G., Nonet, M.L., and Richmond, J.E. (2008). Direct interactions between *C. elegans* RAB-3 and Rim provide a mechanism to target vesicles to the presynaptic density. *Neurosci Lett* 444, 137-142.
- Gracheva, E.O., Maryon, E.B., Berthelot-Grosjean, M., and Richmond, J.E. (2010). Differential Regulation of Synaptic Vesicle Tethering and Docking by UNC-18 and TOM-1. *Front Synaptic Neurosci* 2, 141.
- Guan, Z., Buhl, L.K., Quinn, W.G., and Littleton, J.T. (2011). Altered gene regulation and synaptic morphology in *Drosophila* learning and memory mutants. *Learn Mem* 18, 191-206.
- Hallermann, S., Kittel, R.J., Wichmann, C., Weyhersmuller, A., Fouquet, W., Mertel, S., Oswald, D., Eimer, S., Depner, H., Schwarzel, M., *et al.* (2010). Naked dense bodies provoke depression. *The Journal of neuroscience : the official journal of the Society for Neuroscience* 30, 14340-14345.
- Hammarlund, M., Palfreyman, M.T., Watanabe, S., Olsen, S., and Jorgensen, E.M. (2007). Open syntaxin docks synaptic vesicles. *PLoS Biol* 5, e198.
- Hatsuzawa, K., Lang, T., Fasshauer, D., Bruns, D., and Jahn, R. (2003). The R-SNARE motif of tomosyn forms SNARE core complexes with syntaxin 1 and SNAP-25 and down-regulates exocytosis. *The Journal of biological chemistry* 278, 31159-31166.
- Hayashi, T., McMahon, H., Yamasaki, S., Binz, T., Hata, Y., Sudhof, T.C., and Niemann, H. (1994). Synaptic vesicle membrane fusion complex: action of clostridial neurotoxins on assembly. *The EMBO journal* 13, 5051-5061.
- Hermann, G.J., Scavarda, E., Weis, A.M., Saxton, D.S., Thomas, L.L., Salesky, R., Somhegyi, H., Curtin, T.P., Barrett, A., Foster, O.K., *et al.* (2012). *C. elegans* BLOC-1 functions in trafficking to lysosome-related gut granules. *PLoS One* 7, e43043.
- Hu, Z., Tong, X.J., and Kaplan, J.M. (2013). UNC-13L, UNC-13S, and Tomosyn form a protein code for fast and slow neurotransmitter release in *Caenorhabditis elegans*. *Elife* 2, e00967.

- Hunt, J.M., Bommert, K., Charlton, M.P., Kistner, A., Habermann, E., Augustine, G.J., and Betz, H. (1994). A post-docking role for synaptobrevin in synaptic vesicle fusion. *Neuron* 12, 1269-1279.
- Ilardi, J.M., Mochida, S., and Sheng, Z.H. (1999). Snapin: a SNARE-associated protein implicated in synaptic transmission. *Nat Neurosci* 2, 119-124.
- Iseki, M., Matsunaga, S., Murakami, A., Ohno, K., Shiga, K., Yoshida, K., Sugai, M., Takahashi, T., Hori, T., and Watanabe, M. (2002). A blue-light-activated adenylyl cyclase mediates photoavoidance in *Euglena gracilis*. *Nature* 415, 1047-1051.
- Jahn, R., Lang, T., and Sudhof, T.C. (2003). Membrane fusion. *Cell* 112, 519-533.
- Jorgensen, E.M., Hartweg, E., Schuske, K., Nonet, M.L., Jin, Y., and Horvitz, H.R. (1995). Defective recycling of synaptic vesicles in synaptotagmin mutants of *Caenorhabditis elegans*. *Nature* 378, 196-199.
- Khvotchev, M., Dulubova, I., Sun, J., Dai, H., Rizo, J., and Sudhof, T.C. (2007). Dual modes of Munc18-1/SNARE interactions are coupled by functionally critical binding to syntaxin-1 N terminus. *The Journal of neuroscience : the official journal of the Society for Neuroscience* 27, 12147-12155.
- Kim, B.Y., Sahara, Y., Yamamoto, A., Kominami, E., Kohsaka, S., and Akazawa, C. (2006). The interaction of mammalian Class C Vps with nSec-1/Munc18-a and syntaxin 1A regulates pre-synaptic release. *Biochem Biophys Res Commun* 350, 691-697.
- Kim, J.S., Lilley, B.N., Zhang, C., Shokat, K.M., Sanes, J.R., and Zhen, M. (2008). A chemical-genetic strategy reveals distinct temporal requirements for SAD-1 kinase in neuronal polarization and synapse formation. *Neural Dev* 3, 23.
- Kohn, R.E., Duerr, J.S., McManus, J.R., Duke, A., Rakow, T.L., Maruyama, H., Moulder, G., Maruyama, I.N., Barstead, R.J., and Rand, J.B. (2000). Expression of multiple UNC-13 proteins in the *Caenorhabditis elegans* nervous system. *Molecular biology of the cell* 11, 3441-3452.
- Kramer, L., and Ungermann, C. (2011). HOPS drives vacuole fusion by binding the vacuolar SNARE complex and the Vam7 PX domain via two distinct sites. *Molecular biology of the cell* 22, 2601-2611.
- Littleton, J.T., Stern, M., Perin, M., and Bellen, H.J. (1994). Calcium dependence of neurotransmitter release and rate of spontaneous vesicle fusions are altered in *Drosophila* synaptotagmin mutants. *Proceedings of the National Academy of Sciences of the United States of America* 91, 10888-10892.
- Ma, C., Su, L., Seven, A.B., Xu, Y., and Rizo, J. (2013). Reconstitution of the vital functions of Munc18 and Munc13 in neurotransmitter release. *Science* 339, 421-425.

- Madison, J.M., Nurrish, S., and Kaplan, J.M. (2005). UNC-13 interaction with syntaxin is required for synaptic transmission. *Curr Biol* 15, 2236-2242.
- Maruyama, I.N., and Brenner, S. (1991). A phorbol ester/diacylglycerol-binding protein encoded by the *unc-13* gene of *Caenorhabditis elegans*. *Proceedings of the National Academy of Sciences of the United States of America* 88, 5729-5733.
- Masuda, E.S., Huang, B.C., Fisher, J.M., Luo, Y., and Scheller, R.H. (1998). Tomosyn binds t-SNARE proteins via a VAMP-like coiled coil. *Neuron* 21, 479-480.
- Matos, M.F., Mukherjee, K., Chen, X., Rizo, J., and Sudhof, T.C. (2003). Evidence for SNARE zippering during Ca²⁺-triggered exocytosis in PC12 cells. *Neuropharmacology* 45, 777-786.
- McEwen, J.M., Madison, J.M., Dybbs, M., and Kaplan, J.M. (2006). Antagonistic regulation of synaptic vesicle priming by Tomosyn and UNC-13. *Neuron* 51, 303-315.
- Nagahama, T., Suzuki, T., Yoshikawa, S., and Iseki, M. (2007). Functional transplant of photoactivated adenylyl cyclase (PAC) into *Aplysia* sensory neurons. *Neurosci Res* 59, 81-88.
- O'Connor, V., Heuss, C., De Bello, W.M., Dresbach, T., Charlton, M.P., Hunt, J.H., Pellegrini, L.L., Hodel, A., Burger, M.M., Betz, H., *et al.* (1997). Disruption of syntaxin-mediated protein interactions blocks neurotransmitter secretion. *Proceedings of the National Academy of Sciences of the United States of America* 94, 12186-12191.
- Oyler, G.A., Higgins, G.A., Hart, R.A., Battenberg, E., Billingsley, M., Bloom, F.E., and Wilson, M.C. (1989). The identification of a novel synaptosomal-associated protein, SNAP-25, differentially expressed by neuronal subpopulations. *The Journal of cell biology* 109, 3039-3052.
- Pan, P.Y., Tian, J.H., and Sheng, Z.H. (2009). Snapin facilitates the synchronization of synaptic vesicle fusion. *Neuron* 61, 412-424.
- Pang, Z.P., Shin, O.H., Meyer, A.C., Rosenmund, C., and Sudhof, T.C. (2006). A gain-of-function mutation in synaptotagmin-1 reveals a critical role of Ca²⁺-dependent soluble N-ethylmaleimide-sensitive factor attachment protein receptor complex binding in synaptic exocytosis. *The Journal of neuroscience : the official journal of the Society for Neuroscience* 26, 12556-12565.
- Perin, M.S., Fried, V.A., Mignery, G.A., Jahn, R., and Sudhof, T.C. (1990). Phospholipid binding by a synaptic vesicle protein homologous to the regulatory region of protein kinase C. *Nature* 345, 260-263.
- Pobbati, A.V., Razeto, A., Boddener, M., Becker, S., and Fasshauer, D. (2004). Structural basis for the inhibitory role of tomosyn in exocytosis. *The Journal of biological chemistry* 279, 47192-47200.

Poskanzer, K.E., Marek, K.W., Sweeney, S.T., and Davis, G.W. (2003). Synaptotagmin I is necessary for compensatory synaptic vesicle endocytosis in vivo. *Nature* 426, 559-563.

Price, A., Wickner, W., and Ungermann, C. (2000). Proteins needed for vesicle budding from the Golgi complex are also required for the docking step of homotypic vacuole fusion. *The Journal of cell biology* 148, 1223-1229.

Raymond, C.K., Howald-Stevenson, I., Vater, C.A., and Stevens, T.H. (1992). Morphological classification of the yeast vacuolar protein sorting mutants: evidence for a prevacuolar compartment in class E vps mutants. *Mol Biol Cell* 3, 1389-1402.

Renger, J.J., Ueda, A., Atwood, H.L., Govind, C.K., and Wu, C.F. (2000). Role of cAMP cascade in synaptic stability and plasticity: ultrastructural and physiological analyses of individual synaptic boutons in *Drosophila* memory mutants. *J Neurosci* 20, 3980-3992.

Richmond, J. (2009). Dissecting and recording from the *C. Elegans* neuromuscular junction. *J Vis Exp*.

Richmond, J.E., Davis, W.S., and Jorgensen, E.M. (1999). UNC-13 is required for synaptic vesicle fusion in *C. elegans*. *Nat Neurosci* 2, 959-964.

Richmond, J.E., Weimer, R.M., and Jorgensen, E.M. (2001). An open form of syntaxin bypasses the requirement for UNC-13 in vesicle priming. *Nature* 412, 338-341.

Rostaing, P., Weimer, R.M., Jorgensen, E.M., Triller, A., and Bessereau, J.L. (2004). Preservation of immunoreactivity and fine structure of adult *C. elegans* tissues using high-pressure freezing. *J Histochem Cytochem* 52, 1-12.

Saifee, O., Wei, L., and Nonet, M.L. (1998). The *Caenorhabditis elegans* unc-64 locus encodes a syntaxin that interacts genetically with synaptobrevin. *Molecular biology of the cell* 9, 1235-1252.

Sakisaka, T., Baba, T., Tanaka, S., Izumi, G., Yasumi, M., and Takai, Y. (2004). Regulation of SNAREs by tomosyn and ROCK: implication in extension and retraction of neurites. *The Journal of cell biology* 166, 17-25.

Sakisaka, T., Yamamoto, Y., Mochida, S., Nakamura, M., Nishikawa, K., Ishizaki, H., Okamoto-Tanaka, M., Miyoshi, J., Fujiyoshi, Y., Manabe, T., *et al.* (2008). Dual inhibition of SNARE complex formation by tomosyn ensures controlled neurotransmitter release. *J Cell Biol* 183, 323-337.

Sato, T.K., Rehling, P., Peterson, M.R., and Emr, S.D. (2000). Class C Vps protein complex regulates vacuolar SNARE pairing and is required for vesicle docking/fusion. *Mol Cell* 6, 661-671.

Schiavo, G., Benfenati, F., Poulain, B., Rossetto, O., Polverino de Laureto, P., DasGupta, B.R., and Montecucco, C. (1992). Tetanus and botulinum-B neurotoxins

block neurotransmitter release by proteolytic cleavage of synaptobrevin. *Nature* 359, 832-835.

Schiavo, G., Matteoli, M., and Montecucco, C. (2000). Neurotoxins affecting neuroexocytosis. *Physiological reviews* 80, 717-766.

Schluter, O.M., Basu, J., Sudhof, T.C., and Rosenmund, C. (2006). Rab3 superprimes synaptic vesicles for release: implications for short-term synaptic plasticity. *The Journal of neuroscience : the official journal of the Society for Neuroscience* 26, 1239-1246.

Schoch, S., Deak, F., Konigstorfer, A., Mozhayeva, M., Sara, Y., Sudhof, T.C., and Kavalali, E.T. (2001). SNARE function analyzed in synaptobrevin/VAMP knockout mice. *Science* 294, 1117-1122.

Schonthaler, H.B., Fleisch, V.C., Biehlmaier, O., Makhankov, Y., Rinner, O., Bahadori, R., Geisler, R., Schwarz, H., Neuhauss, S.C., and Dahm, R. (2008). The zebrafish mutant *lbc/vam6* resembles human multisystemic disorders caused by aberrant trafficking of endosomal vesicles. *Development* 135, 387-399.

Schwaerzel, M., Jaeckel, A., and Mueller, U. (2007). Signaling at A-kinase anchoring proteins organizes anesthesia-sensitive memory in *Drosophila*. *The Journal of neuroscience : the official journal of the Society for Neuroscience* 27, 1229-1233.

Sieburth, D., Madison, J.M., and Kaplan, J.M. (2007). PKC-1 regulates secretion of neuropeptides. *Nature neuroscience* 10, 49-57.

Siksou, L., Varoqueaux, F., Pascual, O., Triller, A., Brose, N., and Marty, S. (2009). A common molecular basis for membrane docking and functional priming of synaptic vesicles. *Eur J Neurosci* 30, 49-56.

Sollner, T., Bennett, M.K., Whiteheart, S.W., Scheller, R.H., and Rothman, J.E. (1993). A protein assembly-disassembly pathway in vitro that may correspond to sequential steps of synaptic vesicle docking, activation, and fusion. *Cell* 75, 409-418.

Stevens, D.R., Wu, Z.X., Matti, U., Junge, H.J., Schirra, C., Becherer, U., Wojcik, S.M., Brose, N., and Rettig, J. (2005). Identification of the minimal protein domain required for priming activity of Munc13-1. *Curr Biol* 15, 2243-2248.

Stierl, M., Stumpf, P., Udvari, D., Gueta, R., Hagedorn, R., Losi, A., Gartner, W., Petereit, L., Efetova, M., Schwarzel, M., *et al.* (2011). Light modulation of cellular cAMP by a small bacterial photoactivated adenylyl cyclase, bPAC, of the soil bacterium *Beggiatoa*. *The Journal of biological chemistry* 286, 1181-1188.

Stigloher, C., Zhan, H., Zhen, M., Richmond, J., and Bessereau, J.L. (2011). The presynaptic dense projection of the *Caenorhabditis elegans* cholinergic neuromuscular junction localizes synaptic vesicles at the active zone through SYD-2/liprin and UNC-10/RIM-dependent interactions. *The Journal of neuroscience : the official journal of the Society for Neuroscience* 31, 4388-4396.

Striegel, A.R., Biela, L.M., Evans, C.S., Wang, Z., Delehoy, J.B., Sutton, R.B., Chapman, E.R., and Reist, N.E. (2012). Calcium binding by synaptotagmin's C2A domain is an essential element of the electrostatic switch that triggers synchronous synaptic transmission. *The Journal of neuroscience : the official journal of the Society for Neuroscience* 32, 1253-1260.

Sudhof, T.C., and Rizo, J. (1996). Synaptotagmins: C2-domain proteins that regulate membrane traffic. *Neuron* 17, 379-388.

Sutton, R.B., Fasshauer, D., Jahn, R., and Brunger, A.T. (1998). Crystal structure of a SNARE complex involved in synaptic exocytosis at 2.4 Å resolution. *Nature* 395, 347-353.

Thakur, P., Stevens, D.R., Sheng, Z.H., and Rettig, J. (2004). Effects of PKA-mediated phosphorylation of Snapin on synaptic transmission in cultured hippocampal neurons. *J Neurosci* 24, 6476-6481.

Tian, J.H., Wu, Z.X., Unzicker, M., Lu, L., Cai, Q., Li, C., Schirra, C., Matti, U., Stevens, D., Deng, C., *et al.* (2005). The role of Snapin in neurosecretion: snapin knock-out mice exhibit impaired calcium-dependent exocytosis of large dense-core vesicles in chromaffin cells. *J Neurosci* 25, 10546-10555.

Trimble, W.S., Cowan, D.M., and Scheller, R.H. (1988). VAMP-1: a synaptic vesicle-associated integral membrane protein. *Proceedings of the National Academy of Sciences of the United States of America* 85, 4538-4542.

Vites, O., Rhee, J.S., Schwarz, M., Rosenmund, C., and Jahn, R. (2004). Reinvestigation of the role of snapin in neurotransmitter release. *J Biol Chem* 279, 26251-26256.

Washbourne, P., Cansino, V., Mathews, J.R., Graham, M., Burgoyne, R.D., and Wilson, M.C. (2001). Cysteine residues of SNAP-25 are required for SNARE disassembly and exocytosis, but not for membrane targeting. *The Biochemical journal* 357, 625-634.

Weber, T., Zemelman, B.V., McNew, J.A., Westermann, B., Gmachl, M., Parlati, F., Sollner, T.H., and Rothman, J.E. (1998). SNAREpins: minimal machinery for membrane fusion. *Cell* 92, 759-772.

Weimer, R.M., Gracheva, E.O., Meyrignac, O., Miller, K.G., Richmond, J.E., and Bessereau, J.L. (2006). UNC-13 and UNC-10/rim localize synaptic vesicles to specific membrane domains. *J Neurosci* 26, 8040-8047.

Weimer, R.M., and Richmond, J.E. (2005). Synaptic vesicle docking: a putative role for the Munc18/Sec1 protein family. *Current topics in developmental biology* 65, 83-113.

Weissenberger, S., Schultheis, C., Liewald, J.F., Erbguth, K., Nagel, G., and Gottschalk, A. (2011). PACalpha--an optogenetic tool for in vivo manipulation of cellular cAMP

levels, neurotransmitter release, and behavior in *Caenorhabditis elegans*. *Journal of neurochemistry* *116*, 616-625.

Weisskopf, M.G., Castillo, P.E., Zalutsky, R.A., and Nicoll, R.A. (1994). Mediation of hippocampal mossy fiber long-term potentiation by cyclic AMP. *Science* *265*, 1878-1882.

Wurmser, A.E., Sato, T.K., and Emr, S.D. (2000). New component of the vacuolar class C-Vps complex couples nucleotide exchange on the Ypt7 GTPase to SNARE-dependent docking and fusion. *J Cell Biol* *151*, 551-562.

Xu, J., Pang, Z.P., Shin, O.H., and Sudhof, T.C. (2009). Synaptotagmin-1 functions as a Ca²⁺ sensor for spontaneous release. *Nat Neurosci*.

Yamamoto, Y., Mochida, S., Kurooka, T., and Sakisaka, T. (2009). Reciprocal intramolecular interactions of tomosyn control its inhibitory activity on SNARE complex formation. *The Journal of biological chemistry* *284*, 12480-12490.

Yao, L.H., Rao, Y., Varga, K., Wang, C.Y., Xiao, P., Lindau, M., and Gong, L.W. (2012). Synaptotagmin 1 is necessary for the Ca²⁺ dependence of clathrin-mediated endocytosis. *The Journal of neuroscience : the official journal of the Society for Neuroscience* *32*, 3778-3785.

Yizhar, O., Matti, U., Melamed, R., Hagalili, Y., Bruns, D., Rettig, J., and Ashery, U. (2004). Tomosyn inhibits priming of large dense-core vesicles in a calcium-dependent manner. *Proceedings of the National Academy of Sciences of the United States of America* *101*, 2578-2583.

Yoshihara, M., and Littleton, J.T. (2002). Synaptotagmin I functions as a calcium sensor to synchronize neurotransmitter release. *Neuron* *36*, 897-908.

Yoshihara, M., Suzuki, K., and Kidokoro, Y. (2000). Two independent pathways mediated by cAMP and protein kinase A enhance spontaneous transmitter release at *Drosophila* neuromuscular junctions. *The Journal of neuroscience : the official journal of the Society for Neuroscience* *20*, 8315-8322.

Zhang, J.Z., Davletov, B.A., Sudhof, T.C., and Anderson, R.G. (1994). Synaptotagmin I is a high affinity receptor for clathrin AP-2: implications for membrane recycling. *Cell* *78*, 751-760.

Zhou, B., Cai, Q., Xie, Y., and Sheng, Z.H. (2012). Snapin recruits dynein to BDNF-TrkB signaling endosomes for retrograde axonal transport and is essential for dendrite growth of cortical neurons. *Cell Rep* *2*, 42-51.

Zufall, F. (1993). Cyclic AMP-gated cation channels of olfactory receptor neurons. *Exs* *66*, 135-145.

VITA

Szi-chieh Yu, BS, MS

University of Illinois at Chicago, Department of Biological Sciences
840 W. Taylor St. Rm4311, Chicago, IL, 60607. (312) 996-5190

EDUCATION

Ph.D. in Molecular, Cellular and Developmental Biology,
University of Illinois at Chicago (2007–present)

Master's in Biotechnology, University of Pennsylvania (2005–2006)

Bachelor in Life Sciences, National Chung Hsing University – Taiwan (2000–2004)

PROFESSIONAL EXPERIENCE

Ph.D. (08/2007–present)

Department of Biological Sciences, University of Illinois at Chicago

Thesis title: Regulators of synaptic vesicle docking and priming.

Advisor: Janet E. Richmond

Exchange Student/ Research Assistant (04/2011–08/2011 and 05/2012–08/2012)

University of Göttingen/ European Neuroscience Institute – Germany

Thesis title: Regulators of synaptic vesicle docking and priming.

Study of synaptic protein mechanisms regulating neurotransmission by using cryo-electron microscopy in *Drosophila melanogaster*.

Advisor: Janet E. Richmond

Technician and Independent Study (11/2005–07/2007)

Department of Biology, University of Pennsylvania

Project: Construction, characterization, and evolutionary fate of double mutator strains in Escherichia coli.

Advisor: Paul Sniegowski

Research Assistant (06/2004–06/2005)

Institute of Biomedical Science, Academia Sinica – Taiwan

Project: Hepatoma-derived growth factor (HDGF) structure-function study.

Advisor: Tai-huang Huang

Research Internship (07/2002–08/2003)

Graduate Institute of Zoology, National Taiwan University – Taiwan

Project1: Identification and genetic diversity of microsatellite markers of tiger shrimps
Penaeus Monodon

Project2: Microsatellite markers development in two species of plants (*Durio* and
Asplenium) for population genetic analysis

Advisor: Hon-Tsen Yu

PUBLICATIONS

Edwards SL, **Yu SC**, Hoover CM, Phillips BC, Richmond JE, Miller KG. "An organelle gatekeeper function for *C. elegans* UNC-16 (JIP3) at the axon initial segment." *Genetics*. (2013) May;194(1):143-61

Yu SC, Klosterman SM, Martin AA, Gracheva EO, Richmond JE. "Differential roles for Snapin and Synaptotagmin in the synaptic vesicle cycle." *PLoS one*. (2013) 8(2):e57842

Gnetile CF, **Yu SC**, Serrano SA, Gerrish PJ, Sniegowski PD. "Competition Between high- and higher-mutating strains of *Escherichia coli*." *Biology Letters*. (2011) Jun 23;7(3):422-4

Chen K, Gracheva EO, **Yu SC**, Sheng Q, Richmond JE, Featherstone DE. "Neurexin in Embryonic *Drosophila* Neuromuscular Junctions." *PLoS one*. (2010) Jun 14;5(6):e11115

ORAL PRESENTATIONS

Yu SC, Klosterman SM, Martin AA, and Richmond JE. "Differential regulation of the synaptic vesicle cycle by snapin and synaptotagmin" 5th East Asia Worm Meeting, Jun27-30, 2012

Yu SC, Klosterman SM, Martin AA, and Richmond JE. "Differential regulation of the synaptic vesicle cycle by snapin and synaptotagmin" *EMBO conference series-C. elegans Neurobiology*. Heidelberg, Germany. Jun14-17, 2012

Edwards SL, **Yu SC**, Phillips BC, Richmond JE, Miller KG. "Kinesin Acts with JIP3 and Dynein to Restrict the Flow of Golgi and Endosomal Organelles into Axons." *Neuronal Development, Synaptic Function and Behavior C. elegans Topic Meeting*. Madison, WI. Jun 27-30, 2010

POSTERS

Klosterman SM, **Yu SC**, Burdina AO and Richmond JE. "VPS-39 promotes synaptic vesicle fusion in *C. elegans*." *The Genetics Society of America Conferences: 19th International C. elegans Meeting*. Los Angeles, CA. Jun 26-30, 2013

Hoover C, Edwards SL, **Yu SC**, Kittelmann M, Eimer S, Richmond JE, Miller KG. "A Novel UNC-43 (CaM Kinase II) Dense Core Vesicle Trafficking Pathway Blocks UNC-31 (CAPS) - Dependent Secretion from Neuronal Cell Somas." *The Genetics Society of America Conferences: 19th International C. elegans Meeting*. Los Angeles, CA. Jun 26-30, 2013

Klosterman SM, **Yu SC** Martin AA, and Richmond JE. “vps-39 promotes synaptic vesicle fusion in *C. elegans*” *EMBO conference series-C. elegans Neurobiology. Heidelberg, Germany. Jun14-17, 2012*

Klosterman SM, **Yu SC**, Burdina AO, and Richmond JE. “Characterization of the novel TOM-1 binding partner, VPS-39, in *C. elegans*” *The Genetics Society of America Conferences: 18th International C. elegans Meeting. Los Angeles, CA. Jun 22-26, 2011*

Klosterman SM, **Yu SC**, Martin AA, Parekh H, Burdina AO, Gracheva EO and Richmond JE. “Characterization of *C. elegans* snapin mutants.” *Society of Neuroscience meeting. Chicago, IL. Oct 17-21, 2009*

Klosterman SM, **Yu SC**, Martin AA, Parekh H, Burdina AO, Gracheva EO and Richmond JE. “Characterization of *C. elegans* snapin mutants.” *The Genetics Society of America Conferences: 17th International C. elegans Meeting. Los Angeles, CA. Jun 24-28, 2009*

Lee WT, Sue SC, Wang CH, Yu JG, **Yu SC**, Lee SC, Wu WJ, Wu WG, and Huang TH. “The HATH domain of human hepatoma-derived growth factor can form a domain-swapped dimer with much higher affinity for heparin as cell internalization.”

HONORS

“An Organelle Gatekeeper Function for Caenorhabditis elegans UNC-16 (JIP3) at the Axon Initial Segment” article was selected for **F1000prime** and was recommended by faculty member Robert K. Herman (2013)

Graduate Award for Research Achievement (2013)

Research Grants for Doctoral Candidates and Young Academics and Scientists, DAAD (Deutscher Akademischer Austausch Dienst), Germany (2012)

5th East Asia *C. elegans* meeting travel fellowship (2012)

College of Liberal Arts & Sciences PhD Student travel award (2012)

UIC Graduate Student Council travel award (2012)

UIC Biological Sciences Departmental student travel award (2012)

Cathay Life Scholarship, Cathay Life, Taiwan (2003–2004)

Labor Union Scholarship, Taipei County Driver Labor Union, Taiwan (2003)

Labor Union Scholarship, Taipei County Driver Labor Union, Taiwan (2002)

TEACHING EXPERIENCE

Teaching Assistant (08/2007–05/2008 and 10/2011–present)

UNIVERSITY OF ILLINOIS AT CHICAGO
BIOS221 Genetics Laboratory

PROFESSIONAL MEMBERSHIPS

Genetics Society of America

Society for Neuroscience